PREDICTING FLY ASH PERFORMANCE IN CONCRETE FROM PARTICLE CHARACTERISTICS

By

SHINHYU KANG

Bachelor of Science in Materials Science and Engineering
Kyonggi University
Suwon, Republic of Korea
2010

Master of Science in Materials Science and Engineering
Kyonggi University
Suwon, Republic of Korea
2012

Submitted to the Faculty of the
Graduate College of the
Oklahoma State University
in partial fulfillment of
the requirements for
the Degree of
DOCTOR OF PHILOSOPHY
May, 2020

PREDICTING FLY ASH PERFORMANCE IN

CONCRETE FROM PARTICLE CHARACTERISTICS

Dissertation Approved:

Dr. M. Tyler Ley

Dissertation Adviser

Dr. Bruce W. Russell

Dr. Julie A. Hartell

Dr. Nicholas F. Materer

ACKNOWLEDGEMENTS

First, I greatly appreciate my advisor, Dr. Tyler Ley for giving me a chance to work with him during my Doctorate. This degree would have not happened without your support, patience, encouragement, and guidance. I will forever be indebted to you. I also would like to thank my committee members, Dr. Bruce Russell, Dr. Julie Hartell, and Dr. Nicholas Materer who generously agreed to serve on my committee and support me. The professional knowledge and encouragement that they shared made me keep going on my research.

I would like to extend my thanks to all my colleagues and friends at Oklahoma State University. I would especially like to thank Dr. Taahwan Kim for helping and supporting me mentally and physically to get over those days. I would like to thank Dr. Daniel Cook for reviewing all my papers and giving me valuable comments to enhance them. Jeffrey M. Davis, Dr. Qinang Hu, Dr. Mehdi Khanzadeh, Zane Lloyd, Mark Finnell, Nick Seader, Nathaniel Morris, Mayra Salazar, Anna Rywelski, and Amir Behravan; it was a pleasure to work with all of you on my research. I would also like to thank all of the undergraduate students that helped me during my doctorate research.

I would like to express my sincere thankfulness to my beloved and supportive family, especially my parents for unconditionally loving, encouraging, supporting and believing in me. A special thank you must go to my best friend as well as my beautiful and wonderful wife, Eunyoung, for her love, trust, and support over the years. I would like to give my special thanks to my precious and adorable daughter, Joey. Thank you for coming to this world as my daughter at the end of my degree. I could not have done this journey without my family.

Name: SHINHYU KANG

Date of Degree: MAY, 2020

Title of Study: PREDICTING FLY ASH PERFORMANCE IN CONCRETE FROM PARTICLE CHARACTERISTICS

Major Field: CIVIL ENGINEERING

Abstract: While fly ash is widely used as supplementary cementitious material (SCM) in concrete, the demands of fly ash have been increased in producing high-performance concrete. Fly ash can contribute to the strength gain and improve the durability of concrete because of its pozzolanic and cementitious properties. Even though fly ash can be classified either Class C or Class F based on the contents of CaO according to ASTM C618, this classification has not always shown to be useful to predict performance in concrete. Because of the unpredictability of the performance of fly ash this limits the amount of fly ash used in concrete. This study aims to develop predictive models for the compressive strength, electrical resistivity and apparent diffusion coefficient of fly ash concrete materials. A novel approach called the Particle Model is employed to construct the predictive models for different curing dates and replacement levels. This includes investigating thousands of fly ash particles using automated scanning electron microscopy (ASEM) and classifying them into nine distinct groups based on the characteristics of the individual particle with the help of machine learning. This work has given promising linear predictive equations and important insights into how different fly ash particles contribute to the compressive strength, electrical resistivity and apparent diffusion coefficient of concrete over time. These are an important step to build accurate predictive models for fly ash performance in concrete. In addition, the possibility of predicting the apparent diffusion coefficient using electrical resistivity was evaluated by investigating the practical relationship between two performances. The results in this dissertation could be of interest to a broad readership seeking more knowledge about the impacts of fly ash on compressive strength, electrical resistivity and apparent diffusion coefficient in concrete, usage of fly ash in concrete, and advanced technique for predicting the performances of concrete with by-products.

TABLE OF CONTENTS

Chapter Page

Chapter Page

Chapter Page

Chapter Page

Chapter Page

LIST OF TABLES

Table Page

Table Page

Table Page

LIST OF FIGURES

Figure Page

Figure Page

CHAPTER I

INTRODUCTION

1.1 Introduction

Fly ash is currently being used in many places as one of the supplementary cementitious materials (SCMs) in concrete. Fly ash is fine spherical particles resulting from the combustion of pulverized coal in the power plants. About 12.5 million tons or 35% of the total fly ash produced in the United States in 2018 was used as a partial replacement of portland cement in concrete [1]. Any improvements to the utilization of fly ash or understanding of fly ash properties could help not only for the environment but also in economic impact.

ASTM C618 [2] is widely used to classify fly ash as either Class C or F based on the bulk chemical composition, and past studies of the reactivity of fly ash largely relied on bulk characterization methods, such as X-ray fluorescence (XRF) or X-ray diffraction (XRD) [3-5]. While understanding the bulk chemical composition is useful, it only describes the average behavior of the system. Practically, each coal particle independently undergoes different physical and chemical changes during the combustion process at the power plant. Therefore, the composition of each individual particle of fly ash is a result of all these processes [6]. Because of this, there is no universal method to predict the performance of fly ash in concrete [2-5].

However, there may be more to learn about the performance of fly ash by studying individual particles. A method for a better understanding of the characteristics of fly ash and its performance would greatly benefit in the concrete industry.

A technique using automated scanning electron microscopy (ASEM) is able to rapidly measure the physical and chemical information of thousands of individual particles within a reasonable timeframe [6-11]. This can provide potential insights into the performance of fly ash in cement-based materials through the study of the individual fly ash particles. In addition, the ASEM allows the investigation of the impacts of particle size and chemical composition of fly ash in performances and helps to study the relationship among the performances.

A novel approach called the Particle Model is introduced to predict the compressive strength of fly ash concrete [8]. The Particle Model uses a machine learning, self-organizing map (SOM), to classify thousands of fly ash particles in distinct groups based on the particle information and construct the linear model for predicting the performance of cement-based materials including fly ash. This can be applied to a specific period of hydration date and other concrete performance such as electrical resistivity and diffusion. Furthermore, the coefficients from the derived predictive models can provide important insights into the effectiveness of different fly ash particles over time into the performances of concrete materials. The work presented provides new insights into creating predictive models for the performance of fly ash in concrete. This could help users better characterize different fly ash sources and use even higher volumes of fly ash in concrete.

1.2 Research objectives

The main tasks of this dissertation are to:

- Develop a statistical approach to classify the fly ash particles into distinct groups using a machine learning method based on the characteristics of the individual fly ash particles.

- Develop and extend the application of a novel approach to drive the predictive models for the compressive strength, electrical resistivity and diffusion coefficient of the cement-based materials including fly ash at different hydration times and replacement levels called the Particle Model.
- Investigate the impacts of fly ash on each performance by using the determined groups of fly ash particles and the predictive models.
- Study the correlation between electrical resistivity and the iodide diffusion coefficient.

1.3 Overview of dissertation

In this dissertation, work is presented in six chapters in the paper-based format including the first chapter which is the introduction of the dissertation.

The second chapter presents the usefulness of the Particle Model to predict the compressive strength of fly ash concrete. The Particle Model uses machine learning through a Self-Organizing Map (SOM) algorithm to classify the thousands of fly ash particles into distinct groups. Predictive models for compression strength of 20% and 40% fly ash replacement levels are developed for seven different curing times between 3 and 180 days. This chapter in the present format was submitted for publication in Cement and Concrete Research.

In the third chapter, the Particle Model is applied to predict the surface electrical resistivity of fly ash concrete. Predictive models for predicting the surface electrical resistivity are presented for each 20% and 40% fly ash replacement levels at seven different curing times between 3 and 180 days. This chapter in the present format was submitted for publication in Construction and Building Materials.

The fourth chapter extends the use of the Particle Model to investigate the diffusion properties of fly ash-cement paste. Predictive models for predicting the apparent I diffusion coefficient for 20% fly ash

replacement level are developed at three different curing times which are 45, 90, and 135 days. This chapter in the present format was prepared for publication in Cement and Concrete Composites.

The fifth chapter describes the empirical correlation between the surface electrical resistivity and the apparent iodide diffusion coefficient by employing the Nernst-Einstein equation for the concrete materials with partially replacing the cement to fly ash. The possibility of determining of apparent diffusion coefficient through the electrical resistivity is evaluated for service life prediction. This chapter in the present format was prepared for publication in Construction and Building Materials.

Finally, in chapter six, the major conclusions of this dissertation are summarized followed by the recommendations for future research.

The research presented in this dissertation is based on work performed by the author at Oklahoma State University.

Contributors/co-authors to this study are: Dr. Mohammed Aboustait, Dr. Taehwan Kim, Jeffrey Davis, Dr. Qinang Hu, Zane Lloyd, and Dr. Tyler Ley.

Dr. Aboustait developed the ASEM method to analyze the fly ash particles, and Dr. Kim improved the reliability of the ASEM method by employing the data correction process by using CalcZAF to complete the chemical analysis of the individual particles. The data of seven out of twenty-six fly ash sources were analyzed by Dr. Aboustait and Dr. Kim. Jeffrey Davis developed the SOM analysis with the R program for determining distinct groups of the fly ash particles and classifying the individual particles into the groups. Furthermore, he developed the code for multiple linear regression (MLR) modeling by using the R program to help derive the predictive models of fly ash concrete. Dr. Hu created the code using MATLAB for calculating the apparent iodide diffusion coefficient and surface concentration of the radiographs of the paste samples. Zane Lloyd measured and collected all the data of compressive strength and surface electrical resistivity for 40% fly ash concrete. Dr. Ley is the

advisor, and he guides the directions of the dissertation and papers. Their contributions are acknowledged and greatly appreciated.

References

[1] A. C. A. Association, "2018 Production and Use Survey Results News Release," American Coal Ash Association, Washington, D.C.2019.

[2] *ASTM C618, Standard Specification for Coal Fly Ash and Raw or Calcined Natural Pozzolan for Use in Concrete*, 2019.

[3] S. Diamond, "On the Glass Present in Low-Calcium and in High-Calcium Flyashes," (in English), *Cement and Concrete Research,* vol. 13, no. 4, pp. 459-464, 1983.

[4] L. X. Du, E. Lukefahr, and A. Naranjo, "Texas Department of Transportation Fly Ash Database and the Development of Chemical Composition-Based Fly Ash Alkali-Silica Reaction Durability Index," (in English), *Journal of Materials in Civil Engineering,* vol. 25, no. 1, pp. 70-77, Jan 2013.

[5] S. C. White and E. D. Case, "Characterization of fly ash from coal-fired power plants," *Journal of Materials Science,* vol. 25, no. 12, pp. 5215-5219, 1990/12/01 1990.

[6] M. Aboustait, T. Kim, M. T. Ley, and J. M. Davis, "Physical and chemical characteristics of fly ash using automated scanning electron microscopy," (in English), *Construction and Building Materials,* vol. 106, pp. 1-10, Mar 1 2016.

[7] T. Kim, M. Moradian, and M. T. Ley, "Dissolution and leaching of fly ash in nitric acid using automated scanning electron microscopy," *Advances in Civil Engineering Materials,* vol. 7, no. 1, pp. 291-307, 2018.

[8] T. Kim, J. M. Davis, M. T. Ley, S. Kang, and P. Amrollahi, "Fly ash particle characterization for predicting concrete compressive strength," (in English), *Construction and Building Materials,* vol. 165, pp. 560-571, Mar 20 2018.

[9] S. Ghosal, J. L. Ebert, and S. A. Self, "Chemical composition and size distributions for fly ashes," *Fuel processing technology,* vol. 44, no. 1-3, pp. 81-94, 1995.

[10] Y. Chen, N. Shah, F. E. Huggins, G. P. Huffman, W. P. Linak, and C. A. Miller, "Investigation of primary fine particulate matter from coal combustion by computer-controlled scanning electron microscopy," *Fuel Processing Technology,* vol. 85, no. 6-7, pp. 743-761, 2004.

[11] T. Kim, M. T. Ley, S. Kang, J. M. Davis, S. Kim, and P. Amrollahi, "Using particle composition of fly ash to predict concrete strength and electrical resistivity," *Cement and Concrete Composites,* vol. 107, p. 103493, 2020/03/01/ 2020.

CHAPTER II

PREDICTING THE COMPRESSIVE STRENGTH OF FLY ASH CONCRETE WITH THE PARTICLE MODEL

Abstract

A novel approach called the Particle Model is used to predict the compressive strength of fly ash concrete. Thousands of fly ash particles are classified into the nine groups based on the chemical information of each particle based on the Particle Model. Predictive models for compression strength for 20% and 40% fly ash replacement levels are developed for seven different curing times between 3 and 180 days. The R-squared value for the compressive strength prediction of the Particle Model is ≈ 0.99, while the Class C and F classification model is < 0.50. Furthermore, the results show that the Particle Model is able to predict the compressive strength within +/- 10% for 95% of all measurements at 20% fly ash replacement and for 81% of all measurements at 40% replacement. The coefficients in the derived predictive models give important insights into the effectiveness of different fly ash particles over time. This work shows that the Particle Model is a promising method to make predictions of the performance of fly ash in concrete.

Keywords: Fly ash; Concrete; Compressive strength; ASEM; Particle Model; SOM

2.1 Introduction

Fly ash is a fine powder from the combustion of pulverized coal. About 14.1 million tons or 36% of the total fly ash produced in the United States in 2017 was used as a partial replacement of portland cement in concrete [1]. Fly ash can improve the overall performance and economy of concrete [2-5]. Fly ash is typically used at a 15-35% replacement level by mass in concrete [6]. This rate of fly ash replacement is typically limited to 20% as it is hard to predict the performance of fly ash in concrete and so this replacement level typically produces acceptable performance. Since fly ash is a waste product that would typically be landfilled if not used in concrete [7], higher replacement levels in concrete allow significant improvements in the sustainability of these mixtures. However, tools are needed to help practitioners realize when they can use higher replacement levels and how this might impact the properties and performance of the concrete.

The bulk characterization methods such as X-ray fluorescence (XRF) has been used in the previous studies to investigate the properties of fly ash and predict performance [8-11]. Unfortunately, some fly ashes with similar bulk chemical compositions can have dramatically different performance [12]. Thus, the bulk chemical composition alone cannot fully explain the fly ash properties and cannot be used to predict the performance of fly ash concrete. Previous research showed that fly ash particles are not uniform but do have repeating patterns in composition [13, 14]. Further studies using scanning electron microscopy (SEM) and automated scanning electron microscopy (ASEM) with energy dispersive X-ray spectrometry (EDS) have identified nine repeating patterns in the chemical composition of fly ash particles [14-17].

After investigating thousands of particles from different sources a method to organize and predict the performance of the fly ash was developed called the Particle Model [18]. Fig. 2.1 provides an overview of the entire process. The Particle Model uses machine learning through a Self-Organizing Map (SOM) algorithm to classify the numerous fly ash particles into nine distinct

groups [18]. The concrete performance was then measured and linear regression was used to construct a numerical model to predict the compressive strength of concrete that contains fly ash. This paper extends previous research to show that the Particle Model can be used to predict the compressive strength of fly ash concrete with 20% and 40% replacement and also for a wider range of materials.

It is outside the scope of this paper to provide detailed explanations of why different fly ash particles impact the properties of the concrete, or to comprehensively predict the compressive strength of concrete in all cases. Instead, this work is aimed at showing the usefulness of the Particle Model to develop predictive tools to predict the performance of concrete and help users become more comfortable with using higher volumes of fly ash in their concrete.

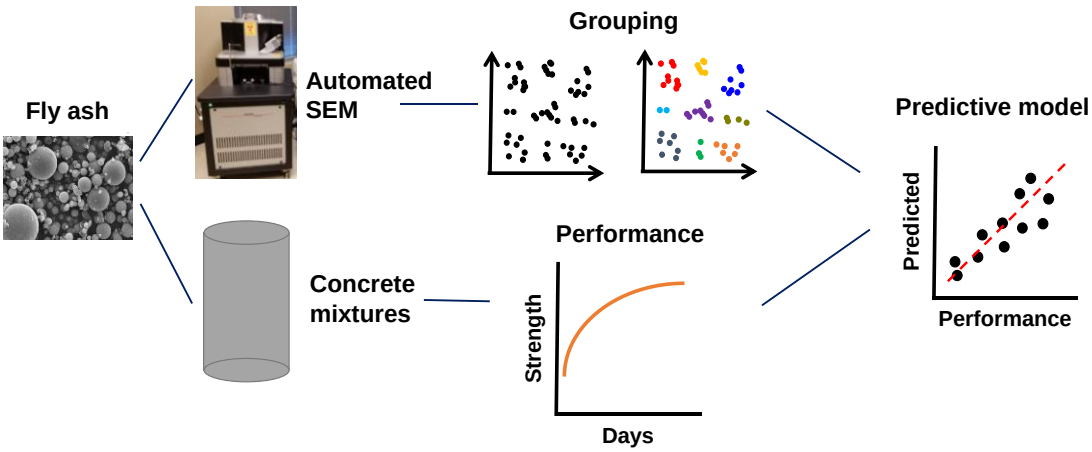

Fig. 2.1 The schematic diagram of the overall progress.

2.2 Experimental Method

2.2.1 Raw materials

Twenty-six different fly ashes were investigated in this study. All the fly ash sources were produced in the United States from various coal sources, coal power plant designs, and collection methods. Fly ashes investigated in this study were classified into fifteen Class C and eleven Class

F fly ashes according to ASTM C618 [19]. The ASEM method was used to collect a large collection of data by analyzing each individual fly ash particle. ASTM C150 Type I [20] ordinary portland cement (OPC) was used for all concrete mixtures. Table 2.1 shows the chemical and phase composition of cement used in this study. Limestone and natural sand from the state of Oklahoma were used as coarse and fine aggregate, respectively. The specific gravities for the coarse and fine aggregate were the same as 2.60, and the absorptions were 0.64% and 0.55%, respectively.

Table 2.1 Properties of Type I portland cement.

Element	**Composition (%)**	**Phase**	**Composition (%)**
SiO_2	20.77		
Al_2O_3	4.57	C_3S	52.13
Fe_2O_3	2.62		
CaO	62.67		
MgO	2.37	C_2S	20.22
SO_3	3.18		
Na_2O	0.19		
K_2O	0.32	C_3A	7.68
TiO_2	0.34		
P_2O_5	0.14		
SrO	0.22	C_4AF	7.97
BaO	0.07		

2.2.2 Fly ash particle investigation with the ASEM

The ASEM method was used to investigate the properties of all twenty-six fly ashes. This method uses SEM-EDS (Aspex Explorer PSEM-EDS) with an image analysis operating system and has important advantages over the conventional analysis of bulk chemistry using conventional XRF

[13, 21, 22]. One of the primary advantages of the ASEM is that the method can investigate the chemical composition, size and shape of approximately 500 particles per hour without human intervention. This means that the ASEM can rapidly measure the physical and average chemical information of thousands of individual particles within a reasonable timeframe. Two thousand particles were examined from each fly ash and grouped based on the eleven elements. Two thousand particles have been shown to be a representative sample for fly ash [13].

Since fly ash particles are not flat this violates one of the fundamental assumptions of classical quantitative EDS analysis. The correction models have been developed by Armstrong and Love-Scott [23, 24] and Armstrong – Buseck [25, 26] to take into account the shape of the particle and make corrections to the collected k-ratios of 11 elements (Si, Al, Fe, Ca, Mg, S, Na, K, Ti, P, and Sr). A previous study measured the chemical composition for 50 Class C fly ash particles three times. The results showed that the highest standard deviation (SD) was 1.60% [18]. This indicates the analysis results using ASEM was consistent. More detailed results for the consistency of the ASEM method can be found in Appendix A. The accuracy, reliability, and repeatability of the ASEM method when compared to XRF analysis have been presented in other publications and shown to be < 5% absolute difference for > 90% of comparisons [13, 18, 27]. This indicates that the two methods agree. Comparisons for the materials in this work are presented in Appendix B. Furthermore, the particle size distribution (PSD) has been compared between ASEM and acoustic attenuation spectroscopy and found to be similar [28]. More details over the ASEM method, sample preparation, analysis with ASEM and data processing, can be found in Appendix C.

2.2.3 Sample preparation for compressive strength testing

2.2.3.1 Concrete mixture design

Twelve Class C and seven Class F were used for concrete mixtures. Fly ash sources were chosen based on a wide range of different chemical compositions. To investigate the fly ash

performances in a concrete mixture design, 0%, 20%, and 40% replacement rates by mass of cement were produced for each fly ash source. The 0% replacement mixture was prepared for the control specimens which contained 100% portland cement, and therefore no fly ash was included in the mixture. Table 2.2 shows the mixture proportions for the control specimens without fly ash, the mixture with 20% fly ash replacement, and the mixture with 40% fly ash replacement. A constant 0.45 water-to-cementitious material ratio (w/cm) was used for all the mixtures. No chemical admixtures were added to these mixtures to minimize the variables.

Table 2.2 Mixture proportions for concrete compressive strength testing.

Mix Design	**Cement (kg/m^3)**	**Fly Ash (kg/m^3)**	**Coarse Aggregate (kg/m^3)**	**Fine Aggregate (kg/m^3)**	**Water (kg/m^3)**	**W/CM**
Control	283	0	863	564	127	0.45
20% Fly Ash	227	57	862	562	127	0.45
40% Fly Ash	170	113	858	557	127	0.45

2.2.3.2 Concrete mixing procedure and sample preparation

The moisture content of both coarse and fine aggregate was investigated before the mixing process to correct the batch proportion for each mixture ingredient. Both coarse and fine aggregates were brought into the temperature-controlled mixing facility at least a day before and their batch weights corrected for the moisture content. All the mixes were conducted according to the following steps with the adjusted mixture proportion. First, before mixing, all aggregates were collected from outside storage piles and brought into a temperature-controlled room (23°C) for at least 24 hours. Aggregates were then placed in the mixer and spun, and then a representative sample was taken for moisture correction. The aggregates should be properly sealed to prevent

water loss until the mixing. At the time of mixing, all aggregate and approximately one half of the mixing water was loaded into the mixer and mixed for three minutes. This allows the aggregates to approach the saturated surface dry (SSD) condition and ensures that the aggregates were evenly distributed. Then, all the materials (the cement, fly ash, and the remaining water) were added into the mixer and mixed for three minutes. The mixture was rested for two minutes while the sides of the mixing drum were scraped. After this time, the mixer was started to mix the concrete for another three minutes.

2.2.3.3 Sample preparation and testing

The unit weight, slump, and air content were measured for each mixture [29-31]. The results are reported in other publications [32]. Using ASTM C31 [33], samples were cast in 100 mm x 200 mm cylindrical containers and cured at 23°C and 100% RH for 24 hours in the curing room after sealing the container. The samples were then demolded and placed back into the curing room until the sample was ready for compressive strength testing according to ASTM C39 [34]. Three samples were tested at the curing times of 3, 7, 14, 28, 56, 90, and 180 days.

2.2.4 Particle Model Development

Two thousand particles were collected from each fly ash, and thus 52,000 fly ash particles from twenty-six fly ashes were collected by using ASEM. Each particle has 12 different variables, including eleven pieces of chemical composition data (Na_2O, MgO, Al_2O_3, SiO_2, P_2O_5, SO_3, K_2O, CaO, TiO_2, Fe_2O_3, and SrO_2) and its average diameter. This means that 624,000 pieces of data were collected through the ASEM particle analysis.

The SOM analysis was completed 200 times to determine the distinct groups. The SOM method is a useful way to deal with a large database and find distinct groups [35]. A previous study found

a nine group geometry worked best for the clustering analysis [18], and therefore, a nine group geometry was continued to be used for this work.

Each particle was grouped by using a spectral angle analysis. This has been discussed in previous publications and additional information is provided in Appendix D. A threshold or maximum spectral angle of 0.4 rad is used to exclude particles that do not fit any of the groups. Each particle was placed in the group with the lowest spectral angle.

These nine groups were used to derive predictive models for the compressive strength at 3, 7, 14, 28, 56, 90, and 180 days. The percentage of each group was used to conduct a multiple linear regression (MLR) analysis. In addition, the model analysis was applied not only for 20% but also for 40% fly ash replacement to predict the compressive strength. Therefore, the initial multivariable linear model equation was derived with the format of Eq.(2.1):

$$\text{Compressive Strength} = \{a(\text{Group 1}) + b(\text{Group 2}) + c(\text{Group 3}) + d(\text{Group 4}) + e(\text{Group 5}) + f(\text{Group 6}) + g(\text{Group 7}) + h(\text{Group 8}) + i(\text{Group 9})\} / Z \quad \text{Eq.(2.1)}$$

where Z is a conversion factor to determine the units of the compressive strength. The unit of strength is psi when the Z is 1 (one) and the value of Z is 145.03 if the desired units of strength are MPa. The lowercase letters represent the determined coefficients from the model analysis. Each of the coefficients reflects the effect of the individual groups on compressive strength at a specific curing time, where the potential influence of the remaining independent variables on the groups has been taken into account.

The probability value (Pr(>|t|)) from the MLR was then used to determine the statistical significance of variables on the results. This was done because there were concerns of overfitting the data with these nine groups and the Pr(>|t|) allowed the groups to be reduced to only those that are statistically significant. The R-squared value of each model was investigated for 20% and 40% fly ash replacement concrete at all individual curing times to evaluate the linear fit to the

model. The detailed procedure of the MLR analysis is found in Appendix E. All the data and model processing was conducted using the R programming environment [36, 37].

2.2.5 Bootstrapping

To evaluate the robustness of the derived predictive models, the bootstrap method was applied. Ideally, the data can be collected by repeating a large number of mixtures for the same experiment to evaluate the validity of the derived predictive models, but this is impractical. Instead, the bootstrap was implemented to investigate the robustness of the Particle Model over the R-squared value. The bootstrapping is a resampling method where the data are sampled with replacement from the original sample to generate simulated results [36]. This allows creating many R-squared values by running the predictive models with simulated samples in a timely manner. Furthermore, the results from the bootstrapping can be used to calculate a variety of sample statistics such as the mean (average) and SD of the created R-squared values to compare the R-squared value of the original model.

The size of the bootstrapping sample was the same as the original dataset and is chosen at random from the existing data set. This means that some data points can be chosen multiple times in the simulated sample while others may not be selected at all. This procedure has been used by others [38]. The bootstrapping was conducted with 500 times for each model. Then, the mean of the R-squared values from the bootstrapping was investigated and compared with the R-squared value of the derived predictive model. This was applied to each curing time for both 20% and 40% replacement.

2.3 Results and discussion

2.3.1 PSD and bulk chemical composition of raw fly ash from ASEM

Fig. 2.2 shows the cumulative PSDs of fifteen Class C and eleven Class F fly ashes investigated in this study. Most of the fly ash particles ranged between 0.5 μm and 30 μm in diameter. The range of D50 for Class C fly ashes is between 1.5 μm to 3 μm while Class F is between 1.5 μm to 2.5 μm. Previous research investigated the effect of fly ash mean particle size on the compressive strength at 7d, 28d, and 120d, and the results showed that there were no significant changes in the compressive strength for fly ash with a mean particle size between 2 to 5 μm [39]. The largest and smallest mean particle size in this study is 4.3 μm (C10) and 1.9 μm (C1). Because of this, the particle size information of the fly ashes was not included in the model.

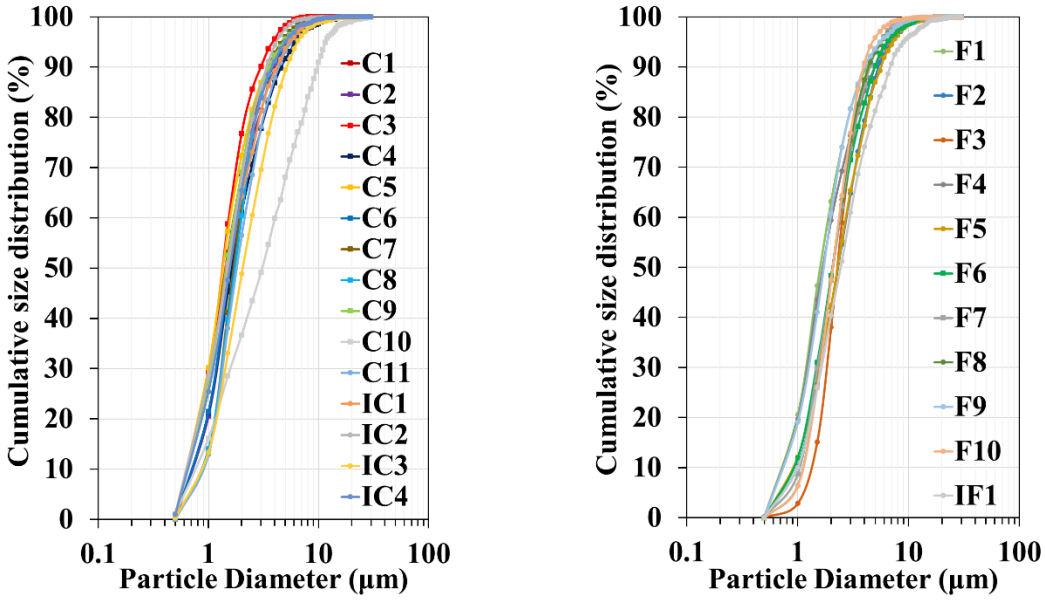

(a) Cumulative PSDs for Class C fly ashes (b) Cumulative PSDs for Class F fly ashes

Fig. 2.2 Comparison of the particle size distribution by number fraction of (a) Cumulative PSDs for fourteen Class C fly ashes and (b) Cumulative PSDs for eleven Class F fly ashes.

All the fly ashes are classified as either Class C or F fly ash according to ASTM C618. This means that Class C fly ash has > 18% of CaO while Class F fly ash has < 18% of CaO [19]. Table 2.3 shows the bulk chemical composition result from the ASEM method for twenty-six fly ash

sources. The fly ashes with “C#” and “IC#” represent Class C fly ash while the fly ashes with “F#” and “IF#” represent Class F fly ash.

Table 2.3 Bulk chemical composition from the ASEM method.

Source	SiO_2	Al_2O_3	Fe_2O_3	CaO	MgO	SO_3	Na_2O	K_2O	TiO_2	P_2O_5	SrO
C1	36.20	21.72	5.35	23.15	5.38	0.67	3.58	1.01	0.80	1.90	0.23
C2	35.82	19.18	5.60	26.88	5.49	0.98	3.00	0.88	0.73	1.25	0.18
C3	25.32	19.26	5.22	32.50	7.76	2.60	3.42	0.63	1.08	1.89	0.32
C4	36.70	22.82	4.53	22.45	4.33	1.19	3.44	0.95	1.28	1.09	1.22
C5	31.25	22.46	5.38	26.06	5.95	0.56	4.30	0.84	0.84	2.11	0.23
C6	27.66	22.88	4.23	21.54	4.52	2.55	12.61	0.76	1.27	0.67	1.32
C7	35.28	20.61	4.74	24.72	4.93	0.74	4.26	1.23	1.64	0.82	1.00
C8	40.11	22.61	4.54	19.45	5.72	0.76	3.74	0.91	0.64	1.42	0.10
C9	31.49	24.02	5.96	25.71	5.35	0.99	3.72	0.61	0.94	1.12	0.10
C10	36.04	19.30	5.06	22.70	7.77	1.97	4.78	0.57	1.03	0.32	0.47
C11	30.96	20.77	6.38	27.15	7.14	1.59	3.45	0.73	0.78	0.83	0.23
IC1	31.82	22.87	5.68	28.24	5.52	1.08	2.28	1.02	0.78	0.46	0.25
IC2	25.15	21.20	6.22	30.47	7.78	1.04	4.02	0.56	1.22	2.18	0.15
IC3	29.66	21.03	5.92	30.29	5.35	1.87	2.22	0.55	1.04	1.61	0.46
IC4	29.85	17.66	4.73	31.75	9.32	1.19	2.57	0.76	0.83	1.08	0.24
F1	48.76	23.79	7.39	12.53	2.97	0.48	0.86	2.05	0.78	0.09	0.29
F2	50.40	20.91	3.89	17.09	3.69	0.54	1.04	1.37	0.70	0.05	0.32
F3	48.81	26.62	6.65	9.30	1.95	0.28	1.75	1.93	1.46	0.14	1.10
F4	45.34	27.39	4.00	14.61	3.59	0.70	1.48	0.65	1.09	0.37	0.76
F5	53.18	25.36	11.21	2.06	0.19	0.89	0.97	4.43	0.71	0.03	0.96
F6	51.87	25.71	12.32	2.50	0.32	0.67	1.61	4.13	0.66	0.05	0.16
F7	51.92	26.31	8.01	3.28	0.54	1.69	4.04	2.53	0.87	0.61	0.14
F8	56.90	23.94	3.38	6.21	2.11	0.10	4.05	1.70	0.34	1.20	0.07
F9	48.27	25.01	5.86	12.59	3.32	0.49	1.33	1.77	1.12	0.18	0.06

F10	53.59	27.76	2.79	10.53	2.50	0.47	0.33	1.27	0.45	0.28	0.02
IF1	58.33	21.87	6.87	3.67	1.42	0.59	2.17	4.25	0.22	0.36	0.24

2.3.2 Data processing

2.3.2.1 Determination of distinct groups

Table 2.4 shows the nine different groups were found with unique chemical compositions. The standard error of each group after 200 independent SOM analyses is < 0.10%. This is quite low, indicating that the nine different groups are representative compositions obtained from 52,000 particles. More details about the SOM analysis and error analysis are found in Appendix F.

Table 2.4 Chemical composition in percent of the nine groups from the SOM analysis.

Group	**SiO_2**	**Al_2O_3**	**Fe_2O_3**	**CaO**	**MgO**	**SO_3**	**Na_2O**	**K_2O**	**TiO_2**	**P_2O_5**	**SrO**
Group 1	10.56	5.42	77.81	2.80	0.72	0.98	0.91	0.18	0.28	0.20	0.10
Group 2	8.35	33.41	6.35	33.71	6.62	2.06	0.47	0.01	0.81	6.96	1.14
Group 3	8.67	15.83	8.17	42.63	9.34	6.21	0.23	0.03	2.00	6.49	0.28
Group 4	38.35	31.09	4.48	6.65	2.89	1.29	12.13	1.95	0.56	0.20	0.37
Group 5	36.16	26.69	4.64	20.99	6.55	0.43	2.35	0.13	1.29	0.30	0.43
Group 6	23.86	21.54	4.80	34.81	7.90	1.54	0.45	0.01	1.70	2.90	0.43
Group 7	48.75	32.36	6.39	3.82	1.65	0.42	2.97	2.85	0.43	0.02	0.32
Group 8	60.58	14.82	4.75	7.11	2.75	0.33	5.90	2.83	0.46	0.04	0.39
Group 9	84.46	5.43	2.03	2.19	0.51	0.20	2.62	2.06	0.10	0.00	0.38

Fig. 2.3 shows a graphical comparison of the different particle groups. All individual groups show a unique composition of the eleven oxides. For example, Group 1 shows extremely high contents of Fe_2O_3 (77.81%) while Group 9 is mainly composed of SiO_2 (84.46%) which is

presumably crystalline quartz. More details about different groups will be discussed later in the paper.

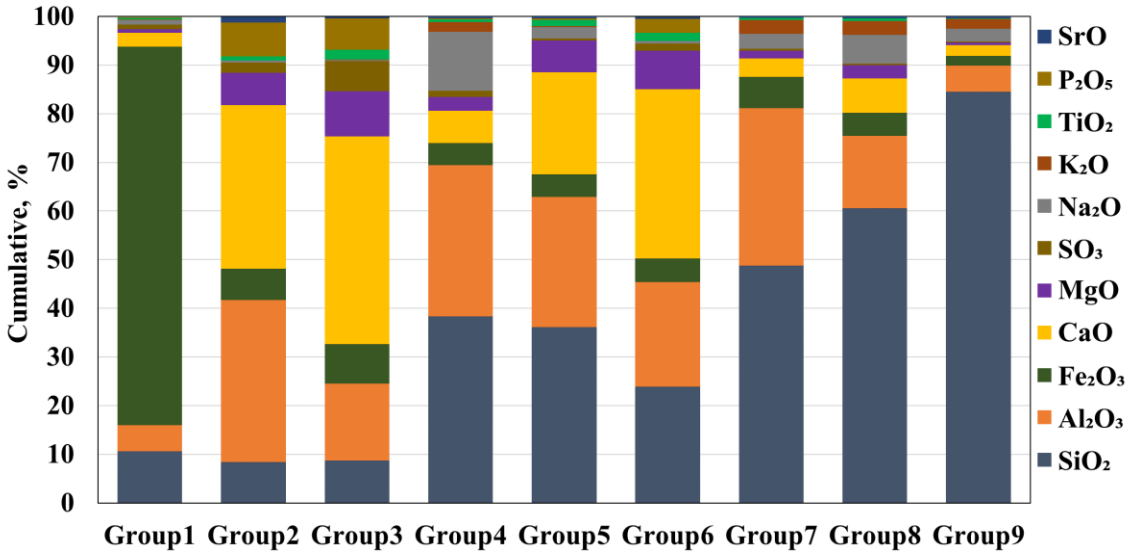

Fig. 2.3 The cumulative plot for chemicals of determined nine groups.

The amount of each group in the twenty-six fly ash sources is shown in Table 2.5. The results indicate that this approach is able to sort > 91% for each fly ash source into one of the nine groups. Excluded particles are not used in the compressive strength models.

Table 2.5 Comprehensive group composition result of the twenty-six fly ash sources.

Source	Group 1	Group 2	Group 3	Group 4	Group 5	Group 6	Group 7	Group 8	Group 9	Total
C1	0.50	8.75	16.20	13.10	21.00	21.75	4.55	5.40	5.35	96.60
C2	0.15	8.25	23.80	18.70	12.80	17.65	1.40	6.80	7.60	97.15
C3	0.30	8.55	32.20	10.30	11.80	21.25	0.25	4.90	2.90	92.45
C4	0.10	8.65	15.70	21.40	21.00	19.00	4.00	2.95	3.05	95.85
C5	0.25	7.70	27.90	21.80	12.90	16.95	0.90	3.20	4.05	95.65
C6	0.30	11.85	7.20	37.80	13.55	13.60	0.00	5.30	1.80	91.40
C7	0.15	10.05	22.90	17.25	11.95	18.55	2.40	6.35	7.50	97.10
C8	0.20	9.35	6.85	18.35	25.65	18.95	4.15	7.30	5.05	95.85

C9	0.20	11.65	10.00	20.15	25.85	21.05	0.70	3.50	3.05	96.15
C10	0.20	14.40	14.35	10.75	15.85	26.70	0.90	5.75	5.60	94.50
C11	0.15	12.60	19.85	13.80	15.50	22.75	1.30	4.95	5.10	96.00
IC1	0.25	5.75	15.30	11.70	20.70	20.45	11.00	6.70	5.15	97.00
IC2	0.00	10.75	22.40	13.95	15.35	25.40	0.05	5.15	3.30	96.35
IC3	0.25	6.70	26.00	16.70	14.50	19.45	4.65	4.15	4.05	96.45
IC4	0.05	7.60	30.25	5.95	11.35	30.10	0.80	3.60	2.65	92.35
F1	1.10	0.95	7.15	0.50	22.60	11.75	39.85	8.65	6.10	98.65
F2	0.40	0.60	6.55	0.40	22.30	13.75	36.70	11.30	6.15	98.15
F3	5.80	0.60	2.55	0.35	15.40	4.05	51.15	11.85	1.85	93.60
F4	0.30	5.05	11.95	1.65	18.45	13.15	37.45	4.30	3.90	96.20
F5	1.80	0.15	0.25	0.05	1.05	0.30	75.20	7.50	8.60	94.90
F6	2.55	0.35	0.55	0.10	1.30	0.70	71.80	8.60	8.70	94.65
F7	1.80	0.10	0.15	36.00	1.00	0.55	43.15	4.70	6.50	93.95
F8	0.80	0.95	0.30	6.50	8.50	1.60	48.80	13.45	12.35	93.25
F9	0.50	2.55	6.45	0.85	20.40	13.00	37.55	7.50	7.90	96.70
F10	0.25	0.55	1.50	0.35	14.70	4.45	56.90	10.25	7.65	96.60
IF1	1.80	0.35	0.75	0.85	2.45	1.70	51.95	20.90	11.15	91.90

2.3.2.2 Predicting compressive strength

The ASTM C618 [19] classification method is widely used to approximately compare the performance of different fly ashes despite this not being recommended. Fig. 2.4 shows the comparison between the measured strength and the average values for Class C or F fly ash at 20% and 40% replacement rates. The actual measured values were shown as points on the plot with the same color as the matching trend line. Despite having similar bulk chemical classification as per ASTM C618 the strength performance was variable. This further shows the challenge of using ASTM C618 classification methods to predict the compressive strength of concrete containing fly ash.

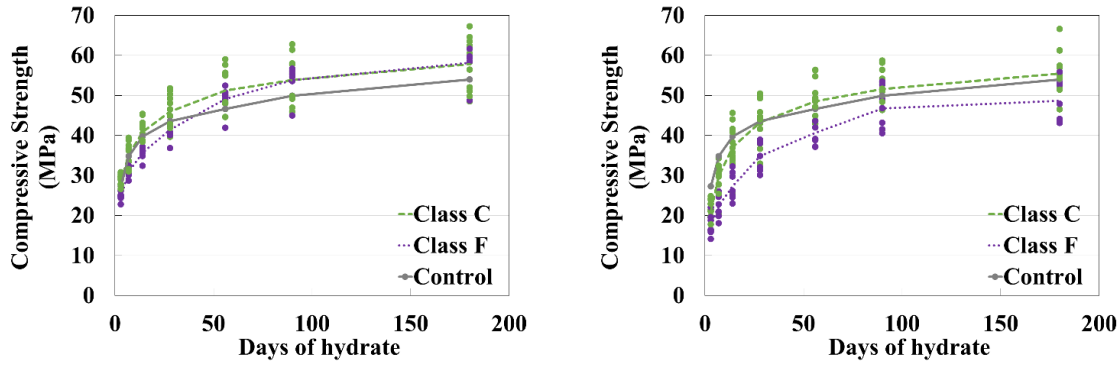

(a) 20% fly ash replacement (b) 40% fly ash replacement

Fig. 2.4 Comparison results between actual and predicted compressive strength with the type of fly ash used: (a) 20% fly ash replacement concrete and (b) 40% fly ash replacement concrete.

To highlight the benefits of using the different particle group classification, a comparison is made between the compressive strength results for fly ash with similar bulk chemistry but different compressive strengths and the results are shown in Fig. 2.5. The difference in the oxide contents (%) from each comparison in Fig. 2.5(a), C1 vs. C2 and F5 vs. IF1, is < 5% in all eleven oxides. On the other hand, the particle group composition of these four ashes varied for all nine groups in Fig. 2.5(b), and some groups showed quite big differences. For example, the differences in group composition for Group 3 and Group 5 between C1 and C2 are 7.6% and 8.3%, respectively. Furthermore, the differences in group composition for Group 7 and Group 8 between F5 and IF1 are 25.9% and 17.6%, respectively.

The compressive strength results at 20% and 40% fly ash replacement are presented in Fig. 2.5(c) and Fig. 2.5(d), respectively. The results of 20% fly ash replacement are shown as solid lines while 40% fly ash replacement results are shown as dashed lines. The results show that concrete with 40% replacement of fly ash C1 and C2 had a difference at 180d of 9.7 MPa but similar results with 20% replacement. In addition, fly ash F5 and IF1 at 20% replacement shows a difference of 9.7 MPa at 180d and similar results with 40% replacement. Again, the bulk chemical composition of C1 is quite similar to C2, and that of F5 is quite similar to IF1. This

indicates that the compressive strength is not accurately predicted by bulk chemical composition in this example. More in-depth analysis is needed to compare how the fly ash groups perform.

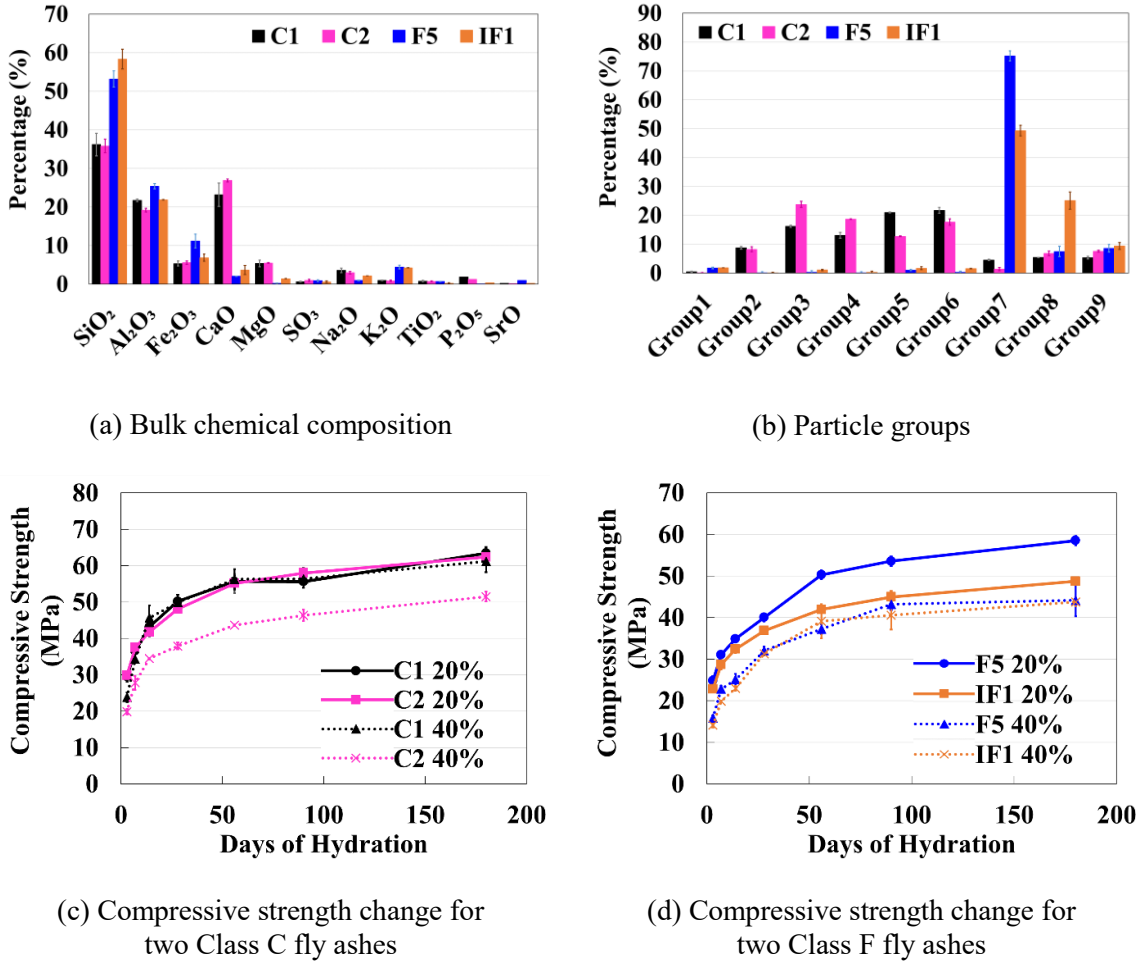

(a) Bulk chemical composition

(b) Particle groups

(c) Compressive strength change for two Class C fly ashes

(d) Compressive strength change for two Class F fly ashes

Fig. 2.5 Comparisons of (a) Bulk chemical composition, (b) Particle groups, (c) Compressive strength change for C1 vs. C2, and (d) Compressive strength change for F5 and IF1.

2.3.3 Accuracy of the Particle Model

Fig. 2.6 shows the relationship between the measured and predicted value using the Particle Model for all curing times on 20% and 40% fly ash replacement. The detailed results of the predictive models for 20% and 40% fly ash replacement at different hydration time is found in Appendix G. The slope of the trend line for 20% and 40% replacement are 1.00 and 0.99 respectively, and the R-squared value of each trend line for 20% and 40% replacement are 0.95

and 0.93. This shows the compressive strength is accurately predicted by using the Particle Model for each curing time.

According to ASTM C39, the acceptable range of three individual cylinder strengths for the test of 100 by 200 mm (4 by 8 inch) cylinders made from a well-mixed sample of concrete under laboratory conditions is 10.6% [34]. This is a helpful number to evaluate the accuracy of the Particle Model. Values of +/- 10% are shown in Fig. 2.6 as dashed red lines. For the 20% fly ash replacement shown in Fig. 2.6(a), 127 out of 133 measurements or 95% of all measurements are within +/- 10%, and the remaining 6 predictions are within +/- 15%. For the concrete with 40% fly ash replacement in Fig. 2.6(b), 108 out of 133 or 81% of the measurements are within +/- 10% and the 94% predictions are within +/- 15%. This indicates that the Particle Model works well, and the derived equations are reliable to predict the compressive strength from periods between 3d and 180d with both 20% and 40% replacement.

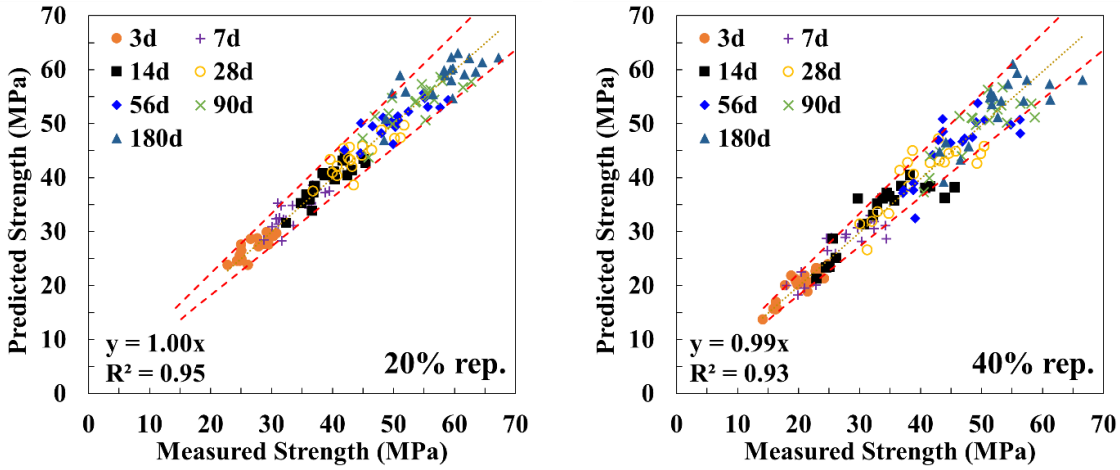

(a) 20% fly ash replacement (b) 40% fly ash replacement

* Red dash line: The range of +/– 10% of the predicted and measured strength.

Fig. 2.6 The relationship between the predicted and measured value for strength by using the Particle Model for (a) 20% fly ash concrete and (b) 40% fly ash concrete.

With the Particle Model, a model based on the current ASTM C618 classification method (Class C or F) was created for each day of hydration. It should be noted that Class C and F model did not use any of the fly ash particle data from ASEM or the nine groups. The R-squared value of Class C and F classification model was investigated for 20% and 40% fly ash replacement concrete at all individual curing time and compared to the R-squared value from Particle Model. Table 2.6 shows the R-squared value comparison results between Class C and F model and Particle Model results for all the analyses. Low R-squared value indicates a weak linear fit for the model while high R-squared value indicates the model explains all the variability of the response data around its mean. The R-squared value for all the Particle Models is close to 0.99 while the Class C and F classification model had R-squared values < 0.50 for all the measurements. These high R-squared values show that the Particle Model closely matches the measured compressive strength results.

Table 2.6 R-squared value from C and F classification model and Particle model at different curing times on different mixtures.

Days of hydration	**20% replacement**		**40% replacement**	
	C-F Model	**Particle Model**	**C-F Model**	**Particle Model**
3 days	0.494	0.997	0.458	0.992
7 days	0.423	0.996	0.495	0.989
14 days	0.478	0.998	0.438	0.988
28 days	0.256	0.997	0.397	0.991
56 days	0.065	0.997	0.365	0.992
90 days	0.000	0.996	0.184	0.993
180 days	0.000	0.996	0.318	0.993

Table 2.7 shows the results of the bootstrapping for the Particle Model over the R-squared value. The mean of 500 R-squared values through the bootstrap method is compared with the R-squared value of the derived predictive model in Table 2.6 at each measurement time for both 20% and

40% fly ash concrete. It should be noted here again that this helps to determine the robustness of the Particle Model. The results present that the mean R-squared value from the bootstrapping shows the same or almost the same each other to the R-squared value of the derived predictive model. The maximum, minimum and SD are also investigated over the R-squared values from the bootstrapping. It shows that the range of difference between the maximum and minimum R-squared value is from 0.002 to 0.014 which is quite narrow. Furthermore, all the investigated SDs are under 0.003 which indicates the variance of the bootstrap results is quite small. Thus, the Particle Model can be considered as a robust tool to predict the compressive strength of fly ash concrete for the materials investigated.

Table 2.7 The results of the bootstrapping for the Particle Model over the R-squared value.

Mixture	Days of hydration	The mean of the R-squared values	Max	Min	SD
20% Fly ash	3 days	0.997	0.999	0.995	0.0006
	7 days	0.997	0.998	0.994	0.0007
	14 days	0.998	0.999	0.997	0.0004
	28 days	0.997	0.999	0.994	0.0007
	56 days	0.997	0.999	0.995	0.0006
	90 days	0.997	0.999	0.995	0.0007
	180 days	0.997	0.999	0.994	0.0008
40% Fly ash	3 days	0.993	0.997	0.987	0.0014
	7 days	0.990	0.995	0.984	0.0016
	14 days	0.988	0.996	0.981	0.0026
	28 days	0.991	0.996	0.988	0.0013
	56 days	0.992	0.996	0.986	0.0015
	90 days	0.993	0.997	0.989	0.0013
	180 days	0.993	0.997	0.990	0.0013

2.3.4 Effects of each individual group on compressive strength

Fig. 2.7 and 2.8 show the coefficients of each group for the linear model used to predict the compression strength between 3 and 180 days for 20% and 40% replacement. The value of > 0 indicates that the group helps to increase the compressive strength while ages without a value for a coefficient mean that those groups did not affect the strength at that time period. For example, since Group 6 and 8 have a coefficient of zero between 7 and 56 days for 20% fly ash replacement, these groups are found to not be statistically significant during these periods of time (from 7 days to 56 days). The numerical value for each group shows how significant it is at each time. Positive values are shown to increase strength and negative values will decrease strength. Further discussion over the contribution of each group will be discussed later in this paper.

The impacts of Group 2, 3, 5, 7, and 9 for both 20% and 40% replacement show a steady increase over time. This means that these groups continue to contribute to strength over time. At 20% replacement Group 4 did not show an improvement in strength after 3 days, and at 40% replacement, it did not contribute to strength. Groups 6 and 8 show either no meaningful contribution or a decrease in strength for both 20% and 40% replacement. Finally, Group 1 shows a difference in performance at 20% and 40% replacement. At 20% replacement Group 1 shows an increase in contribution up to 56 days and then a decrease in strength after that, but no contribution of Group 1 was found at 40% replacement.

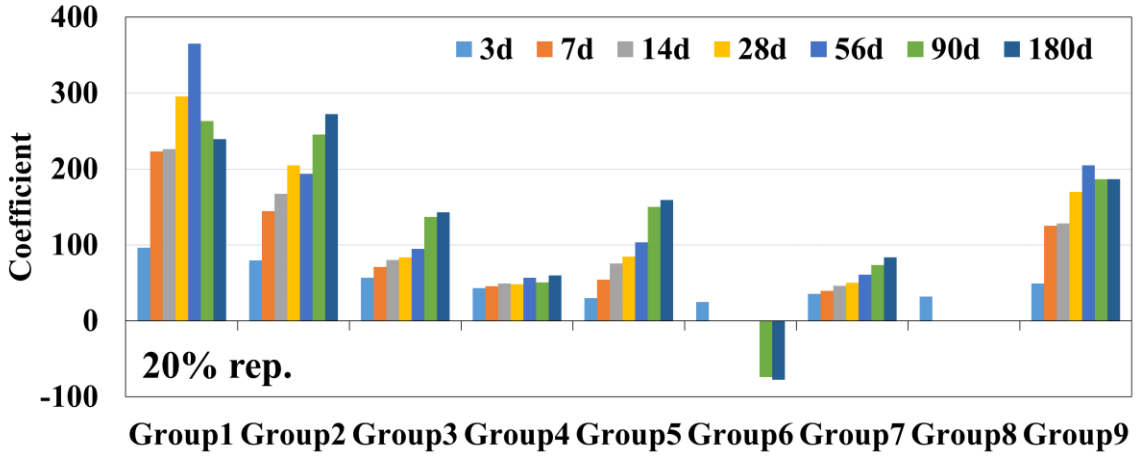

Fig. 2.7 The coefficient comparison for 20% replacement of fly ash within a concrete mixture.

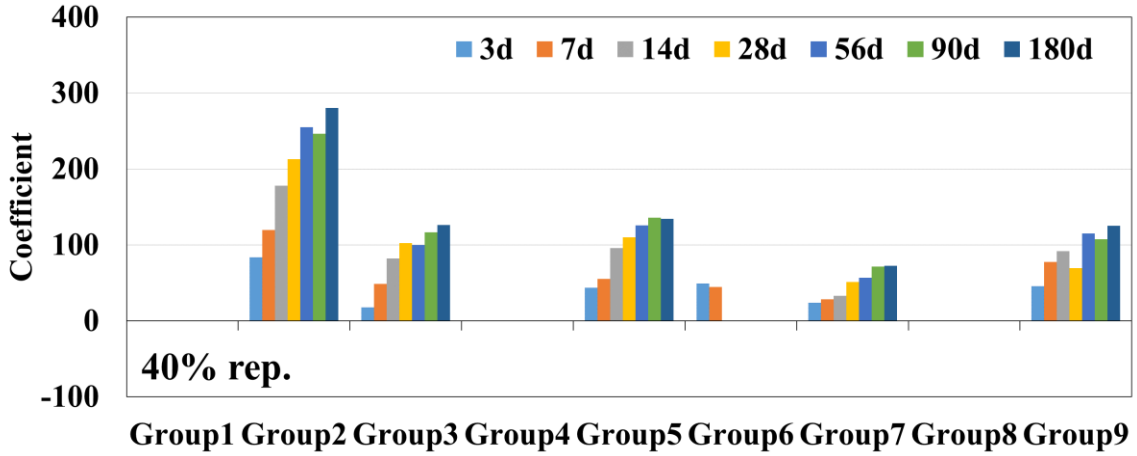

Fig. 2.8 The coefficient comparison for 40% replacement of fly ash within a concrete mixture.

2.3.4.1 Discussion of Group 2, 3, 5, and 7

These groups are likely composed of reactive glasses. Group 2 and 3 have high contents of Al_2O_3 and CaO with relatively small SiO_2 contents (about 8%). Furthermore, Group 5 has a high content of SiO_2, Al_2O_3, and CaO while Group 7 has high contents of SiO_2 and Al_2O_3 with relatively small CaO.

Group 2 and 3 have relatively higher contents of P_2O_5 and MgO than other groups, and these materials may form magnesium phosphate and aluminum phosphate. The magnesium phosphate

can decrease set, increase early strength, and show good durability including resistance to chemical attack and permeation [40]. Aluminum phosphate will also increase strength [41].

It is also possible that several glassy phases can exist in these four groups such as calcium-rich aluminosilicates, aluminosilicate and calcium silicates. Those glassy phases have been found in fly ash in several previous studies and suggested as reactive glassy phases [5, 42-45]. Durdziński et al. [43] studied the reactivity of four glassy phases in fly ash for 365 days of hydration. They have shown calcium-rich aluminosilicates were the most reactive, and the aluminosilicates also had a high reactivity [43]. It is well known that the calcium-rich glassy phases are much more reactive than those with low or moderate calcium content phases [43, 45]. Thus, Group 2, 3, 5 and 7 are likely more reactive phases than other groups.

2.3.4.2 Discussion of Group 9

Group 9 has ≈ 85% SiO_2 content. Previous studies over fly ash have shown a silicon-rich phase containing almost no impurities was mainly observed as crystalline silica which is quartz [46, 47]. Quartz is commonly observed in fly ash [5]. Furthermore, on both 20% and 40% fly ash concrete, Group 9 relatively has a high impact on the compressive strength than other groups for the first 180d of hydration. Further, the impact was almost constant after 56d of hydration.

Popovics has suggested the strength increase on the fly ash concrete could be either attributed to the reduction in initial porosity of the paste by fine particles of fly ash and quartz powder, or to the acceleration of hydration of the cement phase due to nucleation effects from fly ash particles for C-S-H gel [48]. It is also possible that some soluble silica exists in Group 9. The soluble silica could react with the aluminum to form a C-A-S-H gel with a dense microstructure. This would lower the porosity and create a finer gel pore system [49].

2.3.4.3 Discussion of Group 4, 6, and 8

The particles in these groups show a poor reactivity. Even though these groups have a similar chemical composition to the calcium-rich alumino-silicate (Group 6) and aluminum silicate (Group 4 and 8), there may be some reason that these particles have a poor reactivity. Previous studies have found low reactive materials such as mullite (a crystalline aluminosilicate) in low calcium fly ashes [50]. Group 4 has a high percentage of SiO_2 and Al_2O_3 with a CaO content of about 6%. Therefore, Group 4 may contain high amounts of mullite. Group 8 contains high SiO_2 ($\approx$ 60%) and some Na_2O and K_2O. This material is more likely a conglomerate of non-reactive phases like feldspar (K, Na)$A1Si_3O_8$, mullite, and quartz [51].

Group 6 has higher CaO and MgO content than the other groups and also has some SiO_2 and Al_2O_3. Group 6 seemed to have a similar chemical composition to Group 3 but there is about a 15% difference in SiO_2 content. The chemical composition of Group 6 could be gehlenite $Ca_2Al(AlSiO_7)$ and akermanite $Ca_2Mg(Si_2O_7)$ which have shown to not be chemically active in concrete [5]. Merwinite ($Ca_3Mg(SiO_4)_2$), a non-reactive phase that is commonly found in high-calcium fly ash may also be found in Group 6 [5]. It is also possible that the MgO causes an unsoundness problem in the concrete. This might be why these materials are observed to have a negative coefficient or a loss in strength over time.

2.3.4.4 Discussion of Group 1

Group 1 contains 77.81% of Fe_2O_3 content and this particle has the largest coefficient for 3, 7, 14, 28, and 56 days on 20% replacement while there is no impact at all to the strength over time for 40% replacement. Furthermore, the impact of Group 1 at 20% fly ash replacement concrete decreases after 56d while the impact of other groups increases. Previous studies used Fe-rich materials such as iron powder and iron waste as the partial replacement of cement to investigate the impact on the compressive strength [52-55]. The studies have found that the Fe-rich material

increased the first 28 days of hydration. One reason for this may be the strong electrostatic attractive forces of the Fe-rich particle. This has been suggested as a cause for the increase in strength at early ages [52]. This work went on to show that there is no impact on the properties after the optimum amount of Fe-rich material was reached [52]. Thus, it is possible that a 40% replacement of fly ash provides an excessive amount of this material and so there is no impact on the measured strength.

2.3.5 Practical Implications

This work builds on previous studies to show that understanding the reactivity of the individual fly ash particles is a helpful tool to predict and ultimately understand the performance of fly ash within concrete. The Particle Model takes this concept and creates a numerical tool for prediction. This work has given useful predictive equations that can be used at both 20% and 40% replacement volume of fly ash within the concrete and should help build confidence in the use of higher replacement levels of fly ash. This work also shows that it is possible to build accurate predictive models for fly ash performance in concrete.

Because of the change in coal-fired power plant emissions, the supply of fly ash has been reduced in some regions. Because the Particle Model is performance-based then it may allow greater usage of fly ash that does not meet current specifications. Further, the Particle Model may be able to serve as the basis for a performance-based classification system for fly ash beyond the current bulk composition analysis in ASTM C 618.

2.4 Conclusion

Twenty-six fly ash sources were investigated by using the ASEM to collect the properties of 52,000 fly ash particles. The Particle Model was used to investigate the fly ash concrete with nineteen fly ash sources and predict compressive strength at 20% and 40% replacement in

concrete after 3, 7, 14, 28, 56, 90, and 180 days of curing. Insights about each fundamental type or group are made as well as their contribution to the compressive strength over time.

The following contributions were made:

1. Over 91% of the fly ash particles can be classified into nine groups based on the chemical composition data.
2. The Particle Model is able to predict the compressive strength within +/- 10% for 95% of all measurements at 20% fly ash replacement and for 81% of all measurements at 40% replacement.
3. The R-squared value for the compressive strength prediction of the Particle Model is ≈ 0.99, while the Class C and F classification model is < 0.50 for the time periods investigated and for 20% and 40% fly ash replacement.
4. Group 2, 3, 5, 7, and 9 are correlated with strength gain for both 20% and 40% fly ash replacement and show similar trends at both replacement levels.
5. Group 4, 6, and 8 have a poor contribution or a reduction to the compressive strength for 20% and 40% replacement.
6. Group 1 showed the largest contribution coefficient over the first 56 days for 20% replacement while there is no impact for the compressive strength for 40% replacement.

This paper presents a useful approach to fly ash classification and accurate prediction of performance in concrete at 20% and 40% replacement levels. This work also shows that these contributions depend on the replacement levels, the chemical composition of each type of particle, and the age of curing.

Acknowledgments

This work was sponsored by funding from the Illinois Department of Transportation [Project ICT R27-180], and the FHWA [EAR project # BAA No. 693JJ3-18-BAA-0001]. The authors would like to thank Dr. Daniel Cook and Mr. Jeff Davis for their assistance and discussion on this work.

Reference

[1] A. C. A. Association, "2017 Production and Use Survey Results News Release," American Coal Ash Association, Washington, D.C.2018.

[2] M. A. Bérubé, J. Duchesne, and D. Chouinard, "Why the Accelerated Mortar Bar Method ASTM C 1260 is Reliable for Evaluating the Effectiveness of Supplementary Cementing Materials in Suppressing Expansion Due to Alkali-Silica Reactivity," *Cement, Concrete and Aggregates,* vol. 17, no. 1, pp. 26-34, 1995.

[3] S. G. Shashiprakash and M. D. A. Thomas, "Sulfate Resistance of Mortars Containing High-Calcium Fly Ashes and Combinations of Highly Reactive Pozzolans and Fly Ash," *Special Publication,* vol. 199, pp. 221-238, 6/1/2001 2001.

[4] B. Mather, "Use of Concrete of Low Portland Cement Content in Combination with Pozzolans and Other Admixtures in Construction of Concrete Dams," *J Am Concr Inst,* Article vol. 71, no. 12, pp. 589-599, 1974.

[5] A. Committee, "232.2R-18: Report for the Use of Fly Ash in Concrete," *Technical Documents,* 4/23/2018 2018.

[6] R. B. Holland, K. E. Kurtis, and L. F. Kahn, "7 - Effect of different concrete materials on the corrosion of the embedded reinforcing steel," in *Corrosion of Steel in Concrete Structures*, A. Poursaee, Ed. Oxford: Woodhead Publishing, 2016, pp. 131-147.

[7] M. E. Kalinski and P. K. Yerra, "Hydraulic conductivity of compacted cement–stabilized fly ash," *Fuel,* vol. 85, no. 16, pp. 2330-2336, 2006.

[8] S. K. Das and Yudhbir, "A simplified model for prediction of pozzolanic characteristics of fly ash, based on chemical composition," (in English), *Cement and Concrete Research,* vol. 36, no. 10, pp. 1827-1832, Oct 2006.

[9] S. Diamond, "On the Glass Present in Low-Calcium and in High-Calcium Flyashes," (in English), *Cement and Concrete Research,* vol. 13, no. 4, pp. 459-464, 1983.

[10] L. X. Du, E. Lukefahr, and A. Naranjo, "Texas Department of Transportation Fly Ash Database and the Development of Chemical Composition-Based Fly Ash Alkali-Silica Reaction Durability Index," (in English), *Journal of Materials in Civil Engineering,* vol. 25, no. 1, pp. 70-77, Jan 2013.

[11] S. C. White and E. D. Case, "Characterization of fly ash from coal-fired power plants," *Journal of Materials Science,* vol. 25, no. 12, pp. 5215-5219, 1990/12/01 1990.

[12] S. Schlorholtz, K. Bergeson, and T. Demirel, "Monitoring of Fluctuations in the Physical and Chemical Properties of a High-Calcium Fly Ash," *MRS Proceedings,* vol. 113, p. 107, 1987, Art. no. 107.

[13] M. Aboustait, T. Kim, M. T. Ley, and J. M. Davis, "Physical and chemical characteristics of fly ash using automated scanning electron microscopy," (in English), *Construction and Building Materials,* vol. 106, pp. 1-10, Mar 1 2016.

[14] Q. Hu, M. Aboustait, M. T. Ley, J. C. Hanan, V. Rose, and R. Winarski, "Combined three-dimensional structure and chemistry imaging with nanoscale resolution," (in English), *Acta Materialia,* vol. 77, pp. 173-182, Sep 15 2014.

[15] Q. Hu, M. T. Ley, J. Davis, J. C. Hanan, R. Frazier, and Y. Zhang, "3D chemical segmentation of fly ash particles with X-ray computed tomography and electron probe microanalysis," *Fuel,* vol. 116, pp. 229-236, 2014.

[16] T. Kim, Q. Hu, M. T. Ley, M. Aboustait, and J. W. Bullard, "Using Particle Characterization to Study Fly Ash Dissolution and Leaching in Water and KOH

Solution," *ACI Materials Journal,* vol. 116, no. 4, 2019.

[17] T. Kim, M. Moradian, and M. T. Ley, "Dissolution and leaching of fly ash in nitric acid using automated scanning electron microscopy," *Advances in Civil Engineering Materials,* vol. 7, no. 1, pp. 291-307, 2018.

[18] T. Kim, J. M. Davis, M. T. Ley, S. Kang, and P. Amrollahi, "Fly ash particle characterization for predicting concrete compressive strength," (in English), *Construction and Building Materials,* vol. 165, pp. 560-571, Mar 20 2018.

[19] *ASTM C618, Standard Specification for Coal Fly Ash and Raw or Calcined Natural Pozzolan for Use in Concrete*, 2019.

[20] *ASTM C150, Standard Specification for Portland Cement*, 2019.

[21] R. P. Gupta, T. F. Wall, I. Kajigaya, S. Miyamae, and Y. Tsumita, "Computer-controlled scanning electron microscopy of minerals in coal - Implications for ash deposition," (in English), *Progress in Energy and Combustion Science,* vol. 24, no. 6, pp. 523-543, 1998.

[22] C. A. O'Keefe, T. M. Watne, and J. P. Hurley, "Development of advanced scanning electron microscopy techniques for characterization of submicron ash," (in English), *Powder Technology,* vol. 108, no. 2-3, pp. 95-102, Mar 20 2000.

[23] J. T. Armstrong, "Quantitative Elemental Analysis of Individual Microparticles with Electron Beam Instruments," in *Electron Probe Quantitation*, K. F. J. Heinrich and D. E. Newbury, Eds. Boston, MA: Springer US, 1991, pp. 261-315.

[24] G. Love and V. D. Scott, "Evaluation of a New Correction Procedure for Quantitative Electron-Probe Microanalysis," (in English), *Journal of Physics D-Applied Physics,* vol. 11, no. 10, pp. 1369-1376, 1978.

[25] J. T. Armstrong and P. R. Buseck, "Quantitative Chemical-Analysis of Individual Microparticles Using Electron-Microprobe - Theoretical," (in English), *Analytical Chemistry,* vol. 47, no. 13, pp. 2178-2192, 1975.

[26] J. T. Armstrong and P. R. Buseck, "A General Characteristic Fluorescence Correction for the Quantitative Electron Microbeam Analysis of Thick Specimens, Thin-Films and Particles," (in English), *X-Ray Spectrometry,* vol. 14, no. 4, pp. 172-182, 1985.

[27] M. Aboustait *et al.*, *Innovative prediction of fly ash performance in concrete*. Midwest City, OK: Oklahoma Transportation Center, 2013.

[28] C. P. Aichele *et al.*, "A comparison of automated scanning electron microscopy (ASEM) and acoustic attenuation spectroscopy (AAS) instruments for particle sizing," *Colloids and Surfaces A: Physicochemical and Engineering Aspects,* vol. 479, pp. 46-51, 2015/08/20/ 2015.

[29] *ASTM C138, Standard Test Method for Density (Unit Weight), Yield, and Air Content (Gravimetric) of Concrete*, 2017.

[30] *ASTM C143, Standard Test Method for Slump of Hydraulic-Cement Concrete*, 2015.

[31] *ASTM C231, Standard Test Method for Air Content of Freshly Mixed Concrete by the Pressure Method*, 2017.

[32] Z. Lloyd, "Investigation of the Quality Control of Waste Products for Concrete," Master, Civil Engineering, Oklahoma State University, Stillwater, OK, 2019.

[33] *ASTM C31, Standard Practice for Making and Curing Concrete Test Specimens in the Field*, 2019.

[34] *ASTM C39, Standard Test Method for Compressive Strength of Cylindrical Concrete Specimens*, 2018.

[35] T. Kohonen, *Self-Organizing Maps*, Third ed. (Springer Series in Information Sciences). Springer, Berlin, Heidelberg, 1997.

[36] M. J. Crawley, *The R Book*, Second ed. Imperial College London at Silwood Park, UK: John Wiley & Sons Ltd, 2012.

[37] R. C. Team, "R: a language and environment for statistical computing. Vienna, Austria: R

Foundation for Statistical Computing; 2015. R Foundation for Statistical Computing," ed, 2016.

[38] M. Kuhn and K. Johnson, *Applied predictive modeling*. Springer, 2013.

[39] G. Li and X. Wu, *Influence of fly ash and its mean particle size on certain engineering properties of cement composite mortars*. 2005, pp. 1128-1134.

[40] Z. Li, Z. Ding, and Y. Zhang, "Development of sustainable cementitious materials," in *Proceedings of the international workshop on sustainable development and concrete technology*, 2004, vol. 1, no. 1, pp. 55-76: Iowa State University.

[41] N. Abdel-Rahman and N. M. Naghoj, "Silica Phosphate in Engineering Materials," in *Challenges of Concrete Construction: Volume 6, Concrete for Extreme Conditions*, 2002, pp. 101-107.

[42] D. M. Roy, K. Luke, and S. Diamond, "Characterization of fly ash and its reactions in concrete," *MRS Online Proceedings Library Archive,* vol. 43, 1984.

[43] P. T. Durdzinski, C. F. Dunant, M. Ben Haha, and K. L. Scrivener, "A new quantification method based on SEM-EDS to assess fly ash composition and study the reaction of its individual components in hydrating cement paste," (in English), *Cement and Concrete Research,* vol. 73, pp. 111-122, Jul 2015.

[44] K. L. Aughenbaugh, "Fly ash-based geopolymers: identifying reactive glassy phases in potential raw materials," Doctor of Philosophy, Civil, Architectural, and Environmental Engineering, The University of Texas at Austin, The University of Texas at Austin, 2013.

[45] K. L. Aughenbaugh, R. T. Chancey, P. Stutzman, M. C. Juenger, and D. W. Fowler, "An examination of the reactivity of fly ash in cementitious pore solutions," *Materials and Structures,* vol. 46, no. 5, pp. 869-880, 2013.

[46] V. M. Malhotra and P. K. Mehta, *High-performance, high-volume fly ash concrete : materials, mixture proportioning, properties, construction practice, and case histories*.

Ottawa, Canada: Supplementary Cementing Materials for Sustainable Development, Inc., 2002.

[47] K. Kiattikomol, C. Jaturapitakkul, S. Songpiriyakij, and S. Chutubtim, "A study of ground coarse fly ashes with different finenesses from various sources as pozzolanic materials," (in English), *Cement & Concrete Composites,* vol. 23, no. 4-5, pp. 335-343, Aug-Oct 2001.

[48] S. Popovics, "A Model for Estimation of the Contribution of Fly Ash to Concrete Strength in Blended Cements in Construction," vol. Blended cements in construction, no. Elsevier Applied Science, ed. by R. N. Swamy, 1991.

[49] Y. Ma, J. Hu, and G. Ye, "The effect of activating solution on the mechanical strength, reaction rate, mineralogy, and microstructure of alkali-activated fly ash," *Journal of Materials Science,* vol. 47, no. 11, pp. 4568-4578, 2012/06/01 2012.

[50] S. Gomes, M. François, M. Abdelmoula, P. Refait, C. Pellissier, and O. Evrard, "Characterization of magnetite in silico-aluminous fly ash by SEM, TEM, XRD, magnetic susceptibility, and Mössbauer spectroscopy," *Cement and Concrete Research,* vol. 29, no. 11, pp. 1705-1711, 1999/11/01/ 1999.

[51] D. Stark and M. S. Y. Bhatty, "Alkali-Silica Reactivity: Effect of Alkali in Aggregate on Expansion," V. H. Dodson, Ed. West Conshohocken, PA: ASTM International, 1986, pp. 16-30.

[52] P. Sikora, E. Horszczaruk, K. Cendrowski, and E. Mijowska, "The Influence of Nano-Fe_3O_4 on the Microstructure and Mechanical Properties of Cementitious Composites," (in English), *Nanoscale Research Letters,* vol. 11, Apr 11 2016.

[53] S. Ghannam, H. Najm, and R. Vasconez, "Experimental study of concrete made with granite and iron powders as partial replacement of sand," (in English), *Sustainable Materials and Technologies,* vol. 9, pp. 1-9, Sep 2016.

[54] M. A. Largeau, R. Mutuku, and J. Thuo, "Effect of Iron Powder (Fe_2O_3) on Strength, Workability, and Porosity of the Binary Blended Concrete," *Open Journal of Civil Engineering,* vol. Vol.08No.04, p. 15, 2018, Art. no. 88279.

[55] K. Noori and H. Ibrahim, *Mechanical Properties of Concrete Using Iron Waste as a Partial Replacement of Sand*. 2018.

CHAPTER III

USING THE PARTICLE MODEL TO PREDICT ELECTRICAL RESISTIVITY PERFORMANCE OF FLY ASH IN CONCRETE

Abstract

The electrical resistivity performance of fly ash in concrete is not easy to predict due to the diverse sources of fly ash and their varying reactivity. This paper aims to develop predictive models for the electrical resistivity of fly ash concrete by applying the Particle Model. The Particle Model rapidly examines individual fly ash particles without human intervention and is used to derive predictive models for 20% and 40% fly ash replacement levels in concrete at seven different periods of hydration. The R-squared values of predictive models in the Particle Model show significant improvement over using the classification method based on Class C and F for both fly ash replacement at all investigated time periods. The derived predictive models are able to accurately estimate the electrical resistivity within +/- 10% for 80% of all measurements at 20% fly ash replacement and within +/- 10% for 75% of all measurements at 40% fly ash replacement. These investigations provide important insights into how the Particle Model can help predict the electrical resistivity of fly ash concrete at different mixtures and hydration times.

Keywords: Electrical resistivity; Fly ash; Concrete; ASEM; Particle Model; Grouping; SOM

3.1 Introduction

Electrical resistivity gives direct insight into the rate of corrosion within concrete once the chloride threshold level has been exceeded and corrosion has been initiated [1]. Furthermore, the corrosion process of steel in reinforced concrete can be evaluated with the help of electrical resistivity of concrete, and the correlations between the electrical resistivity of concrete and the corrosion have been found in other studies [2-6]. Electrical resistivity is also being evaluated as a means to evaluate mass transport into concrete and has been proposed as a quality control tool for concrete [7-9]. Several factors influence the performance of electrical resistivity including: cement chemistry, the cement content, water-to-cement ratio, admixtures, and supplementary cementitious materials such as fly ash [10].

Fly ash is used as a partial replacement of the portland cement to improve the overall durability of concrete [11-14] and is generally used at 15-35% replacement of cement by mass because this range has been found to be an acceptable level of replacement without major negative effects on the performance [15]. Previous studies have investigated the impacts of fly ash in concrete and tried to predict the performance of fly ash by using bulk chemical characterization methods such as X-ray fluorescence (XRF) [16-19]. However, fly ash sources with similar bulk chemistry can have dramatically different performance [20]. This indicates that bulk chemical characteristics are not always useful to predict the properties of concrete. Furthermore, it is hard to predict the performance of higher replacement levels of fly ash in concrete. These higher replacement levels can reduce the overall cost, possibly increase durability, and improve the sustainability of the concrete [13]. Thus, a technique is needed to provide accurate predictions for the electrical resistivity performance of fly ash concrete. This has the ability to increase the usage of fly ash in concrete and improve the service life of concrete structures.

While bulk chemistry does not provide predictable insights into the performance of the fly ash in concrete, studies with scanning electron microscopy (SEM) and automated scanning electron microscopy (ASEM) show that there are repeating patterns in chemical composition found within fly ash particles [21, 22]. To gain more insights, a method called the Particle Model is developed in a previous study to produce predictive models for compressive strength [23]. This is based on using an ASEM to classify thousands of individual fly ash particles [23-28] and then machine learning with the Self-Organizing Map (SOM) algorithm was applied to classify the fly ash particles into nine distinct groups based on these few major repeatable patterns of chemical compositions [23]. These groups are then able to predict the compressive strength at different times with 90% of the predicted values within +/- 10% of the measured values [29].

The current work expands the application of the Particle Model by predicting electrical resistivity as demonstrated in Fig. 3.1. The aim of this work is to provide important insights into how the application of the Particle Model can be extended on the electrical resistivity prediction at 20% and 40% replacement by mass at different hydration times. This paper provides some important insights to evaluate the impact of fly ash in concrete and improve the durability of concrete, although a full investigation is outside the scope of this work.

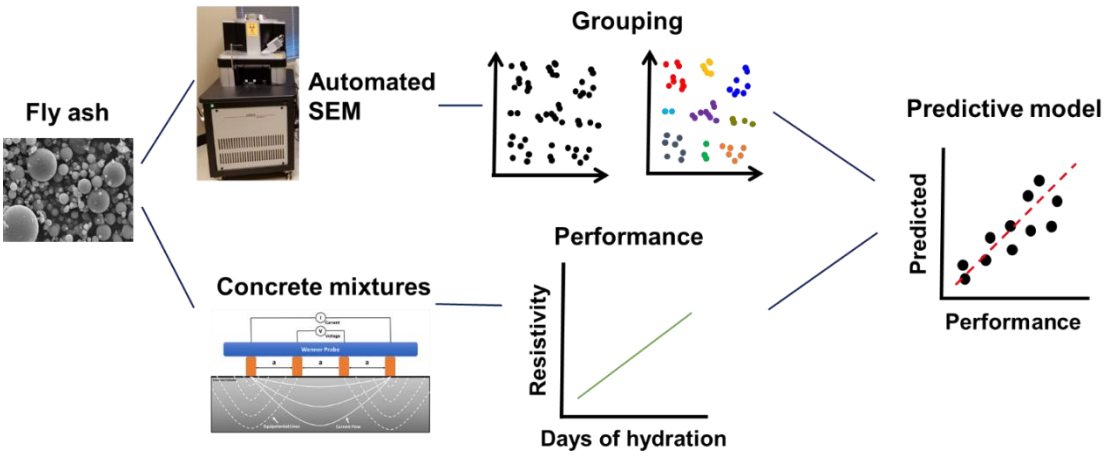

Fig. 3.1 The schematic diagram of the overall procedure of the work in this study.

3.2 Experimental Method

3.2.1 Materials

An ASTM C150 Type I ordinary portland cement (OPC) [30] was used in this study. The chemical and phase composition of the cement is presented in Table 3.1. Crushed limestone meeting ASTM C33 #57 was used as a coarse aggregate and ASTM C33 natural river sand was used as a fine aggregate [31]. The specific gravity for the coarse and fine aggregate was the same as 2.60, and the degree of absorptions for the aggregates was 0.64% and 0.55%, respectively. Twenty-six different fly ashes were investigated. All of the fly ash sources were produced in the United States from various coal sources, power plant designs, and collection methods. These fly ashes were classified into fifteen Class C and eleven Class F fly ashes in accordance with ASTM C618 [32].

Table 3.1 Properties of the cement.

Element	**Composition (%)**	**Phase**	**Composition (%)**
SiO_2	20.8	C_3S	52.1
Al_2O_3	4.6		
Fe_2O_3	2.6	C_2S	20.2
CaO	62.7		
MgO	2.4	C_3A	7.7
SO_3	3.2		
Na_2O	0.2	C_4AF	8.0
K_2O	0.3		

3.2.2 Investigation of fly ash particles with the ASEM

The ASEM was used to investigate the properties of fly ash and to collect thousands of individual fly ash particle data. The ASEM method used SEM-EDS (Aspex Explorer PSEM-EDS) with the image analysis operating system. Two thousand particles were analyzed from each fly ash because this amount of particles has been shown to be a representative sample for fly ash [25]. One of the important advantages of the ASEM over the conventional analysis of bulk chemistry is the effectiveness of measurement time [25, 33, 34]. The ASEM method enabled researchers to investigate the chemical composition, size, and shape of approximately 500 particles per hour without human intervention. This means that the ASEM can rapidly measure the physical and average chemical information of thousands of individual particles within a reasonable timeframe.

One challenge with the ASEM method was that the fly ash particle has a spherical shape, but not a flat shape; so this violated one of the assumptions of the classical quantitative EDS analysis. The correction models developed by Armstrong and Love-Scott [35, 36] and Armstrong – Buseck were used to address this [37, 38]. These models took into account the shape of the particle and make corrections in the collected k-ratios of eleven investigated elements (Na, Mg, Al, Si, P, S, K, Ca, Ti, Fe, and Sr). Furthermore, the particle size distribution (PSD) was compared between ASEM and acoustic attenuation spectroscopy and found to be similar [39]. The consistency of the ASEM method was discussed in the previous study [23], and details can be found in Appendix A. The accuracy, reliability, and repeatability of the ASEM method when compared to XRF analysis were presented in other publications and shown to be less than a 5% absolute difference for > 90% of comparisons [23, 25, 40]. More details over the ASEM method, sample preparation, analysis with ASEM, and data processing can be found in Appendix C.

3.2.3 Concrete specimen preparation

3.2.3.1 Concrete mixture design

Based on a wide range of different chemical composition, twelve Class C and seven Class F fly ash sources were chosen for concrete mixtures. The 20% and 40% fly ash replacement rates by mass of cement were produced for each fly ash source to investigate the fly ash performances in a concrete mixture design. In addition, a concrete mixture with 100% portland cement or 0% of fly ash replacement was prepared as the control specimens for performance. Table 3.2 shows mixture proportions for the mixtures with different fly ash replacement levels. A constant 0.45 water-to-cementitious material ratio (w/cm) was used for all the mixtures. To minimize the variables, no chemical admixtures were used in any mixtures.

Table 3.2 Mixture proportions for concrete specimens.

Mixture design	**W/C**	**Cement (kg/m^3)**	**Fly ash (kg/m^3)**	**Water (kg/m^3)**	**Coarse aggregate (kg/m^3)**	**Fine aggregate (kg/m^3)**
Control	0.45	283	0	127	863	564
20% fly ash	0.45	227	57	127	862	562
40% fly ash	0.45	170	113	127	858	557

3.2.3.2 Concrete mixing procedure and sample preparation

The moisture content for both coarse and fine aggregates was determined before the mixing process and the batch proportions for the aggregates and water were adjusted. Both aggregates were brought into the temperature-controlled mixing facility at least a day before conducting the moisture correction, and their batch weights were corrected for the moisture content. After adjusting the mixture proportion, all the mixtures were mixed according to the following steps. All aggregates were collected from the outside storage piles, and they were stored in a

temperature-controlled room (23°C) for at least 24 hours. The aggregates were then placed in the mixer and spun; after that, a representative sample was taken for moisture correction. It should be noted here that aggregates have to be properly sealed to prevent water loss before the mixing. At the time of mixing, all aggregates and approximately one half of the mixing water were loaded into the mixer; they were being mixed for three minutes. This allowed the aggregates to approach the saturated surface dry (SSD) condition and to ensure that the aggregates were evenly distributed. All the materials (the cement, fly ash, and the remaining water) were added into the mixer and were being mixed for three minutes. Then the mixture was rested for two minutes while the sides of the mixing drum were scraped. After that, the mixer was started to mix the concrete for three more minutes as well.

3.2.4 Testing of concrete samples

The unit weight, slump, and air content were measured for each mixture [41-43]. The results were reported in the previous publication [44]. Concrete samples were then formed in 100 mm by 200 mm cylindrical containers according to ASTM C31 [45]; they were being cured at 23°C and 100% RH for 24 h in the curing room after sealing the container. The samples were demolded and placed into the curing room until the samples were ready for the surface resistivity test.

A non-destructive surface resistivity test, the four-point Wenner probe, was performed to measure the electrical resistivity of the concrete according to AASHTO T358 [46] at 3, 7, 14, 28, 56, 90, and 180 days of hydration. Before the measurement, four lines were marked on the circular face of each concrete cylinder at 0, 90, 180, and 270 degrees for measurement. Three cylinders were measured so that twelve measurements were collected for each fly ash concrete at each chosen curing time. The average value of twelve measurements was used as the representative electrical resistivity for each fly ash at specific curing time. All the specimens were in the saturated surface dry (SSD) status while the resistivity test was conducted.

3.2.5 The Particle Model development

The SOM algorithm and the maximum spectral angle method were used for the model development process of the Particle Model. The SOM helped to determine nine distinct groups of fly ash particles with unique chemical makeup. The data of the 52,000 particles were extracted from twenty-six sources of fly ashes, and each particle had eleven pieces of chemical composition data (Na_2O, MgO, Al_2O_3, SiO_2, P_2O_5, SO_3, K_2O, CaO, TiO_2, Fe_2O_3, and SrO_2). The maximum spectral angle method helped to classify the fly ash particles into the determined nine groups. More details of the maximum spectral angle method can be found in the previous publication [18] and Appendix D.

A multiple linear regression (MLR) analysis was conducted by using the percentage of each of the nine groups found within fly ash to derive predictive models for the electrical resistivity at 3, 7, 14, 28, 56, 90, and 180 days of hydration. This model analysis was applied to both 20% and 40% fly ash replacement of the concrete. The initial linear model to predict the electrical resistivity was derived as the format of Eq.(3.1):

$$\text{Resistivity } (k\Omega\cdot cm) = a(\text{Group 1}) + b(\text{Group 2}) + c(\text{Group 3}) + d(\text{Group 4}) + e(\text{Group 5}) + f(\text{Group 6}) + g(\text{Group 7}) + h(\text{Group 8}) + i(\text{Group 9}) \quad \text{Eq.(3.1)}$$

Where, lowercase from “a” to “i” in the equation indicates the coefficient of each group determined from statistical analysis. The group # indicates the percentage of each group of fly ash.

The initial model was evaluated with the probability value (Pr(>|t|)) from the MLR to determine the statistical significance of the variables. The R-squared value of each model was investigated for 20% and 40% fly ash replacement concrete at all individual curing times to

evaluate the linear fit to the model. More details can be found in Appendix H. All the data and model processing was conducted within the R programming environment [47, 48].

3.2.6 Bootstrapping

The robustness of the derived predictive models was evaluated with the help of the bootstrap method. Ideally, the data can be collected by repeating a large number of mixtures for the same experiment to evaluate the validity of the generated predictive models, but this is impractical. Instead, bootstrapping was used to investigate the robustness of the Particle Model over the R-squared value. Bootstrapping is a resampling method where the data are sampled with replacement from the original sample to generate simulated results [47]. This allowed creating numerous R-squared values by running predictive models with simulated samples. Furthermore, the results from the bootstrapping were used to calculate a variety of sample statistics such as the mean (average) and standard deviation (SD) of the created R-squared values to compare the R-squared value of the original model.

The size of the bootstrapping sample was the same as the original dataset and is chosen at random from the existing data set. This means that some data points can be chosen multiple times in the simulated sample while others may not be selected at all. This procedure has been used in previous publications [49, 50]. The bootstrapping was conducted with 500 times for each model. Then, the mean of the R-squared values from the bootstrapping was investigated and compared with the R-squared value of the derived predictive model. This was applied to each curing time for both 20% and 40% replacement.

3.3 Result and Discussion

3.3.1 Investigation of bulk chemical composition

Table 3.3 shows the result of the bulk chemical composition involving the use of ASEM for twenty-six fly ashes. The fly ashes with "C#" and "IC#" represent Class C fly ash, while the fly ashes with "F#" and "IF#" represent Class F fly ash. The fly ash that has greater than 18% of CaO is classified as Class C and the fly ash that has 18% or less of CaO is attributed to Class F according to ASTM C618 [32].

Table 3.3 ASEM bulk chemical composition of each fly ash source.

Source	**SiO_2**	**Al_2O_3**	**Fe_2O_3**	**CaO**	**MgO**	**SO_3**	**Na_2O**	**K_2O**	**TiO_2**	**P_2O_5**	**SrO**
C1	36.2	21.7	5.4	23.2	5.4	0.7	3.6	1.0	0.8	1.9	0.2
C2	35.8	19.2	5.6	26.9	5.5	1.0	3.0	0.9	0.7	1.3	0.2
C3	25.3	19.3	5.2	32.5	7.8	2.6	3.4	0.6	1.1	1.9	0.3
C4	36.7	22.8	4.5	22.5	4.3	1.2	3.4	1.0	1.3	1.1	1.2
C5	31.3	22.5	5.4	26.1	6.0	0.6	4.3	0.8	0.8	2.1	0.2
C6	27.7	22.9	4.2	21.5	4.5	2.6	12.6	0.8	1.3	0.7	1.3
C7	35.3	20.6	4.7	24.7	4.9	0.7	4.3	1.2	1.6	0.8	1.0
C8	40.1	22.6	4.5	19.5	5.7	0.8	3.7	0.9	0.6	1.4	0.1
C9	31.5	24.0	6.0	25.7	5.4	1.0	3.7	0.6	0.9	1.1	0.1
C10	36.0	19.3	5.1	22.7	7.8	2.0	4.8	0.6	1.0	0.3	0.5
C11	31.0	20.8	6.4	27.2	7.1	1.6	3.5	0.7	0.8	0.8	0.2
IC1	31.8	22.9	5.7	28.2	5.5	1.1	2.3	1.0	0.8	0.5	0.3
IC2	25.2	21.2	6.2	30.5	7.8	1.0	4.0	0.6	1.2	2.2	0.2
IC3	29.7	21.0	5.9	30.3	5.4	1.9	2.2	0.6	1.0	1.6	0.5
IC4	29.9	17.7	4.7	31.8	9.3	1.2	2.6	0.8	0.8	1.1	0.2
F1	48.8	23.8	7.4	12.5	3.0	0.5	0.9	2.1	0.8	0.1	0.3
F2	50.4	20.9	3.9	17.1	3.7	0.5	1.0	1.4	0.7	0.1	0.3

F3	48.8	26.6	6.7	9.3	2.0	0.3	1.8	1.9	1.5	0.1	1.1
F4	45.3	27.4	4.0	14.6	3.6	0.7	1.5	0.7	1.1	0.4	0.8
F5	53.2	25.4	11.2	2.1	0.2	0.9	1.0	4.4	0.7	0.0	1.0
F6	51.9	25.7	12.3	2.5	0.3	0.7	1.6	4.1	0.7	0.1	0.2
F7	51.9	26.3	8.0	3.3	0.5	1.7	4.0	2.5	0.9	0.6	0.1
F8	56.9	23.9	3.4	6.2	2.1	0.1	4.1	1.7	0.3	1.2	0.1
F9	48.3	25.0	5.9	12.6	3.3	0.5	1.3	1.8	1.1	0.2	0.1
F10	53.6	27.8	2.8	10.5	2.5	0.5	0.3	1.3	0.5	0.3	0.0
IF1	58.3	21.9	6.9	3.7	1.4	0.6	2.2	4.3	0.2	0.4	0.2

3.3.2 Investigation of the PSD

Fig. 3.2 displays the cumulative PSDs of all twenty-six fly ashes that are investigated using ASEM. The diameter of most fly ash particles ranges from 0.5 to 20 μm. Table 3.4 shows the results of D50 or the average particle size and the SD of two thousand particles for each fly ash source in this study. The range of D50 for Class C fly ashes is from 3.1 μm to 1.5 μm, while the range of D50 for Class F is from 2.4 μm to 1.6 μm. Therefore, the overall range of particle size for Class C fly ashes was slightly wider than the Class F fly ashes in this study.

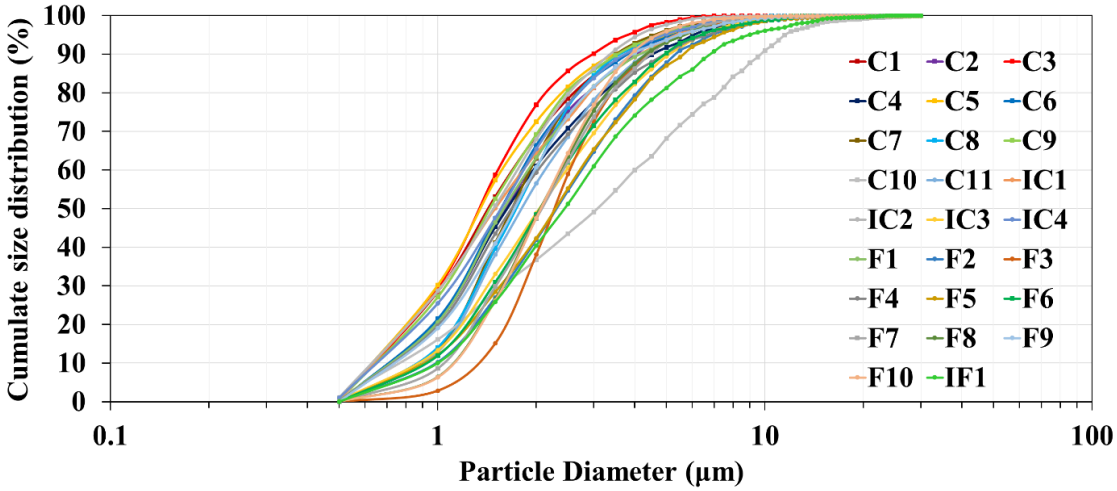

Fig. 3.2 Comprehensive cumulative particle size distribution for fifteen Class C fly ashes and eleven Class F fly ashes.

Table 3.4 D50 and SD for twenty-six fly ash sources.

Class C	D50 (µm)	SD (µm)	Class F	D50 (µm)	SD (µm)
C1	1.4	1.5	F1	1.6	1.7
C2	1.6	1.6	F2	2.3	2.3
C3	1.3	1.0	F3	2.3	1.6
C4	1.6	2.0	F4	1.7	2.1
C5	1.3	1.7	F5	2.3	2.4
C6	1.6	1.6	F6	2.1	2.0
C7	1.7	1.4	F7	2.1	1.7
C8	1.7	1.5	F8	2.0	1.7
C9	1.4	1.6	F9	1.7	1.7
C10	3.1	4.0	F10	2.1	1.6
C11	1.8	1.7	IF1	2.4	3.0
IC1	1.5	1.7			
IC2	1.5	1.2			
IC3	2.0	2.1			
IC4	1.6	1.6			

Fig. 3.3(a) and 3.3(b) describes the relationship between the D50 and the measured resistivity of nineteen sources of fly ash concrete at different curing times comprised of 20% and 40% fly ash replacement rates, respectively. R-squared values of the linear trend line for each relationship are presented below the legend of each hydration time in the figures. All the R-squared values except for 180 days are shown as < 0.5 for 20% fly ash replacement concrete which means the relationship between D50 and the measured electrical resistivity is quite poor. The R-squared values of the linear trend line appear to be < 0.3 for seven curing times in the case of the 40% fly

ash replacement concrete. Thus, the particle size information of the fly ash is not regarded as significant in this study. This means the analysis will focus on the different groups of fly ash particles.

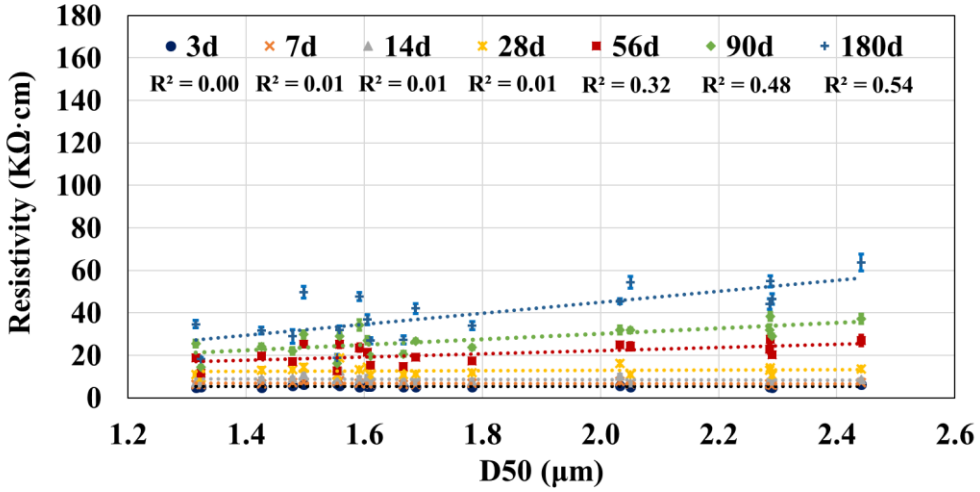

(a) 20% fly ash replacement

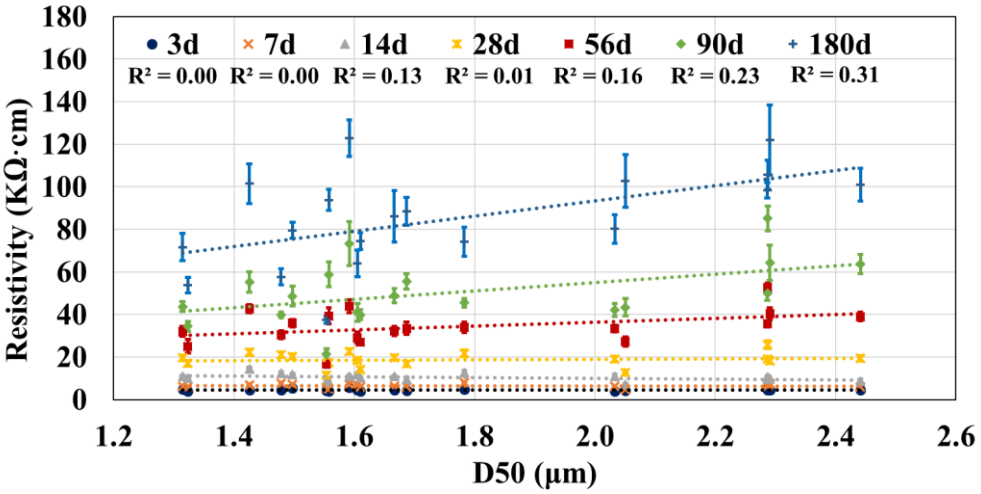

(b) 40% fly ash replacement

Fig. 3.3 Relationship between the D50 and the measured electrical resistivity from concrete with nineteen fly ash sources at different times: (a) 20% and (b) 40% fly ash replacement concrete.

3.3.3 Determination of distinct groups of fly ash particles

The nine determined groups with unique chemical compositions are summarized in Table 3.5, and the graphical comparison of the different groups is presented in Fig. 3.4. For example, Group 2 and 3 show the smallest content of SiO_2 (only 8% for each group), while Group 9 shows the highest content of SiO_2 (84.46%). The value of standard error is investigated for 200 different SOM results, and all the values are < 0.1. More details about the SOM process to find the nine groups and the result of a standard error can be found in Appendix F.

Table 3.5 The chemical composition in percent of the nine distinct groups by mass from the SOM analysis.

Group (%)	**SiO_2**	**Al_2O_3**	**Fe_2O_3**	**CaO**	**MgO**	**SO_3**	**Na_2O**	**K_2O**	**TiO_2**	**P_2O_5**	**SrO**
Group1	10.6	5.4	77.8	2.8	0.7	1.0	0.9	0.2	0.3	0.2	0.1
Group2	8.4	33.4	6.3	33.7	6.6	2.1	0.5	0.0	0.8	7.0	1.1
Group3	8.7	15.8	8.2	42.6	9.3	6.2	0.2	0.0	2.0	6.5	0.3
Group4	38.4	31.1	4.5	6.7	2.9	1.3	12.1	2.0	0.6	0.2	0.4
Group5	36.2	26.7	4.6	21.0	6.6	0.4	2.4	0.1	1.3	0.3	0.4
Group6	23.9	21.5	4.8	34.8	7.9	1.5	0.4	0.0	1.7	2.9	0.4
Group7	48.8	32.4	6.4	3.8	1.7	0.4	3.0	2.9	0.4	0.0	0.3
Group8	60.6	14.8	4.8	7.1	2.8	0.3	5.9	2.8	0.5	0.0	0.4
Group9	84.5	5.4	2.0	2.2	0.5	0.2	2.6	2.1	0.1	0.0	0.4

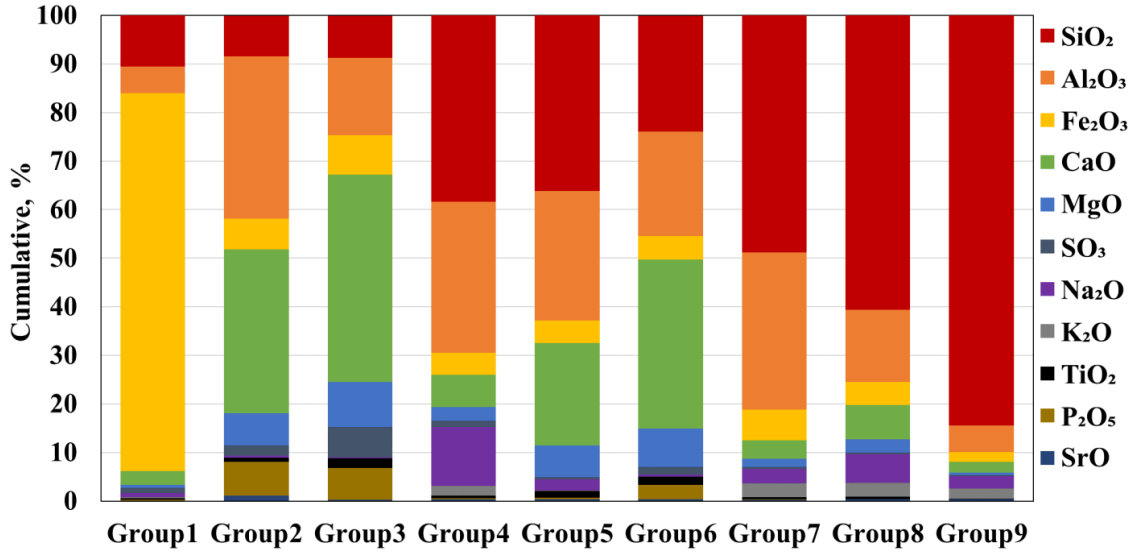

Fig. 3.4 The cumulative plot of the chemical composition of the nine distinct groups.

Table 3.6 shows the comprehensive result of the group composition for the twenty-six fly ash sources. The average of the sum is 95.4% and so, roughly 5% of fly ash particles cannot be considered as one of the nine groups, and are not used in further model analysis.

Table 3.6 Group composition in percent of the twenty-six fly ash sources.

Source	Group 1	Group 2	Group 3	Group 4	Group 5	Group 6	Group 7	Group 8	Group 9	Total
C1	0.5	8.8	16.2	13.1	21.0	21.8	4.6	5.4	5.4	96.6
C2	0.2	8.3	23.8	18.7	12.8	17.7	1.4	6.8	7.6	97.2
C3	0.3	8.6	32.2	10.3	11.8	21.3	0.3	4.9	2.9	92.5
C4	0.1	8.7	15.7	21.4	21.0	19.0	4.0	3.0	3.1	95.9
C5	0.3	7.7	27.9	21.8	12.9	17.0	0.9	3.2	4.1	95.7
C6	0.3	11.9	7.2	37.8	13.6	13.6	0.0	5.3	1.8	91.4
C7	0.2	10.1	22.9	17.3	12.0	18.6	2.4	6.4	7.5	97.1
C8	0.2	9.4	6.9	18.4	25.7	19.0	4.2	7.3	5.1	95.9
C9	0.2	11.7	10.0	20.2	25.9	21.1	0.7	3.5	3.1	96.2
C10	0.2	14.4	14.4	10.8	15.9	26.7	0.9	5.8	5.6	94.5

C11	0.2	12.6	19.9	13.8	15.5	22.8	1.3	5.0	5.1	96.0
IC1	0.3	5.8	15.3	11.7	20.7	20.5	11.0	6.7	5.2	97.0
IC2	0.0	10.8	22.4	14.0	15.4	25.4	0.1	5.2	3.3	96.4
IC3	0.3	6.7	26.0	16.7	14.5	19.5	4.7	4.2	4.1	96.5
IC4	0.1	7.6	30.3	6.0	11.4	30.1	0.8	3.6	2.7	92.4
F1	1.1	1.0	7.2	0.5	22.6	11.8	39.9	8.7	6.1	98.7
F2	0.4	0.6	6.6	0.4	22.3	13.8	36.7	11.3	6.2	98.2
F3	5.8	0.6	2.6	0.4	15.4	4.1	51.2	11.9	1.9	93.6
F4	0.3	5.1	12.0	1.7	18.5	13.2	37.5	4.3	3.9	96.2
F5	1.8	0.2	0.3	0.1	1.1	0.3	75.2	7.5	8.6	94.9
F6	2.6	0.4	0.6	0.1	1.3	0.7	71.8	8.6	8.7	94.7
F7	1.8	0.1	0.2	36.0	1.0	0.6	43.2	4.7	6.5	94.0
F8	0.8	1.0	0.3	6.5	8.5	1.6	48.8	13.5	12.4	93.3
F9	0.5	2.6	6.5	0.9	20.4	13.0	37.6	7.5	7.9	96.7
F10	0.3	0.6	1.5	0.4	14.7	4.5	56.9	10.3	7.7	96.6
IF1	1.8	0.4	0.8	0.9	2.5	1.7	52.0	20.9	11.2	91.9

3.3.4 The accuracy for predicting electrical resistivity

Fig. 3.5(a) and 3.5(b) compares the accuracy of predicting the electrical resistivity using the Class C and F classification method with 20% and 40% replacement rates. The measured values are indicated as the points with the same color as the matching dashed line which is the average values for Class C and F fly ashes at seven different curing times, respectively. Overall, the 40% fly ash replacement concrete shows higher electrical resistivity than the concrete with a 20% fly ash replacement. Furthermore, despite having a similar bulk chemical classification as per ASTM C618, the variability of electrical resistivity is quite high to predict the performance using this classification method. Even though the ASTM C618 classification method is widely used to compare the performance of different fly ashes, these comparison results present the drawbacks

of using ASTM C618 classification methods to predict the resistivity of the concrete containing the fly ash.

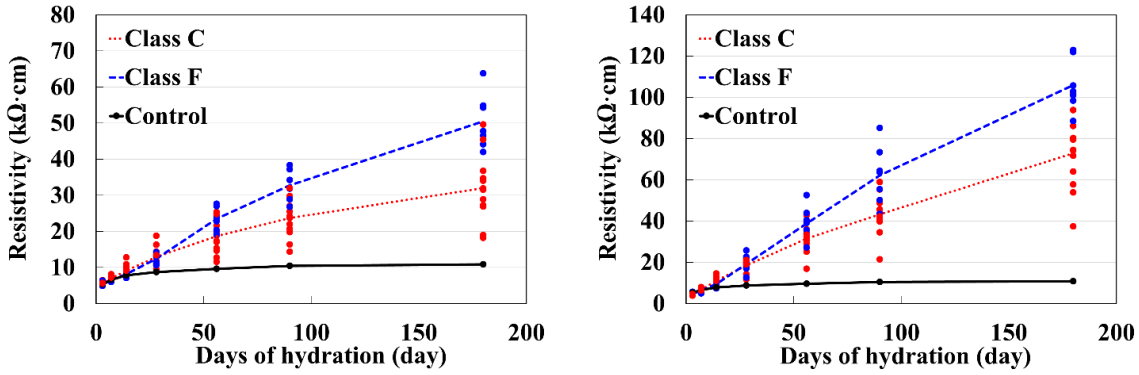

(a) 20% fly ash replacement (b) 40% fly ash replacement

Fig. 3.5 Comparison between the measured and average values of resistivity with the type of fly ash used: (a) 20% fly ash replacement concrete and (b) 40% fly ash replacement concrete.

The comparisons between the calculated value with the predictive models by using the Particle Model and measured value are shown in Fig. 3.6(a) for 20% and (b) for 40% fly ash replacement. The slope of the trend line in the comparisons for both 20% and 40% fly ash replacement is at the level of 0.96 and 0.99, respectively. It should be noted that the perfect fit can be described with a value of 1.00 (one) for the slope. This suggests the results are a very good fit. In addition, the accuracy of the calculated value using the Particle Model is evaluated with the +/- 10% dashed red lines. 107 out of 133 predictions are within +/- 10% while the 14 more predictions are added with the limit of +/- 15%, and the remaining 12 predictions are out of +/- 15% for 20% fly ash replacement as shown in Fig. 3.6(a). In the case of 40% fly ash replacement in Fig. 3.6(b), 98 out of 133 or 75% of the measurements show a difference within a range of +/- 10%, the 10 more predictions are added with the limit of +/- 15%, and the remaining 25 predictions are out of +/- 15%. While there is some variability, overall the resistivity is accurately predicted with the help of the Particle Model. The details about the predictive models for 20% and 40% fly ash replacement at different hydration time is found in Appendix I.

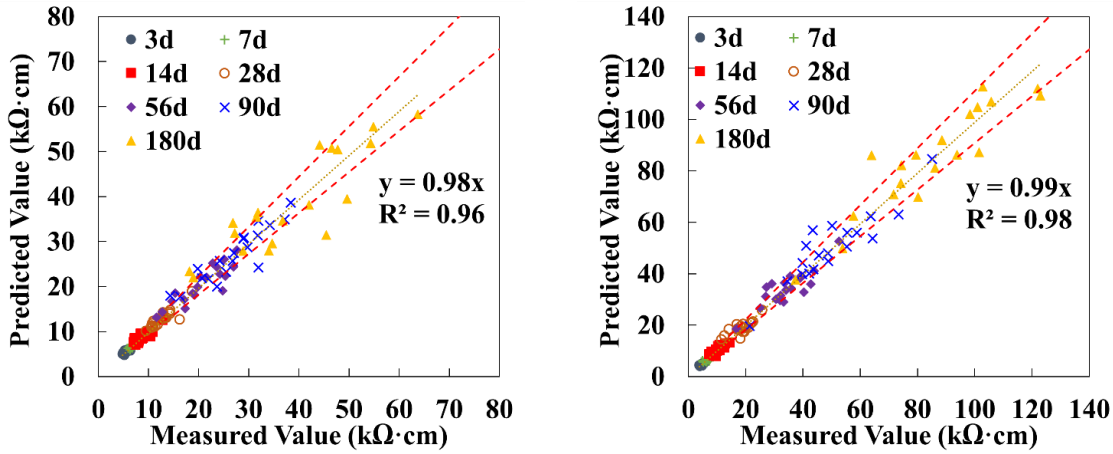

(a) 20% fly ash replacement (b) 40% fly ash replacement

Fig. 3.6 Comprehensive relationship between the calculated and experimental resistivity for (a) 20% fly ash replacement and (b) 40% fly ash replacement.

Table 3.7 shows the comparison results of the R-squared value of predictive models derived by the Particle Model for both 20% and 40% fly ash replacement. Low R-squared value means a weak linear fit for the model while high R-squared value indicates the model explains all the variability of the response data around its mean value. All the R-squared values show greater than 0.98 for both 20% and 40% fly ash replacement concrete. This shows that the Particle Model better reflects the variance of the fly ash properties for resistivity compared to the Class C and F classification.

Table 3.7 Comparison results of the R-squared value revealed with the Particle Model method for different mixtures at different curing times.

Curing (day)	20% fly ash concrete	40% fly ash concrete
3	0.99	0.99
7	0.99	0.99
14	0.99	0.99
28	0.99	0.98
56	0.99	0.98
90	0.99	0.98
180	0.98	0.98

The results of the bootstrapping at each measurement time for both 20% and 40% fly ash concrete are summarized in Table 3.8. The mean of 500 R-squared values through the bootstrap method is compared with the R-squared value of the derived predictive model in Table 3.7. It should be noted here again that this helps to determine the robustness of the Particle Model. The results present that the mean R-squared value from the bootstrapping shows the same or almost the same R-squared value of the derived predictive model. The maximum, minimum and SD are also investigated over the R-squared values from the bootstrapping. The range of difference between the maximum and minimum R-squared value is from 0.003 to 0.016 which is quite narrow. Furthermore, all the investigated SDs are under 0.003 which indicates the variance of the bootstrap results is quite small. Thus, the Particle Model can be considered as a robust tool to predict the electrical resistivity of fly ash concrete for the materials investigated.

Table 3.8 The results of the bootstrapping for the Particle Model over the R-squared value.

Mixture	Days of hydration	The mean of the R-squared values	Max	Min	SD
20% Fly ash	3 days	0.994	0.996	0.992	0.0006
	7 days	0.994	0.996	0.992	0.0006
	14 days	0.991	0.994	0.988	0.0009
	28 days	0.990	0.995	0.986	0.0014
	56 days	0.986	0.991	0.982	0.0014
	90 days	0.988	0.991	0.984	0.0014
	180 days	0.978	0.984	0.972	0.0021
40% Fly ash	3 days	0.990	0.992	0.986	0.0009
	7 days	0.988	0.991	0.984	0.0011
	14 days	0.989	0.992	0.986	0.0009
	28 days	0.985	0.989	0.979	0.0014
	56 days	0.984	0.987	0.978	0.0016
	90 days	0.980	0.986	0.970	0.0024
	180 days	0.983	0.988	0.978	0.0018

3.3.5 Effects of each group on electrical resistivity

The impacts of each group on the electrical resistivity are investigated by comparing the coefficients from predictive models at different hydration times, and the comparison results for 20% and 40% fly ash replacement concrete are shown in Fig. 3.7 and Fig. 3.8, respectively. The coefficients show how different groups impact the electrical resistivity of the concrete at a specific time period, and moreover, further discussion over the impact of each group will be provided. A value > 0 indicates that the group helps to increase the electrical resistivity while the group with the value of < 0 decreased the electrical resistivity at that time period. Ages without a value for a coefficient mean that those groups do not contribute to the electrical resistivity at that

time period. For example, Group 1 shows a coefficient of zero between 3 and 28 days for 20% fly ash replacement, this group is found to not be statistically significant at this curing time. The impacts of Group 4, 5, 7, and 8 show a similar trend of change over time. These groups increase the electrical resistivity between 3 and 180 days of hydration. Group 1 and 9 show almost no meaningful impacts at early age while the significant contribution occurs at later ages. Group 2 shows less than zero coefficients at 20% replacement while it presents > 0 at 40% replacement for all the measured hydration times. Group 3 seems to have a similar trend of coefficient change over time for both replacement to Group 2, but the contribution is negligible as the coefficients are quite small. On the contrary, Group 6 shows relatively small effects to increase the resistivity at 20% replacement while it decreases the resistivity at 40% replacement between 3 and 180 days of hydration.

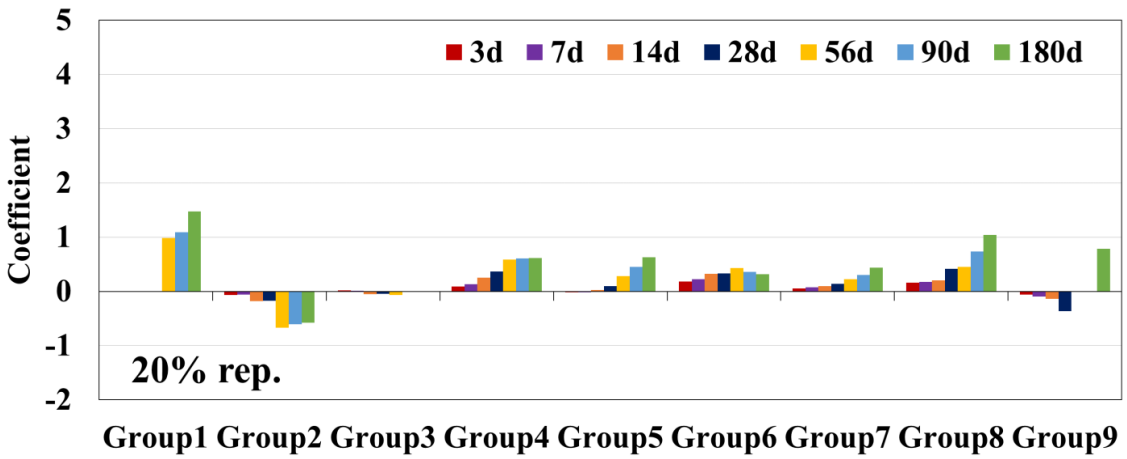

Fig. 3.7 Coefficient comparison for 20% fly ash replacement at different times for each group.

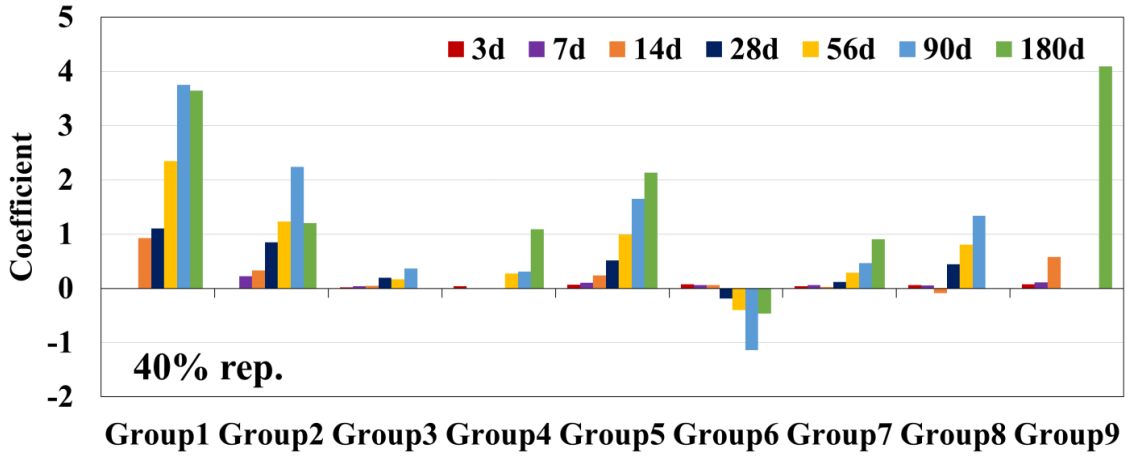

Fig. 3.8 Coefficient comparison for 40% fly ash replacement at different times for each group.

3.3.5.1 Discussion for Group 4, 5, 7 and 8 on the electrical resistivity

Although Group 5 shows quite small negative coefficient (almost zero) at 3 and 7 days at 20% replacement, overall Group 4, 5, 7, and 8 increase the electrical resistivity at rest of all measurement times at both 20% and 40% replacement and the magnitude of their contribution also increases. It is possible that several glassy phases can exist in these groups such as calcium-rich aluminosilicates (especially for Group 5), aluminosilicate and calcium silicates based on the chemical information in Table 3.5. Those glassy phases have been found in fly ash in several previous studies [13, 51-54], and it is well known that the calcium-rich glassy phases are much more reactive than those with low or moderate calcium content phases [52, 54]. Furthermore, these four groups show quite high contents of SiO_2. This means Group 4, 5, 7, and 8 might have a good source to form C-S-H with the portland cement particles. The electrical resistivity is improved by increasing C-S-H phases and decreasing capillary porosity and connectivity of capillary pores [55]. Thus, hydration products with the particles of these groups can increase the resistivity of fly ash concrete.

3.3.5.2 Discussion for Group 1 and 9 on the electrical resistivity

Group 1 shows the largest coefficient at later ages for both 20% and 40% fly ash replacement rates while there were no impacts on early ages (3d, 7d, 14d, and 28d for 20%, and 3d and 7d for 40%). Group 1 has 77.8% of iron oxide (Fe_2O_3), which Fe-rich phases such as magnetite (Fe_2O_3) and hematite (Fe_2O_3) have been found in fly ash and have been known to be largely inert [13, 56]. In addition, a ferrite phase could exist in this group. It is reported that the ferrite particles fill the pores between cement particles resulting in finer pore structure, and more C-S-H gel can be formed because of the reaction between the ferrite particles and the $Ca(OH)_2$ in the hydrating of cement [57, 58]. This could improve the electrical resistivity after 28 days of hydration and be a possible reason why Group 1 does not have any impact at early age for both fly ash replacement.

The impact of Group 9 is almost zero until the 90d of hydration, and then a significant impact is observed for 180 days of hydration for both the 20% and 40% fly ash replacement. This indicates Group 9 affects more on the electrical resistivity at later ages. Group 9 contained 84.5% SiO_2, and this could be a good source of either quartz or a more reactive silicate. Quartz has been observed in almost all fly ashes [13], and a silicon-rich phase containing almost no impurities was found in some previous studies [59, 60]. Furthermore, it should be noted that the reactivity of the quartz and silicate phase is very low and slow [52, 61]. Ehsan et al. [62] have reported the electrical resistivity changes with adding SiO_2 powder (1%, 3%, and 5% of the cementitious materials) with 25% fly ash replacement concrete. The study found that the resistivity increased by increasing the SiO_2 powder at 90 days of hydration while additional Al_2O_3 powder decreases the electrical resistivity [62]. Another study has reported the SiO_2 powder is helpful to improve the water permeability resistance of concrete [63] which means that this could be a possible reason for the impact of Group 9 on resistivity at later ages.

3.3.5.3 Discussion for Group 2, 3, and 6 on the electrical resistivity

Groups 2 and 3 show less than zero or zero coefficients on the resistivity at 20% replacement while the results appear > 0 at 40% replacement between 3 and 180 days of hydration. The coefficients for Group 3 are quite small for both replacements at all the hydration times investigated. On the contrary, Group 6 shows relatively small effects to increase the resistivity at 20% replacement while it decreases the resistivity at 40% replacement between 3 and 180 days of hydration.

Group 2 shows the lowest SiO_2 contents among the nine groups while the contents of CaO, MgO, and SO_3 are relatively higher than the other groups. In addition, the content of Al_2O_3 for Group 2 is the highest among the nine groups. Group 6 also shows relatively higher content of CaO than the other groups and similar content of SiO_2 and Al_2O_3. Various crystalline and glassy phases could exist in those group particles. Several glassy phases such as calcium-rich aluminosilicates, aluminosilicate and calcium silicates can exist in these two groups. Merwinite ($Ca_3Mg(SiO_4)_2$), a common phase in high-calcium fly ash and at the early stages of the devitrification of Mg-containing glasses, could also be considered a phase of Group 6. This material is non-reactive in concrete at normal temperatures [13]. Furthermore, these three groups could be a good source for producing the melilite group which includes Gehlenite $Ca_2Al(AlSiO_7)$ and Akermanite $Ca_2Mg(Si_2O_7)$ phases; these phases are not chemically active in concrete [13]. Thus, investigating the reason for the different trends of Group 2 and Group 6 at different replacement rates is an area of future work.

As discussed, there is almost no contribution from Group 3 on resistivity for both replacements at all the measurement times. This means that the particles in Group 3 can be mainly composed of non-reactive phases although it has some oxides that can possibly be a source of some of the reactive phases.

3.3.6 Practical implications and future applications

The use of fly ash in concrete is typically limited because of the unpredictability of the material. This work has given useful predictive equations that can be used at both 20% and 40% replacement volume of fly ash within the concrete and emphasize that the Particle Method showed a clear path forward for future research efforts that could ultimately make significant changes to predict the electrical resistivity of fly ash concrete. While previous studies have been used the Particle Model to predict the compressive strength with the impact of fly ash particles, this work shows the application of the Particle Model can be extended on accurately predicting the electrical resistivity of the fly ash concrete within 180 days of hydration. This indicates that the Particle Model can not only allow greater usage of fly ash to allow the usage of fly ash that does not meet current specifications by ASTM C618 but also be implemented on predicting other performance of fly concrete.

3.4 Conclusion

The Particle Model is used to create predictive models for the electrical resistivity for 19 different fly ash sources at 20% and 40% replacement of cement in concrete after 3, 7, 14, 28, 56, 90, and 180 days of hydration. With this massive data set, the predicted electrical resistivity values are compared with the measured values and the coefficients from the predictive models were used to interpret the measured chemical consistency of the individual groups. The following contributions are made:

1. The Class C and F classification method does not accurately predict resistivity performance in concrete.
2. The electrical resistivity and the median particle size are not related as all R-squared values of the investigated trend lines are < 0.5 at 20% replacement and < 0.3 for 40% replacement.

3. The electrical resistivity is accurately predicted by the Particle Model within +/- 10% for 80% of all measurements at 20% fly ash replacement and +/- 10% for 75% of all measurements at 40% replacement.
4. The R-squared value is > 0.98 for both 20% and 40% fly ash replacement levels for the Particle Model.
5. Overall, Group 4, 5, 7, and 8 increase the resistivity between 3 and 180 days of hydration at both 20% and 40% replacement. The impact of these groups further increases with additional hydration.
6. Group 1 has the largest coefficient at the later ages for both 20% and 40% replacement while there is no impact at an early age. The impact of Group 9 is ≈ 0 until 90 days of hydration while it has a big impact at 180 days of hydration for both 20% and 40% replacement.
7. Group 2 decreases the resistivity at 20% replacement and increases the resistivity at 40% replacement between 3 and 180 days of hydration. Although the actual value of coefficients for Group 3 is quite small for all the measured hydration times for 20% and 40% fly ash replacement levels, it shows a similar trend of coefficient change to Group 2. On the other hand, Group 6 increases the resistivity at 20% replacement while it decreases the resistivity at the 40% replacement.

Despite there still existing many unknowns, several new insights are found by applying the Particle Model to these fly ashes. This paper offers a novel way to facilitate investigations of fly ash properties in concrete and lead to a better classification of fly ash at both early and later ages at different replacement levels.

Acknowledgment

This work was sponsored by funding from the Illinois Department of Transportation [Project ICT R27-180], and the FHWA [EAR project # BAA No. 693JJ3-18-BAA-0001]. The authors would like to thank Dr. Daniel Cook and Mr. Jeff Davis for their assistance and discussion on this work.

Reference

[1] K. Hornbostel, C.K. Larsen, M.R. Geiker, Relationship between concrete resistivity and corrosion rate–a literature review, Cement and Concrete Composites 39 (2013) 60-72.

[2] O. Sengul, O.E. Gjørv, Electrical resistivity measurements for quality control during concrete construction, ACI Materials Journal 105(6) (2008) 541.

[3] W. Morris, A. Vico, M. Vázquez, Chloride induced corrosion of reinforcing steel evaluated by concrete resistivity measurements, Electrochimica Acta 49(25) (2004) 4447-4453.

[4] B.B. Hope, A.K. Ip, D.G. Manning, Corrosion and electrical impedance in concrete, Cement Concrete Res 15(3) (1985) 525-534.

[5] C. Alonso, C. Andrade, J.A. González, Relation between resistivity and corrosion rate of reinforcements in carbonated mortar made with several cement types, Cement Concrete Res 18(5) (1988) 687-698.

[6] W. López, J.A. González, Influence of the degree of pore saturation on the resistivity of concrete and the corrosion rate of steel reinforcement, Cement Concrete Res 23(2) (1993) 368-376.

[7] O. Gjorv, Durability design and construction quality of concrete structures, PRO 32: International Conference on Advances in Concrete and Structures-ICACS 2003 (Volume 1), RILEM Publications, 2003, p. 309.

[8] C. Andrade, The limit of service life of concrete structures, Encontro Nacional Betão Estrutural (2004) 1-25.

[9] B. Silva, S. Jalali, R. Ferreira, Estimating electrical resistivity based on early age measurements, Proceedings of the international RILEM workshop performance based evaluation and indicators for concrete durability, Madrid, 2006.

[10] P.C. Silva, R.M. Ferreira, H. Figueiras, Electrical resistivity as a means of quality control of concrete–influence of test procedure, XII International Conference on Durability of Building Materials and Components, FEUP Edições, Porto: Distrito de Porto (PT), 2011.

[11] M.A. Bérubé, J. Duchesne, D. Chouinard, Why the Accelerated Mortar Bar Method ASTM C 1260 is Reliable for Evaluating the Effectiveness of Supplementary Cementing Materials in Suppressing Expansion Due to Alkali-Silica Reactivity, Cement, Concrete and Aggregates 17(1) (1995) 26-34.

[12] B. Mather, Use of Concrete of Low Portland Cement Content in Combination with Pozzolans and Other Admixtures in Construction of Concrete Dams, J Am Concr Inst 71(12) (1974) 589-599.

[13] A. Committee, 232.2R-18: Report for the Use of Fly Ash in Concrete, Technical Documents (2018).

[14] S. Shashiprakash, M. Thomas, Sulfate resistance of mortars containing high-calcium fly ashes and combinations of highly reactive pozzolans and fly ash, Special Publication 199 (2001) 221-238.

[15] R.B. Holland, K.E. Kurtis, L.F. Kahn, 7 - Effect of different concrete materials on the corrosion of the embedded reinforcing steel, in: A. Poursaee (Ed.), Corrosion of Steel in Concrete Structures, Woodhead Publishing, Oxford, 2016, pp. 131-147.

[16] S.K. Das, Yudhbir, A simplified model for prediction of pozzolanic characteristics of fly ash, based on chemical composition, Cement Concrete Res 36(10) (2006) 1827-1832.

[17] S. Diamond, On the Glass Present in Low-Calcium and in High-Calcium Flyashes, Cement Concrete Res 13(4) (1983) 459-464.

[18] L.X. Du, E. Lukefahr, A. Naranjo, Texas Department of Transportation Fly Ash Database and the Development of Chemical Composition-Based Fly Ash Alkali-Silica Reaction Durability Index, J Mater Civil Eng 25(1) (2013) 70-77.

[19] S.C. White, E.D. Case, Characterization of fly ash from coal-fired power plants, Journal of Materials Science 25(12) (1990) 5215-5219.

[20] S. Schlorholtz, K. Bergeson, T. Demirel, Monitoring of Fluctuations in the Physical and Chemical Properties of a High-Calcium Fly Ash, MRS Proceedings 113 (1987) 107.

[21] Q. Hu, M.T. Ley, J. Davis, J.C. Hanan, R. Frazier, Y. Zhang, 3D chemical segmentation of fly ash particles with X-ray computed tomography and electron probe microanalysis, Fuel 116 (2014) 229-236.

[22] Q. Hu, M. Aboustait, M.T. Ley, J.C. Hanan, V. Rose, R. Winarski, Combined three-dimensional structure and chemistry imaging with nanoscale resolution, Acta Mater 77 (2014) 173-182.

[23] T. Kim, J.M. Davis, M.T. Ley, S. Kang, P. Amrollahi, Fly ash particle characterization for predicting concrete compressive strength, Constr Build Mater 165 (2018) 560-571.

[24] T. Kim, M. Moradian, M.T. Ley, Dissolution and leaching of fly ash in nitric acid using automated scanning electron microscopy, Advances in Civil Engineering Materials 7(1) (2018) 291-307.

[25] M. Aboustait, T. Kim, M.T. Ley, J.M. Davis, Physical and chemical characteristics of fly ash using automated scanning electron microscopy, Constr Build Mater 106 (2016) 1-10.

[26] S. Ghosal, J.L. Ebert, S.A. Self, Chemical composition and size distributions for fly ashes, Fuel processing technology 44(1-3) (1995) 81-94.

[27] Y. Chen, N. Shah, F.E. Huggins, G.P. Huffman, W.P. Linak, C.A. Miller, Investigation of primary fine particulate matter from coal combustion by computer-controlled scanning electron microscopy, Fuel Processing Technology 85(6-7) (2004) 743-761.

[28] T. Kim, M.T. Ley, S. Kang, J.M. Davis, S. Kim, P. Amrollahi, Using particle composition of fly ash to predict concrete strength and electrical resistivity, Cement and Concrete Composites 107 (2020) 103493.

[29] S. Kang, Z. Lloyd, T. Kim, M.T. Ley, Predicting the Compressive Strength of Fly Ash Concrete with the Particle Model, Manuscript submitted for publication.

[30] ASTM C150, Standard Specification for Portland Cement, American Society for Testing and Materials, West Conshohocken, PA, 2019.

[31] ASTM C33, Standard Specification for Concrete Aggregates, American Society for Testing and Materials, West Conshohocken, PA, 2018.

[32] ASTM C618, Standard Specification for Coal Fly Ash and Raw or Calcined Natural Pozzolan for Use in Concrete, American Society for Testing and Materials, West Conshohocken, PA, 2019.

[33] R.P. Gupta, T.F. Wall, I. Kajigaya, S. Miyamae, Y. Tsumita, Computer-controlled scanning electron microscopy of minerals in coal - Implications for ash deposition, Prog Energ Combust 24(6) (1998) 523-543.

[34] C.A. O'Keefe, T.M. Watne, J.P. Hurley, Development of advanced scanning electron microscopy techniques for characterization of submicron ash, Powder Technol 108(2-3) (2000) 95-102.

[35] J.T. Armstrong, Quantitative Elemental Analysis of Individual Microparticles with Electron Beam Instruments, in: K.F.J. Heinrich, D.E. Newbury (Eds.), Electron Probe Quantitation, Springer US, Boston, MA, 1991, pp. 261-315.

[36] G. Love, V.D. Scott, Evaluation of a New Correction Procedure for Quantitative Electron-Probe Microanalysis, J Phys D Appl Phys 11(10) (1978) 1369-1376.

[37] J.T. Armstrong, P.R. Buseck, Quantitative Chemical-Analysis of Individual Microparticles Using Electron-Microprobe - Theoretical, Anal Chem 47(13) (1975) 2178-2192.

[38] J.T. Armstrong, P.R. Buseck, A General Characteristic Fluorescence Correction for the Quantitative Electron Microbeam Analysis of Thick Specimens, Thin-Films and Particles, X-Ray Spectrom 14(4) (1985) 172-182.

[39] C.P. Aichele, D. Venkataramani, J.E. Smay, M.H. McCann, S. Richter, M. Khanzadeh-Moradllo, M. Aboustait, M.T. Ley, A comparison of automated scanning electron microscopy (ASEM) and acoustic attenuation spectroscopy (AAS) instruments for particle sizing, Colloids and Surfaces A: Physicochemical and Engineering Aspects 479 (2015) 46-51.

[40] M. Aboustait, Q. Hu, R. Frazier, Y. Zhang, B. Tabb, M. Ley, J. Hahan, Innovative prediction of fly ash performance in concrete, Oklahoma Transportation Center, Midwest City, OK, 2013.

[41] ASTM C231, Standard Test Method for Air Content of Freshly Mixed Concrete by the Pressure Method, American Society for Testing and Materials, West Conshohocken, PA, 2017.

[42] ASTM C138, Standard Test Method for Density (Unit Weight), Yield, and Air Content (Gravimetric) of Concrete, American Society for Testing and Materials, West Conshohocken, PA, 2017.

[43] ASTM C143, Standard Test Method for Slump of Hydraulic-Cement Concrete, American Society for Testing and Materials, West Conshohocken, PA, 2015.

[44] Z. Lloyd, Investigation of the Quality Control of Waste Products for Concrete, Civil Engineering, Oklahoma State University, Stillwater, OK, 2019.

[45] ASTM C31, Standard Practice for Making and Curing Concrete Test Specimens in the Field, American Society for Testing and Materials, West Conshohocken, PA, 2019.

[46] AASHTO T 358:2015Method Of Test For Surface Resistivity Indication Of Concrete'S Ability To Resist Chloride Ion Penetration, 2015.

[47] M.J. Crawley, The R Book, Second ed., John Wiley & Sons Ltd, Imperial College London at Silwood Park, UK, 2012.

[48] R.C. Team, R: A Language and Environment for Statistical Computing, Vienna, Austria,

2016.

[49] M. Kuhn, K. Johnson, Applied predictive modeling, Springer2013.

[50] B. Efron, R.J. Tibshirani, An introduction to the bootstrap, CRC press1994.

[51] D.M. Roy, K. Luke, S. Diamond, Characterization of fly ash and its reactions in concrete, MRS Online Proceedings Library Archive 43 (1984).

[52] P.T. Durdzinski, C.F. Dunant, M. Ben Haha, K.L. Scrivener, A new quantification method based on SEM-EDS to assess fly ash composition and study the reaction of its individual components in hydrating cement paste, Cement Concrete Res 73 (2015) 111-122.

[53] K.L. Aughenbaugh, Fly ash-based geopolymers: identifying reactive glassy phases in potential raw materials, Civil, Architectural, and Environmental Engineering, The University of Texas at Austin, The University of Texas at Austin, 2013, p. 292.

[54] K.L. Aughenbaugh, R.T. Chancey, P. Stutzman, M.C. Juenger, D.W. Fowler, An examination of the reactivity of fly ash in cementitious pore solutions, Materials and Structures 46(5) (2013) 869-880.

[55] Z. Liu, Y. Zhang, Q. Jiang, Continuous tracking of the relationship between resistivity and pore structure of cement pastes, Constr Build Mater 53 (2014) 26-31.

[56] G. McCarthy, J. Solem, O. Manz, D. Hassett, Use of a database of chemical, mineralogical and physical properties of North American fly ash to study the nature of fly ash and its utilization as a mineral admixture in concrete, Materials Research Society Symposium Proceedings 178 (1990) 3-34.

[57] M.A. Ahmed, Y.A. Hassanean, K.A. Assaf, M.A. Shawkey, The Effect of Incorporation of Ferrite Nano-particles on Compressive Strength and Resistivity of Self-Compacting Concrete, Open Journal of Civil Engineering 5(01) (2015) 131.

[58] M.A. Largeau, Effect of iron powder patially used as portland cement replacement on the structural properties of concrete, JKUAT-PAUSTI, 2018.

[59] V.M. Malhotra, P.K. Mehta, High-performance, high-volume fly ash concrete : materials, mixture proportioning, properties, construction practice, and case histories, Supplementary Cementing Materials for Sustainable Development, Inc., Ottawa, Canada, 2002.

[60] K. Kiattikomol, C. Jaturapitakkul, S. Songpiriyakij, S. Chutubtim, A study of ground coarse fly ashes with different finenesses from various sources as pozzolanic materials, Cement Concrete Comp 23(4-5) (2001) 335-343.

[61] P.T. Durdzinski, R. Snellings, C.F. Dunant, M. Ben Haha, K.L. Scrivener, Fly ash as an assemblage of model Ca-Mg-Na-aluminosilicate glasses, Cement Concrete Res 78 (2015) 263-272.

[62] E. Mohseni, B.M. Miyandehi, J. Yang, M.A. Yazdi, Single and combined effects of nano-SiO2, nano-Al2O3 and nano-TiO2 on the mechanical, rheological and durability properties of self-compacting mortar containing fly ash, Constr Build Mater 84 (2015) 331-340.

[63] M.R. Sharbaf, S.M. Hejazi, An investigative study on the effects of nano-SiO 2 on compressive strength and permeability of concrete, 5th International Conference on Advanced Computer Theory and Engineering, Cape Town, South Africa, 2012.

CHAPTER IV

PREDICTING ION DIFFUSION IN FLY ASH CEMENT PASTE THROUGH PARTICLE ANALYSIS

Abstract

Mass transport in concrete is an important factor to control the durability of concrete structures. Fly ash is commonly used as an additive to help reduce the mass transport of concrete. Since fly ash is a waste product, it is challenging to predict the performance of fly ash in concrete. This work uses a technique called the Particle Model to predict the reactivity and modification of the diffusion coefficient of the paste with fly ash at a 20% replacement level. The results show 81% of all measurements for the diffusion coefficient can be predicted within the reported variation of the test method (+/- 30%). This work provides a deeper understanding of the impacts of fly ash on the properties of concrete to more accurately predict the performance of the diffusion coefficient at different hydration times.

Keywords: Diffusion coefficient; Surface concentration; Fly ash; Cement paste; ASEM; The Particle Model;

4.1 Introduction

The apparent diffusion coefficient (D_c) is an important factor to control the durability of concrete structures because outside chemicals such as natural chlorides, deicer salts, and sulfate ions will penetrate into concrete and deteriorate the rebar or the concrete matrix itself [1, 2]. Because of the importance of this parameter, performance-based durability specifications commonly use D_c [3, 4]. Fly ash is used as a partial replacement of the portland cement to improve the overall economy, sustainability, and often the durability of the concrete [5-8]. It is known that many fly ashes are helpful to produce concrete with a low D_c in concrete [9-11]. This is achieved through both pozzolanic and secondary cementitious reactions [12, 13].

Fly ash is generally used at 15-35% replacement of cement by mass because this range has been found to be an acceptable level of replacement without major negative effects on the performance [14]. Previous studies have investigated the impacts of fly ash in concrete and tried to predict the performance of fly ash by using bulk chemical characterization methods such as X-ray fluorescence (XRF) [15-18]. However, it is reported that fly ash sources with similar bulk chemistry can have dramatically different performance [19]. In other words, bulk chemical characteristics are not always useful to predict the properties of concrete.

While bulk chemistry does not provide predictable insights into the performance of the fly ash in concrete, studies with scanning electron microscopy (SEM) and automated scanning electron microscopy (ASEM) show that there are repeating patterns in chemical composition found within fly ash particles [20, 21]. To gain more insights, this study applies a method called the Particle Model that is developed in a previous study to produce predictive models for the performance of cement-based materials such as compressive strength and electrical resistivity [22]. This is based on using an ASEM to classify thousands of individual fly ash particles [22-27] and then machine learning with the Self-Organizing Map (SOM) algorithm was applied to classify the fly ash

particles into nine distinct groups based on these few major repeatable patterns of chemical compositions [22]. The predictive models through these groups are then able to predict 90% of the predicted compressive strength and 80% of the predicted electrical resistivity values within +/- 10% of the measured values at different hydration times [28, 29].

To investigate ion diffusion of the fly ash-cement paste, a novel approach using transmission X-ray microscopy (TXM) is applied in this work. This technique is useful as it is non-destructive and rapid to investigate the D_c and surface concentration (C_s). This approach has been used in previous studies to image the movement of the ions in cement-based materials using the potassium iodide (KI) solution as a tracer or contrast agent [30, 31]. Iodide (I) is a great tracer for two reasons; (1) it is strongly X-ray attenuating because of its high atomic number and (2) iodide and chloride ions have been shown similar concentration profiles and about 10% difference of apparent D_c and C_s in the experiments [30, 31]. The current work examines the cement paste to investigate ion diffusion properties such as the apparent iodide D_c and the iodide C_s as the pore structure of the cement paste matrix is related to the ion diffusion in concrete [32]. Moreover, using cement paste is helpful to minimize intervention from aggregates [31]. In all of this work, the term D_{ic} and C_{is} will refer to the iodide diffusion coefficient and iodide surface concentration, respectively.

The current work expands the application of the Particle Model by predicting the D_{ic} of the fly ash-cement paste as demonstrated in Fig. 4.1. The aim of this work is to provide important insights into how the application of the Particle Model can be extended to predict D_{ic} at 20% fly ash replacement by mass at different hydration times. This paper provides some important insights to evaluate the impact of fly ash in cement-based materials and improve the durability of concrete, although providing detailed interpretations of *why* different fly ash particles impact the properties of the cement paste is outside the scope of this work.

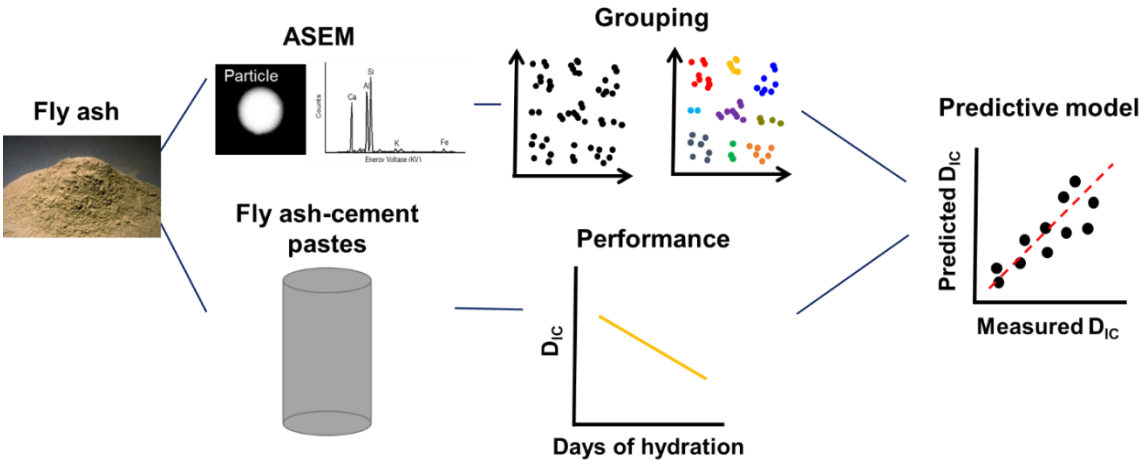

Fig. 4.1 Comprehensive schematic diagram of the process for investigating the diffusion properties.

4.2 Experimental Method

4.2.1 Raw materials

A Type I ordinary portland cement (OPC) by ASTM C150 [33] was used. Table 4.1 shows the chemical and phase composition of cement which was used in this study. Twenty-six different fly ashes were investigated in this study as the replacement material. All the fly ashes were produced from various coal sources, boiler designs, and collection conditions in the United States. Fly ashes in this study were classified into fifteen Class C and eleven Class F fly ashes according to ASTM C618.

Table 4.1 Properties of Type I Portland cement used in concrete mixtures.

Element	Composition (%)	Phase	Composition (%)
SiO_2	20.77		
Al_2O_3	4.57	C_3S	52.13
Fe_2O_3	2.62		
CaO	62.67		
MgO	2.37	C_2S	20.22
SO_3	3.18		
Na_2O	0.19		
K_2O	0.32	C_3A	7.68
TiO_2	0.34		
P_2O_5	0.14		
SrO	0.22	C_4AF	7.97
BaO	0.07		

4.2.2 Fly ash particle characterization by using ASEM method

The ASEM was used to investigate the properties of fly ash and to collect thousands of individual fly ash particle data. The ASEM method used SEM-EDS (Aspex Explorer PSEM-EDS) with the image analysis operating system. Two thousand particles were analyzed from each fly ash because this amount of particles has been shown to be a representative sample for fly ash [24]. One of the important advantages of the ASEM over the conventional analysis of bulk chemistry is the effectiveness of the measurement time [24, 34, 35]. The ASEM method enabled researchers to investigate the chemical composition, size, and shape of approximately 500 particles per hour without human intervention. This means that the ASEM can rapidly measure the physical properties such as shape and size as well as the chemical information of thousands of individual fly ash particles within a reasonable timeframe.

Since fly ash particles are not flat, this violates one of the fundamental assumptions of classical quantitative EDS analysis. The correction models have been developed and presented in previous publications [36-39]. These models have taken into account the shape of the particle and make corrections in the collected k-ratios of eleven investigated elements (Na, Mg, Al, Si, P, S, K, Ca, Ti, Fe, and Sr). A previous study discussed the consistency of the ASEM method with measuring the chemical composition for 50 Class C fly ash particles three times and the results showed that the highest standard deviation (SD) was 1.60% [22], and more details of the results can be found in Appendix A. The accuracy, reliability, and repeatability of the ASEM method when compared to XRF analysis have been presented in other publications and shown to be less than 5% absolute difference for greater than 90% of comparisons which indicates that the two methods largely agree [22, 24, 40]. Comparisons for the materials in this work are presented in Appendix B. The result of the particle size distribution (PSD) with data from ASEM has been compared to acoustic attenuation spectroscopy, and has been found to be similar [41]. Detailed procedure over the ASEM method, sample preparation, analysis with ASEM, and data processing are discussed in Appendix C.

4.2.3 Fly ash-cement paste sample preparation

Nineteen fly ashes were chosen based on a wide range of different chemical compositions for the paste sample preparation. Table 4.2 shows the mixture design of the paste samples. These mixtures have a 0.45 water to cement ratio (w/cm) at a 20% fly ash replacement rate by mass of cement. Thus, a total of twenty mixtures were prepared including one control with 100% OPC and nineteen mixtures with 20% fly ash replacement. All the mixtures were prepared as per ASTM C305 [42].

Vials with dimensions of 9.5 mm x 46 mm were used to prepare the paste samples, and then the samples were sealed and cured at 23°C until either 45, 90, and 135 days. Three samples were prepared for each curing time for each fly ash mixture.

Table 4.2 Mixture design for the paste samples.

Mixture	**Water (g)**	**Cement (g)**	**Fly ash (g)**	**W/C**
OPC	400	888.9	-	0.45
Fly ash	400	711.1	177.8	0.45

4.2.4 Ion penetration test and TXM data analysis

The samples were ponded for 28 days with the 0.6 mol/L of KI solution after curing. The concentration of the KI solution was determined on the experiments in previous publications [30, 31], and this was the optimum concentration to achieve suitable contrast. Next, the radiographs of the ponded samples were taken with the help of a laboratory Skyscan 1172 mCT scanner. The methods and settings used have been described in a previous study [30]. The KI solution was replaced with a new solution every seven days to keep a constant KI concentration. During the diffusion testing, the sample vials were sealed and stored in a container at 23°C.

The D_{ic} and C_{is} were calculated by Fick's second law as shown in Eq.(4.1) [43, 44]. All the data analysis was conducted with the MATLAB programming environment. More details for the experimental setting and theoretical background for the data analysis were reported in previous publications [30, 31] and can be found in Appendix J.

$$C_{(x,t)} = C_s(1 - \mathrm{erf}(\frac{x}{2\sqrt{D_c t}})) \qquad \text{Eq.(4.1)}$$

where, x is the distance from the sample surface, t denotes the time, erf is the error function, D_c is the apparent I diffusion coefficient which is D_{ic} in this work, C_s is the surface I concentration

which is C_{is} in this work, and $C_{(x,t)}$ is the total I concentration at the depth of x from the surface after t.

4.2.5 Particle Model development

The data of the 52,000 particles were extracted from twenty-six sources of fly ashes through the ASEM analysis, and each particle had eleven pieces of chemical composition data (Na_2O, MgO, Al_2O_3, SiO_2, P_2O_5, SO_3, K_2O, CaO, TiO_2, FeO_3, and SrO_2). The SOM algorithm and the maximum spectral angle method of particle classification were used to develop the prediction of the D_{ic}. This approach is called the Particle Model. The SOM helped to determine nine distinct groups of fly ash particles with unique chemical makeup. The unique nine groups were determined through the SOM. More details about the SOM process to determine the nine unique fly ash particle groups can be found in Appendix F. The maximum spectral angle method is used to classify the fly ash particles into the determined nine groups. More details of the maximum spectral angle method and the nine group composition of fly ashes investigated in this study can be found in the previous publication [18] and Appendix D.

A multiple linear regression (MLR) analysis was conducted by using the percentage of each of the nine groups found within fly ash to derive predictive models for the D_{ic} at 45, 90, and 135 days of hydration. The linear model to predict the D_{ic} is shown in Eq.(4.2):

$$D_{ic}\ (x10^{-11},\ m^2/sec) = a(\text{Group 1}) + b(\text{Group 2}) + c(\text{Group 3}) + d(\text{Group 4}) + e(\text{Group 5}) + f(\text{Group 6}) + g(\text{Group 7}) + h(\text{Group 8}) + i(\text{Group 9}) \quad \text{Eq.(4.2)}$$

where the group number indicates the percentage of each group within the fly ash, and the lowercase from “a” to “i” is the coefficient of each group determined from the linear regression analysis. Each of the coefficients reflects the effect of the individual groups on D_{ic} at a specific

curing time, where the potential influence of the remaining independent variables on the groups has been taken into account.

The initial model was evaluated with the probability value (Pr(>|t|)) from the MLR to determine the statistical significance of the variables. To evaluate the linear fit to the model, the R-squared value of each model was investigated at the individual curing times. More details can be found in Appendix K. All the data and model processing was conducted within the R programming environment [45, 46].

4.2.6 Bootstrapping

The robustness of the derived predictive models was evaluated with the help of the bootstrap method. Ideally, the data can be collected by repeating a large number of mixtures for the same experiment to evaluate the validity of the generated predictive models, but this is impractical. Instead, bootstrapping was used to investigate the robustness of the Particle Model over the R-squared value. Bootstrapping is a resampling method where the data are sampled with replacement from the original sample to generate simulated results [45]. This allowed creating numerous R-squared values by running predictive models with simulated samples. Furthermore, the results from the bootstrapping were used to calculate a variety of sample statistics such as the mean (average) and SD of the created R-squared values to compare the R-squared value of the original model.

The size of the bootstrapping sample was the same as the original data set and is chosen at random from the existing data set. This means that some data points can be chosen multiple times in the simulated sample while others may not be selected at all. This procedure has been used in previous publications [47, 48]. The bootstrapping was conducted with 500 times for each model.

Then, the mean of the R-squared values from the bootstrapping was investigated and compared with the R-squared value of the derived predictive model.

4.3 Result and discussion

4.3.1 KI diffusion test

Fig. 4.2 and Fig. 4.3 describe the diffusion test results for D_{ic} and C_{is} at different days of hydration for the fly ash sources investigated. The D_{ic} is decreased with increased days of hydration for all the fly ash sources except for C6. While it is well known that the fly ash helps to reduce the permeability by refining the pore structure of concrete [49], it should be noted that the value of D_{ic} for some of the fly ashes is higher values compared to the OPC. Specifically, at 45 and 90 days of hydration, 8 of the 12 Class C fly ashes show a greater iodide diffusion coefficient than OPC, and at the 135 days of hydration, the number of Class C fly ashes decreases into 6. This means that some of the Class C ashes can have worse performance than OPC when it comes to D_{ic}.

In the case of C_{is}, almost all the fly ash data, except for C6 and C11, show similar values to the OPC. Furthermore, the C_{is} shows similar values with changing the days of hydration for each mixture. Since the C_{is} values do not change significantly, and this is caused by using the same concentration of the KI solution for all the test samples, the Particle Model is not be applied to predicting the C_{is}.

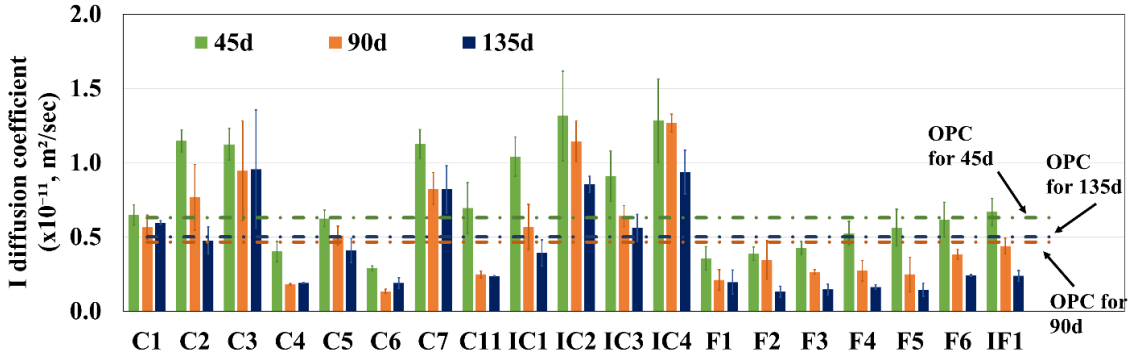

Fig. 4.2 D_{ic} at different days of hydration.

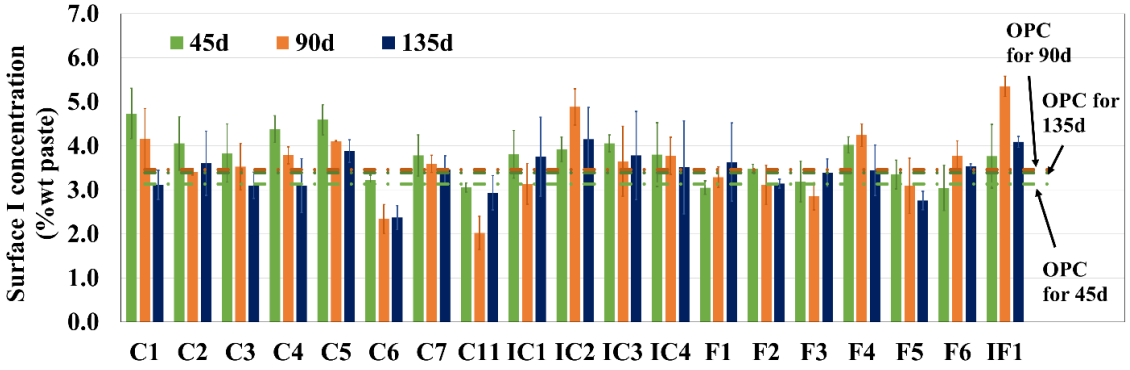

Fig. 4.3 C_{is} at different days of hydration.

4.3.2 Relationship between particle size of fly ash and the paste performances

Fig. 4.4 shows the frequency of PSDs for fifteen Class C and eleven Class F fly ashes by using ASEM, respectively. The fly ashes with "C#" and "IC#" represent Class C fly ash while the fly ashes with "F#" and "IF#" represent Class F fly ash. The results show most of fly ash particles have a size within the range of 0.5 μm and 20 μm in diameter, and the distribution for most fly ashes show a similar trend. D50 mean particle size for all fly ashes are investigated, and the differences between the largest and smallest D50 in Class C and Class F fly ashes are 1.6 μm and 0.8 μm, respectively. Furthermore, the largest and smallest average particle size among twenty-six fly ashes are 4.3 μm (C10) and 1.8 μm (IC2), respectively.

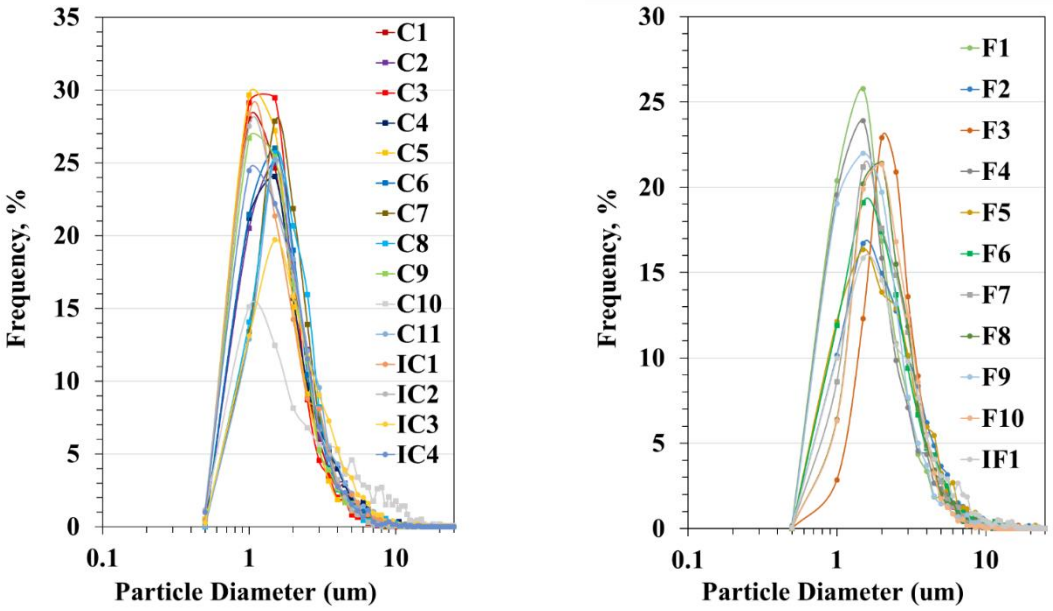

(a) Class C fly ash (b) Class F fly ash

Fig. 4.4 Comparison of the frequency of the PSDs for (a) fourteen Class C fly ashes and (b) eleven Class F fly ashes.

Fig. 4.5 shows the relationship between the D50 particle size of fly ashes and the performances for different days of hydration. Trend lines and R-squared values are investigated to determine the significance of particle size for the predictive model analysis. All investigated R-squared values of the linear trend lines are in the range of 0.00 to 0.29. This means the relationship is quite poor between the particle size of the fly ashes used in this study and the diffusion performances of fly ash pastes. Thus, the particle size information is not used in further model analysis.

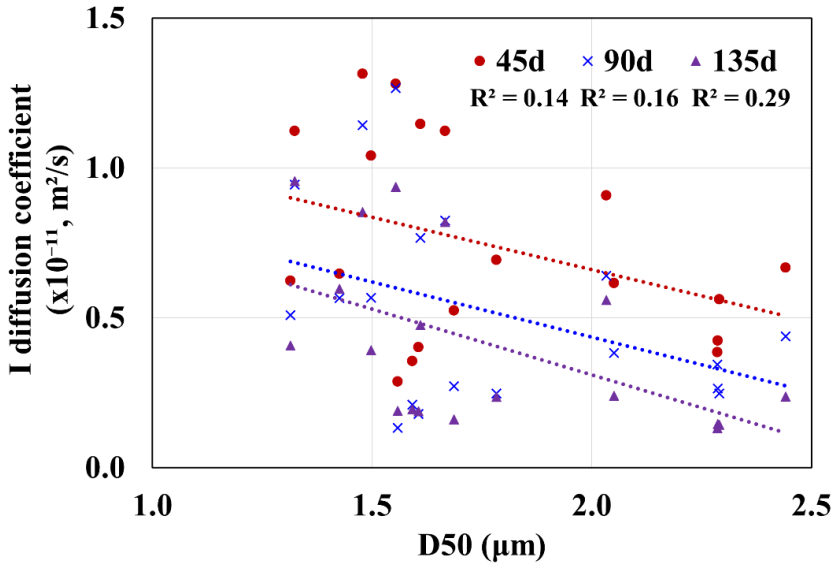

(a) D50 vs. D_{ic}

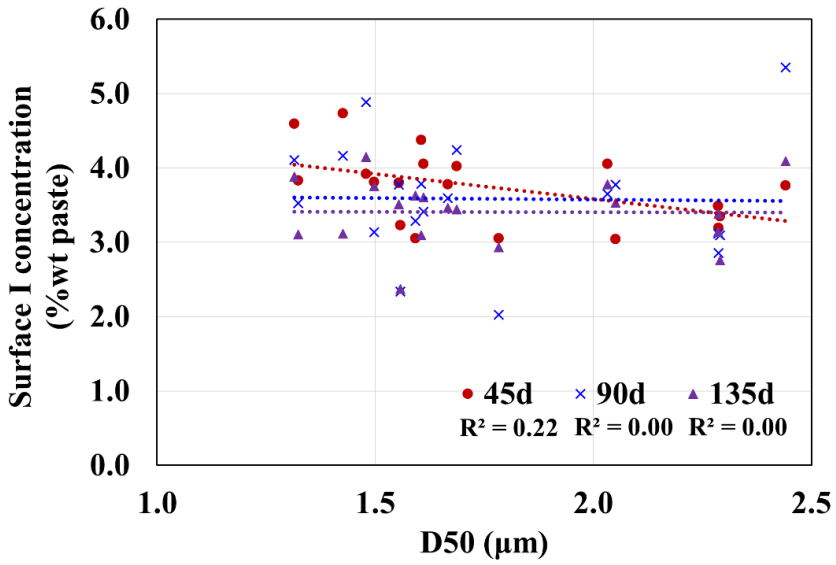

(b) D50 vs. C_{is}

Fig. 4.5 Relationships between the average particle size compared to (a) D_{ic} and (b) C_{is}.

4.3.3 Bulk chemical composition of raw fly ashes by using ASEM

The bulk chemical composition of twenty-six fly ash sources from the ASEM method is investigated, and the results are shown in Table 4.3. The fly ashes are classified as either Class C for greater than 18% of CaO or Class F less than 18% of CaO according to ASTM C618 [50].

Table 4.3 Bulk chemical composition by using the ASEM method.

Source	SiO_2	Al_2O_3	Fe_2O_3	CaO	MgO	SO_3	Na_2O	K_2O	TiO_2	P_2O_5	SrO
C1	36.2	21.7	5.4	23.2	5.4	0.7	3.6	1.0	0.8	1.9	0.2
C2	35.8	19.2	5.6	26.9	5.5	1.0	3.0	0.9	0.7	1.3	0.2
C3	25.3	19.3	5.2	32.5	7.8	2.6	3.4	0.6	1.1	1.9	0.3
C4	36.7	22.8	4.5	22.5	4.3	1.2	3.4	1.0	1.3	1.1	1.2
C5	31.3	22.5	5.4	26.1	6.0	0.6	4.3	0.8	0.8	2.1	0.2
C6	27.7	22.9	4.2	21.5	4.5	2.6	12.6	0.8	1.3	0.7	1.3
C7	35.3	20.6	4.7	24.7	4.9	0.7	4.3	1.2	1.6	0.8	1.0
C8	40.1	22.6	4.5	19.5	5.7	0.8	3.7	0.9	0.6	1.4	0.1
C9	31.5	24.0	6.0	25.7	5.4	1.0	3.7	0.6	0.9	1.1	0.1
C10	36.0	19.3	5.1	22.7	7.8	2.0	4.8	0.6	1.0	0.3	0.5
C11	31.0	20.8	6.4	27.2	7.1	1.6	3.5	0.7	0.8	0.8	0.2
IC1	31.8	22.9	5.7	28.2	5.5	1.1	2.3	1.0	0.8	0.5	0.3
IC2	25.2	21.2	6.2	30.5	7.8	1.0	4.0	0.6	1.2	2.2	0.2
IC3	29.7	21.0	5.9	30.3	5.4	1.9	2.2	0.6	1.0	1.6	0.5
IC4	29.9	17.7	4.7	31.8	9.3	1.2	2.6	0.8	0.8	1.1	0.2
F1	48.8	23.8	7.4	12.5	3.0	0.5	0.9	2.1	0.8	0.1	0.3
F2	50.4	20.9	3.9	17.1	3.7	0.5	1.0	1.4	0.7	0.1	0.3
F3	48.8	26.6	6.7	9.3	2.0	0.3	1.8	1.9	1.5	0.1	1.1
F4	45.3	27.4	4.0	14.6	3.6	0.7	1.5	0.7	1.1	0.4	0.8
F5	53.2	25.4	11.2	2.1	0.2	0.9	1.0	4.4	0.7	0.0	1.0
F6	51.9	25.7	12.3	2.5	0.3	0.7	1.6	4.1	0.7	0.1	0.2
F7	51.9	26.3	8.0	3.3	0.5	1.7	4.0	2.5	0.9	0.6	0.1
F8	56.9	23.9	3.4	6.2	2.1	0.1	4.1	1.7	0.3	1.2	0.1
F9	48.3	25.0	5.9	12.6	3.3	0.5	1.3	1.8	1.1	0.2	0.1
F10	53.6	27.8	2.8	10.5	2.5	0.5	0.3	1.3	0.5	0.3	0.0
IF1	58.3	21.9	6.9	3.7	1.4	0.6	2.2	4.3	0.2	0.4	0.2

4.3.4 Evaluation of the test results and the predictive models

Fig. 4.6 shows the comparison between the measured D_{ic} and the average values for Class C or F fly ash. The actual measured values are shown as points on the plot with the same color as the matching trend line. The results show that the value of D_{ic} varies depending on the fly ash, and Class C fly ash has a much wider range of D_{ic} than Class F fly ash. For example, in the results of 90 days of hydration, the difference between the highest D_{ic} and lowest D_{ic} for Class C fly ashes is 1.02 x 10^{-11} m²/sec while the difference for Class F fly ashes is 0.23 x 10^{-11} m²/sec. This means that it is much harder to predict the D_{ic} of Class C fly ash than Class F fly ash. Furthermore, despite having similar bulk chemical classification as per ASTM C618 the diffusion property is variable. This further shows the challenge of using ASTM C618 classification methods to predict the D_{ic} of concrete containing fly ash.

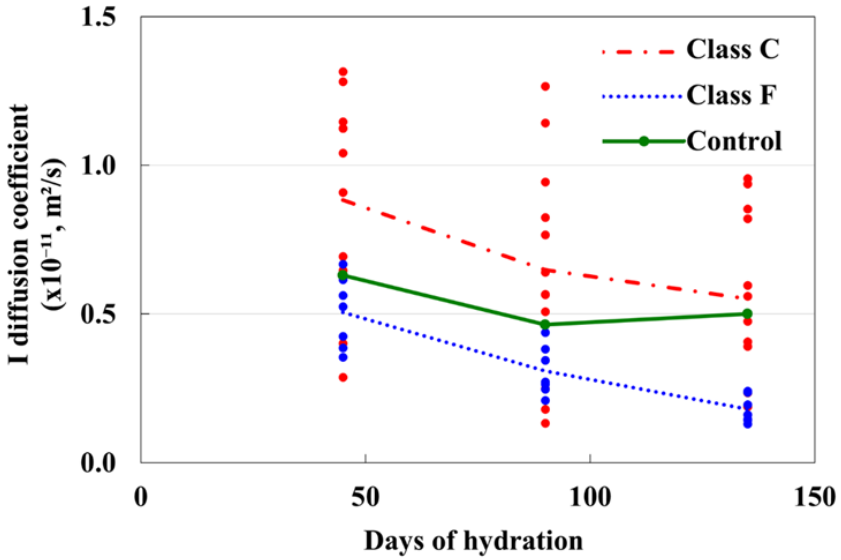

Fig. 4.6 Comparison between actual and predicted D_{ic} with the type of fly ash used.

The comparisons between the predicted D_{ic} from the Particle Model and measured D_{ic} is described in Fig. 4.7. The slope of the trend line in the comparisons is 0.96 with the R-squared value of 0.80. It should be noted that the perfect fit can be described with a value of 1.00 (one) for

the slope. This means that overall the D_{ic} can be closely predicted with the Particle Model. It should be noted that some of the predictions are quite different results to the measured values. For example, the measured D_{ic} of the pastes with C11 fly ash at 135 days of hydration is 0.60 x 10^{-11} m^2/sec while the predicted value is 0.24 x 10^{-11} m^2/sec.

Tang [51] has evaluated the precision of diffusion coefficient through various test methods such as immersion test (Nordtest method NT build 492), rapid migration test (Nordtest method NT build 443), and measurement of chloride ion ingress test (EN 13396), and the study suggests the CV of the reproducibility of these tests are 24%, 28%, and 36%, respectively. The average CV is 29.3% or close to 30% for this work. Moreover, ASTM C1556 (bulk chloride diffusion test) provides 39.8% as the limit of CV to evaluate the precision (single laboratory) of determining the apparent D_c of cementitious mixtures [52]. Even though the test method in this study is different from those methods, these numbers could be a good guideline to evaluate the test results of the current study. A value of +/- 30% has been added as the dashed blue line as a conservative estimate for the variability of the test method. The comparison between the predicted and measured values for the D_{ic} for 57 samples is shown in Fig. 4.7, and 81% of comparisons are within +/- 30%. The detailed results of the predictive models for different hydration time can be found in Appendix L.

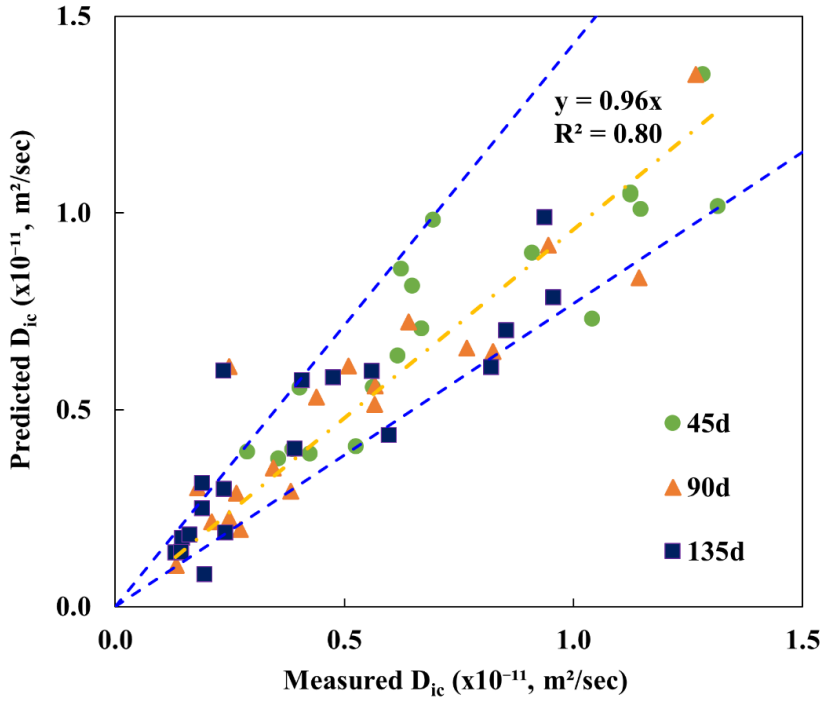

* Blue dash line: The range of +/– 30% of the calculated and measured properties.

Fig. 4.7 Comparison between the calculated and measured value for D_{ic}.

The R-squared value is investigated for the derived predictive models for individual measurement times, and the results are shown in Table 4.4. A low R-squared value means a weak linear fit for the model while a high R-squared value indicates the model explains the majority of the variability of the response data around its mean value. The R-squared values for the three different days of hydration are > 0.90, which is a strong correlation. This shows that the Particle Model is able to accurately predict the D_{ic} with a linear model.

Table 4.4 R-squared value of the predictive models for the D_{ic} at different hydration times.

Days of hydration	**45d**	**90d**	**135d**
R-squared	0.94	0.92	0.90

The results of the bootstrapping at each measurement time are presented in Table 4.5. It should be noted here again that this helps to determine the robustness of the Particle Model. The mean of 500 R-squared values through the bootstrap method is compared with the R-squared value of the derived predictive model in Table 4.4. The results present that the mean R-squared value from the bootstrapping shows the same or almost the same R-squared value of the derived predictive model. The maximum, minimum, and SD of the R-squared values from the bootstrapping are also investigated. The range of difference between the maximum and minimum R-squared value is from 0.07 to 0.14, and all the investigated SDs are under 0.025 which indicates the variance of the bootstrap results is quite small. This means that the Particle Model can be considered as a robust tool to predict the D_{ic} of 20% fly ash cement paste.

Table 4.5 Bootstrapping for the Particle Model over the R-squared value.

Days of hydration	The mean of the R-squared values	Max	Min	SD
45d	0.94	0.98	0.91	0.012
90d	0.92	0.97	0.86	0.018
135d	0.90	0.97	0.83	0.023

4.3.6 Discussion for the contribution of each group

The contribution of each group to the D_{ic} for each time period can be investigated by examining the change in the coefficient over time. The groups with a coefficient value greater than 0 increase the D_{ic} while groups with a coefficient value lesser than 0 decrease the D_{ic}. This means that the groups with the negative coefficient will decrease or improve the D_{ic} while the groups with the positive coefficient values will increase or impair the D_{ic}. The groups that do not have a coefficient mean that those groups did not affect the performance at that time period.

The coefficients of each group are compared for hydration of 45, 90, and 135 days, and the results are shown in Fig. 4.8. The figure shows that Group 2 and 5 decrease the D_{ic}, which can improve permeability, while Group 1, 3, 6, 8, and 9 will increase D_{ic} which can make the permeability worse. Furthermore, Group 4 and 7 do not have any impacts on D_{ic} between 45 to 135 days of hydration. It is interesting to note that the coefficients for the different groups change over time. This suggests that not all fly ash groups have the same impact on the different time periods investigated. More discussions about the impact of each group at different hydration times on D_{ic} will be provided in the following sections.

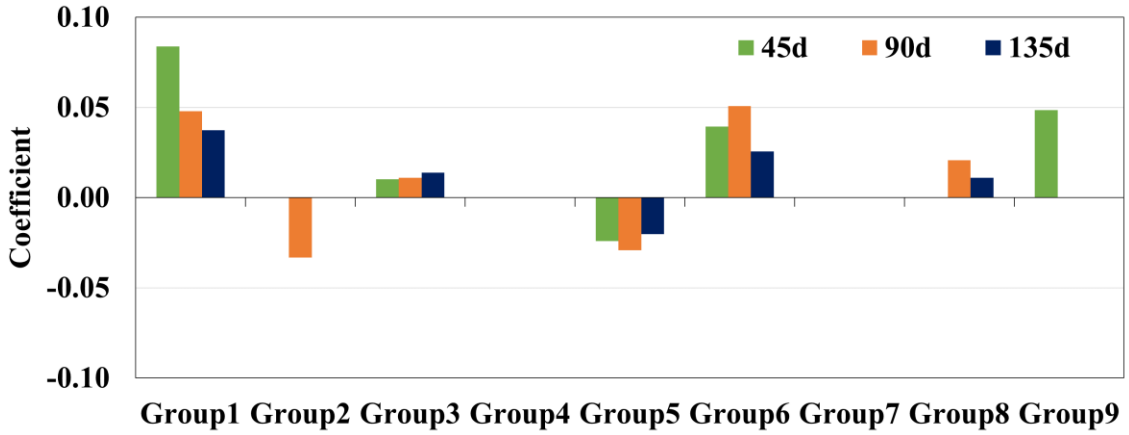

Fig. 4.8 Coefficients of predictive models of each group at different hydration times for D_{ic}.

4.3.6.1 Discussion for Group 2 and 5

According to Fig. 4.8, Group 2 decreases the D_{ic} at 90d, and the coefficients of Group 5 are less than 0 for all the measurements between 45 and 135 days of hydration. This means that Group 2 and 5 can be helped to improve the D_{ic} of the fly ash-cement paste.

It is interesting that only Group 5 shows less than 0 coefficients between 45 and 135 days period. This suggests that Group 5 is critical in improving the D_{ic} of the samples. Group 5 may include high contents of reactive glassy phases such as calcium-rich aluminosilicate. Calcium-rich glassy

phases are much more reactive than those with low or moderate calcium content phases [53, 54]. Furthermore, Group 5 might be a good source to produce C-S-H with a pozzolanic reaction that causes the reduction of capillary production and interconnected pores.

Group 2 shows the lowest SiO_2 content as 8.4%, and only this group has over 30% contents of Al_2O_3 and CaO among the nine groups. In addition, a relatively high amount of MgO is included in Group 2. Various crystalline and glassy phases could exist in those particles. Several glassy phases such as calcium-rich aluminosilicates, aluminosilicate, and calcium silicates can exist in these two groups. Non-reactive phases at normal temperatures such as Merwinite $Ca_3Mg(SiO_4)_2$, Gehlenite $Ca_2Al(AlSiO_7)$, and Akermanite $Ca_2Mg(Si_2O_7)$ phases [7] could also be considered a phase of Group 2. Merwinite is a common phase in high-calcium fly ash and at the early stages of the devitrification of Mg-containing glasses [7]. Calcium hydroxide in the cement paste can react with the reactive Mg-phases to form the insoluble magnesium hydroxide $Mg(OH)_2$ that is capable of reducing the porosity of the cement paste [49]. Thus, investigating the reason for Group 2 about decreasing D_{ic} only at 90 days of hydration is an area of future work.

4.3.6.2 Discussion for Group 1, 3, 6, 8, and 9

Group 1, 3, and 6 show a positive coefficient during all three measurement periods. More specifically, Group 1 and 6 show relatively higher coefficients than the other groups between 45 to 135 days of hydration. This means that the particles in Group 1 and 6 impact the D_{ic} the most. Group 8 shows a positive coefficient at 90d and 135d, and the coefficient is decreased from 90d to 135d while Group 9 increases the D_{ic} at 45d, and it is zero after 45d.

Group 1 has 77.8% of Fe_2O_3, and Fe-rich phases such as magnetite and hematite have been found in fly ash, which is not chemically reactive [7]. Moreover, a ferrite phase could exist in this group. It is reported that the ferrite particles fill the pores between cement particles resulting in finer pore structure, and more C-S-H gel can be formed because of the reaction between the ferrite particles

and the $Ca(OH)_2$ in the hydrating of cement [55, 56]. This could improve the diffusion property, and since this happens after 28 days of hydration, this is a possible reason why the coefficient of Group 1 decreased with increasing hydration time.

Group 3 and 6 have > 6% MgO which is significantly higher than the other groups. Furthermore, these groups have relatively higher CaO and lower Al_2O_3 than Group 2. This can be a good source to form Merwinite which is a common phase in high-calcium fly ash and it is non-reactive in concrete at normal temperatures and it may exist in the particles of these two groups [7]. While Group 3 has a high content of CaO, it also shows the lowest SiO_2 with a quite high content of P_2O_5 among the nine groups. The content of P_2O_5 in Group 6 is also higher than other groups, and the contents of SiO_2 and Al_2O_3 in Group 6 are quite comparable to each other as about 20%. The contents and distribution of pores in concrete can be influenced by high P_2O_5 content fly ash particles because the high contents of P_2O_5 can decompose C_3S forming a series of solid solutions between C_2S and $3CaO{\cdot}P_2O_5$ [57, 58]. Besides, Group 6 can be a source of the melilite group including Gehlenite and Akermanite phases which are not chemically reactive in concrete [7]. Thus, even though further investigation is needed for the phase characterization of each group, the findings in this study provide important insights for the use of fly ash in concrete to improve the D_{ic}.

Group 8 contains high SiO_2 (roughly 60%) and some Na_2O and K_2O. This material is more likely a conglomerate of non-reactive phases like feldspar $(K, Na)AlSi_3O_8$, mullite (a crystalline aluminosilicate), and quartz [59]. Furthermore, the previous study has found low reactive materials such as mullite (a crystalline aluminosilicate) in low calcium fly ashes [60]. Group 9 could be a good source of either quartz or reactive chemical forms such as silicate or aluminosilicate because of the high SiO_2 content as 84.46%, and those phases have been observed in almost all fly ashes [7]. It has been known that the reactivity of quartz and silicate phase is very

low [53, 61]. Those properties could affect the characteristics of pores in fly ash concrete. Practically, the change of the total porosity has been investigated in previous studies by using mercury intrusion porosimetry for the mortar with using the Fe_2O_3 and SiO_2 powder as additives and found the mortar with the additives had higher total porosity than the control mortar with no additives [62, 63].

4.3.6.3 Discussion for Group 4 and 7

Group 4 and 7 have no impacts on D_{ic} between 45d and 135d hydration. Group 4 and 7 show relatively low CaO content with high content SiO_2 and Al_2O_3. Meanwhile, these groups show high contents of alkalis (Na_2O and K_2O) compared to the other groups. Even though the siliceous glass can help to reduce the availability of alkalis for the alkali-silica reaction [7], excessive content of alkali hydroxide can affect the porosity. A previous study reported the evolution of the mercury porosity with a 28 days maximum age of the cement paste which used NaOH and KOH solution [64]. The study found that the cement paste with NaOH and KOH showed higher porosity (22% and 24%, respectively) than the control cement paste (17.5%) which used deionized water as the solution [64]. Besides, additional water-soluble alkalis from the fly ash can cause expansion and damage to the concrete [65].

4.3.7 Practical implications and future applications

This study shows the usefulness of the Particle Model to predict the D_{ic} between 45 and 135 days of hydration for 20% replacement of fly ash paste. This shows that the Particle Model could be a useful tool to evaluate the fly ash powder and predict the performance in hardened concrete. This prediction could be used to help practitioners make wise decisions in choosing a fly ash source that will help them obtain the desired property. This could lead to a new approach to concrete performance design. Furthermore, this approach can be used to determine the interrelationships

among the different fly ash particles and how they contribute to the ultimate properties of the concrete.

4.4 Conclusion

A novel characterization and analysis method called the Particle Model has been used to classify the fly ash particles into nine distinct groups. The predictive models for apparent diffusion coefficient and surface concentration of iodide into cement paste with a 20% replacement of fly ash at 45, 90, and 135 days of hydration. The accuracy of the predictive models is evaluated with the comparison results between the calculated and measured values from the paste samples using nineteen fly ash sources. The impacts of each group on the diffusion coefficient are discussed by interpreting the coefficient changes over time and the measured chemical consistency of the individual groups.

The following contributions are drawn in this study:

1. Between 45 and 135 days of hydration, the apparent iodide diffusion coefficient is decreased over time for all the fly ash sources except for C6. Furthermore, iodide surface concentration shows similar values to the OPC for all the investigated fly ash sources.
2. At 45 and 90 days of hydration, 8 of the 12 Class C fly ashes show a greater iodide diffusion coefficient than OPC, and at the 135 days of hydration, the number of Class C fly ashes decreases into 6.
3. The R-squared values of the relationship between the measured values and mean particle size of nineteen fly ashes are less than 0.3 which means the mean particle size showed poor correlation over the apparent iodide diffusion coefficient.
4. For the apparent iodide diffusion coefficient, all the R-squared values of

predictive models are > 0.95.

5. The predicted and measured apparent iodide diffusion coefficient in paste shows that 81% of all measurements can be predicted within the variation of the test method (+/- 30%) between 45 to 135 days of hydration at 20% fly ash replacement.
6. Group 2 and 5 decreases the apparent iodide diffusion coefficient which means these groups help to improve the mass transport of the sample. Group 5 is the only particle group that showed improvement at all measurement periods while Group 2 showed improvement at 90d.
7. Group 1, 3, and 6 increase the apparent iodide diffusion coefficient between 45 and 135 days of hydration. Group 8 increases the apparent iodide diffusion coefficient at 90d and 135d while Group 9 increases the apparent iodide diffusion coefficient at only 45d. Group 4 and 7 have no impacts on the apparent iodide diffusion coefficient between 45d and 135d hydration.

Future work should be done to better understand the different fly ash groups and also investigate higher replacement levels of fly ash.

Acknowledgments

This work was sponsored by funding from the Illinois Department of Transportation [Project ICT R27-180], and the FHWA [EAR project # BAA No. 693JJ3-18-BAA-0001]. The authors would like to thank Dr. Daniel Cook and Mr. Jeff Davis for their assistance and discussion on this work.

Reference

[1] X. Li, Q. Xu, S. Chen, An experimental and numerical study on water permeability of concrete, Constr Build Mater 105 (2016) 503-510.

[2] S. Sadati, M. Arezoumandi, M. Shekarchi, Long-term performance of concrete surface coatings in soil exposure of marine environments, Constr Build Mater 94 (2015) 656-663.

[3] O. Sengul, Probabilistic Design for the Durability of Reinforced Concrete Structural Elements Exposed to Chloride Containing Environments, Teknik Dergi 22 (2011) 5409-5423.

[4] V. Årskog, O. Sengul, O. Gjørv, Performance-based quality control for concrete durability, Proceedings of International RILEM Workshop on Performance Based Evaluation and Indicators for Concrete Durability. Madrid, 2006, pp. 223-27.

[5] M.A. Bérubé, J. Duchesne, D. Chouinard, Why the Accelerated Mortar Bar Method ASTM C 1260 is Reliable for Evaluating the Effectiveness of Supplementary Cementing Materials in Suppressing Expansion Due to Alkali-Silica Reactivity, Cement, Concrete and Aggregates 17(1) (1995) 26-34.

[6] B. Mather, Use of Concrete of Low Portland Cement Content in Combination with Pozzolans and Other Admixtures in Construction of Concrete Dams, J Am Concr Inst 71(12) (1974) 589-599.

[7] A. Committee, 232.2R-18: Report for the Use of Fly Ash in Concrete, Technical Documents (2018).

[8] S. Shashiprakash, M. Thomas, Sulfate resistance of mortars containing high-calcium fly ashes and combinations of highly reactive pozzolans and fly ash, Special Publication 199 (2001) 221-238.

[9] M. Thomas, Marine performance of PFA concrete, Magazine of Concrete Research 43(156) (1991) 171-185.

[10] O. Al-Amoudi, M. Maslehuddin, I.M. Asi, Performance and correlation of the properties of fly ash cement concrete, Cement, Concrete and Aggregates 18(2) (1996) 71-77.

[11] R.K. Dhir, E.A. Byars, PFA concrete: chloride diffusion rates, Magazine of Concrete Research 45(162) (1993) 1-9.

[12] R.C. Joshi, R. Lohita, Fly ash in concrete: production, properties and uses, CRC Press1997.

[13] K.O. Ampadu, K. Torii, M. Kawamura, Beneficial effect of fly ash on chloride diffusivity of hardened cement paste, Cement Concrete Res 29(4) (1999) 585-590.

[14] R.B. Holland, K.E. Kurtis, L.F. Kahn, 7 - Effect of different concrete materials on the corrosion of the embedded reinforcing steel, in: A. Poursaee (Ed.), Corrosion of Steel in Concrete Structures, Woodhead Publishing, Oxford, 2016, pp. 131-147.

[15] S.K. Das, Yudhbir, A simplified model for prediction of pozzolanic characteristics of fly ash, based on chemical composition, Cement Concrete Res 36(10) (2006) 1827-1832.

[16] S. Diamond, On the Glass Present in Low-Calcium and in High-Calcium Flyashes, Cement Concrete Res 13(4) (1983) 459-464.

[17] L.X. Du, E. Lukefahr, A. Naranjo, Texas Department of Transportation Fly Ash Database and the Development of Chemical Composition-Based Fly Ash Alkali-Silica Reaction Durability Index, J Mater Civil Eng 25(1) (2013) 70-77.

[18] S.C. White, E.D. Case, Characterization of fly ash from coal-fired power plants, Journal of Materials Science 25(12) (1990) 5215-5219.

[19] S. Schlorholtz, K. Bergeson, T. Demirel, Monitoring of Fluctuations in the Physical and Chemical Properties of a High-Calcium Fly Ash, MRS Proceedings 113 (1987) 107.

[20] Q. Hu, M.T. Ley, J. Davis, J.C. Hanan, R. Frazier, Y. Zhang, 3D chemical segmentation of fly ash particles with X-ray computed tomography and electron probe microanalysis, Fuel 116 (2014) 229-236.

[21] Q. Hu, M. Aboustait, M.T. Ley, J.C. Hanan, V. Rose, R. Winarski, Combined three-dimensional structure and chemistry imaging with nanoscale resolution, Acta Mater 77 (2014) 173-182.

[22] T. Kim, J.M. Davis, M.T. Ley, S. Kang, P. Amrollahi, Fly ash particle characterization for predicting concrete compressive strength, Constr Build Mater 165 (2018) 560-571.

[23] T. Kim, M. Moradian, M.T. Ley, Dissolution and leaching of fly ash in nitric acid using automated scanning electron microscopy, Advances in Civil Engineering Materials 7(1) (2018) 291-307.

[24] M. Aboustait, T. Kim, M.T. Ley, J.M. Davis, Physical and chemical characteristics of fly ash using automated scanning electron microscopy, Constr Build Mater 106 (2016) 1-10.

[25] S. Ghosal, J.L. Ebert, S.A. Self, Chemical composition and size distributions for fly ashes, Fuel processing technology 44(1-3) (1995) 81-94.

[26] Y. Chen, N. Shah, F.E. Huggins, G.P. Huffman, W.P. Linak, C.A. Miller, Investigation of primary fine particulate matter from coal combustion by computer-controlled scanning electron microscopy, Fuel Processing Technology 85(6-7) (2004) 743-761.

[27] T. Kim, M.T. Ley, S. Kang, J.M. Davis, S. Kim, P. Amrollahi, Using particle composition of fly ash to predict concrete strength and electrical resistivity, Cement and Concrete Composites (2019) 103493.

[28] S. Kang, Z. Lloyd, T. Kim, M.T. Ley, Predicting the Compressive Strength of Fly Ash Concrete with the Particle Model, Manuscript submitted for publication.

[29] S. Kang, M.T. Ley, Z. Lloyd, T. Kim, Using the Particle Model to Predict Electrical Resistivity Performance of Fly Ash in Concrete, Manuscript submitted for publication.

[30] M. Khanzadeh Moradllo, M.T. Ley, Comparing ion diffusion in alternative cementitious materials in real time by using non-destructive X-ray imaging, Cement and Concrete Composites 82 (2017) 67-79.

[31] M.K. Moradllo, Q. Hu, M.T. Ley, Using X-ray imaging to investigate in-situ ion diffusion in cementitious materials, Constr Build Mater 136 (2017) 88-98.

[32] K. Stanish, R.D. Hooton, M.D. Thomas, Testing the Chloride Penetration Resistance of Concrete: A Literature Review, United States. Federal Highway Administration, 2001.

[33] ASTM C150, Standard Specification for Portland Cement, American Society for Testing and Materials, West Conshohocken, PA, 2019.

[34] R.P. Gupta, T.F. Wall, I. Kajigaya, S. Miyamae, Y. Tsumita, Computer-controlled scanning electron microscopy of minerals in coal - Implications for ash deposition, Prog Energ Combust 24(6) (1998) 523-543.

[35] C.A. O'Keefe, T.M. Watne, J.P. Hurley, Development of advanced scanning electron microscopy techniques for characterization of submicron ash, Powder Technol 108(2-3) (2000) 95-102.

[36] J.T. Armstrong, Quantitative Elemental Analysis of Individual Microparticles with Electron Beam Instruments, in: K.F.J. Heinrich, D.E. Newbury (Eds.), Electron Probe Quantitation, Springer US, Boston, MA, 1991, pp. 261-315.

[37] G. Love, V.D. Scott, Evaluation of a New Correction Procedure for Quantitative Electron-Probe Microanalysis, J Phys D Appl Phys 11(10) (1978) 1369-1376.

[38] J.T. Armstrong, P.R. Buseck, A General Characteristic Fluorescence Correction for the Quantitative Electron Microbeam Analysis of Thick Specimens, Thin-Films and Particles, X-Ray Spectrom 14(4) (1985) 172-182.

[39] J.T. Armstrong, P.R. Buseck, Quantitative Chemical-Analysis of Individual Microparticles Using Electron-Microprobe - Theoretical, Anal Chem 47(13) (1975) 2178-2192.

[40] M. Aboustait, Q. Hu, R. Frazier, Y. Zhang, B. Tabb, M. Ley, J. Hahan, Innovative prediction of fly ash performance in concrete, Oklahoma Transportation Center, Midwest City, OK, 2013.

[41] C.P. Aichele, D. Venkataramani, J.E. Smay, M.H. McCann, S. Richter, M. Khanzadeh-Moradllo, M. Aboustait, M.T. Ley, A comparison of automated scanning electron microscopy (ASEM) and acoustic attenuation spectroscopy (AAS) instruments for particle sizing, Colloids and Surfaces A: Physicochemical and Engineering Aspects 479 (2015) 46-51.

[42] ASTM C305, Standard Practice for Mechanical Mixing of Hydraulic Cement Pastes and Mortars of Plastic Consistency, American Society for Testing and Materials, West Conshohocken, PA, 2014.

[43] J. Crank, The mathematics of diffusion, Oxford university press1979.

[44] S. Sadati, M.K. Moradllo, M. Shekarchi, Long-term durability of onshore coated concrete — chloride ion and carbonation effects, Frontiers of Structural and Civil Engineering 10(2) (2016) 150-161.

[45] M.J. Crawley, The R Book, Second ed., John Wiley & Sons Ltd, Imperial College London at Silwood Park, UK, 2012.

[46] R.C. Team, R: A Language and Environment for Statistical Computing, Vienna, Austria, 2016.

[47] M. Kuhn, K. Johnson, Applied predictive modeling, Springer2013.

[48] B. Efron, R.J. Tibshirani, An introduction to the bootstrap, CRC press1994.

[49] D. Manmohan, P. Mehta, Influence of pozzolanic, slag, and chemical admixtures on pore size distribution and permeability of hardened cement pastes, Cement, Concrete and Aggregates 3(1) (1981) 63-67.

[50] ASTM C618, Standard Specification for Coal Fly Ash and Raw or Calcined Natural Pozzolan for Use in Concrete, American Society for Testing and Materials, West Conshohocken, PA, 2019.

[51] L. Tang, Guideline for practical use of methods for testing the resistance of concrete to chloride ingress, CHLORTEST-EU funded Research Project'Resistance of concrete to chloride ingress-from laboratory tests to in-field performance'G6RD-CT-2002-00855, Deliverable D23 (2008).

[52] ASTM C1556, Standard Test Method for Determining the Apparent Chloride Diffusion Coefficient of Cementitious Mixtures by Bulk Diffusion, American Society for Testing and Materials, West Conshohocken, PA, 2016.

[53] P.T. Durdzinski, C.F. Dunant, M. Ben Haha, K.L. Scrivener, A new quantification method based on SEM-EDS to assess fly ash composition and study the reaction of its individual components in hydrating cement paste, Cement Concrete Res 73 (2015) 111-122.

[54] K.L. Aughenbaugh, R.T. Chancey, P. Stutzman, M.C. Juenger, D.W. Fowler, An examination of the reactivity of fly ash in cementitious pore solutions, Materials and Structures 46(5) (2013) 869-880.

[55] M.A. Ahmed, Y.A. Hassanean, K.A. Assaf, M.A. Shawkey, The Effect of Incorporation of Ferrite Nano-particles on Compressive Strength and Resistivity of Self-Compacting Concrete, Open Journal of Civil Engineering 5(01) (2015) 131.

[56] M.A. Largeau, Effect of iron powder patially used as portland cement replacement on the structural properties of concrete, JKUAT-PAUSTI, 2018.

[57] D.J. Naus, C.H. Mattus, L.R. Dole, Assessment of Potential Phosphate Ion-Cementitious Materials Interactions, Citeseer, 2007.

[58] Z. Li, Z. Ding, Y. Zhang, Development of sustainable cementitious materials, Proceedings of the international workshop on sustainable development and concrete technology, Iowa State University, 2004, pp. 55-76.

[59] D. Stark, M.S.Y. Bhatty, Alkali-Silica Reactivity: Effect of Alkali in Aggregate on Expansion, in: V.H. Dodson (Ed.), ASTM International, West Conshohocken, PA, 1986, pp. 16-30.

[60] S. Gomes, M. François, M. Abdelmoula, P. Refait, C. Pellissier, O. Evrard, Characterization of magnetite in silico-aluminous fly ash by SEM, TEM, XRD, magnetic susceptibility, and Mössbauer spectroscopy, Cement Concrete Res 29(11) (1999) 1705-1711.

[61] P.T. Durdzinski, R. Snellings, C.F. Dunant, M. Ben Haha, K.L. Scrivener, Fly ash as an assemblage of model Ca-Mg-Na-aluminosilicate glasses, Cement Concrete Res 78 (2015) 263-272.

[62] M.Á.S. Barbudo, C.A. Lucio, J.C.G. Ruiz, E.R. Pozo, Combined effect of nano-SiO2 and nano-Fe2O3 on compressive strength, flexural strength, porosity and electrical resistivity in cement mortars, Materiales de construcción (329) (2018) 8.

[63] E. Mohseni, B.M. Miyandehi, J. Yang, M.A. Yazdi, Single and combined effects of nano-SiO2, nano-Al2O3 and nano-TiO2 on the mechanical, rheological and durability properties of self-compacting mortar containing fly ash, Constr Build Mater 84 (2015) 331-340.

[64] G. Sant, A. Kumar, C. Patapy, G. Le Saout, K. Scrivener, The influence of sodium and potassium hydroxide on volume changes in cementitious materials, Cement Concrete Res 42(11) (2012) 1447-1455.

[65] A.D. Buck, K. Mather, Methods for Controlling Effects of Alkali-Silica Reaction in Concrete, ARMY ENGINEER WATERWAYS EXPERIMENT STATION VICKSBURG MS STRUCTURES LAB, 1987.

CHAPTER V

THE RELATIONSHIP BETWEEN THE APPARENT DIFFUSION COEFFICIENT AND ELECTRICAL RESISTIVITY OF FLY ASH CONCRETE

Abstract

Electrical resistivity is a factor that has been suggested as a method to predict mass transport in concrete. This would be of great value because of the low cost, speed, and convenience of electrical resistivity. This study employs the Nernst-Einstein equation to estimate the apparent iodide diffusion coefficient (D_{ic}) by using the surface electrical resistivity (ρ_{sr}) of fly ash concrete. The empirical relationship between the D_{ic} and ρ_{sr} is investigated at three different hydration dates for 19 different fly ash sources at 20% fly ash replacement of the cement. A factor K which shows the correlation between ρ_{sr} and D_{ic} is calculated using the Nernst-Einstein equation, and the regression line is investigated to evaluate the relationship. Comparisons between D_{ic} and ρ_{sr} are made with both Class C and Class F fly ash, and the R-squared values of the regression line for each comparison are examined. This work shows that there is not a single relationship between D_{ic} and ρ_{sr} for the materials and mixtures investigated. However, the results show an accurate prediction of the D_{ic} for class F fly ash is reasonable.

Keywords: Apparent iodide diffusion coefficient, Surface electrical resistivity, Fly ash

5.1 Introduction

The mass transport of outside chemicals into concrete is widely used to evaluate the lifespan of concrete structures. The resistance of concrete against ion ingress is one of the most important factors for designing durable concrete structures [1-3]. Furthermore, the degradation mechanism in reinforced concrete due to the chloride-induced corrosion of reinforcement can cause several structural problems such as cracking, spalling, and delaminating of concrete cover. Previous studies have employed the apparent diffusion coefficient (D_c) as one of the primary parameters to predict the time to corrosion initiation of the reinforcing steel in concrete [4-6]. According to the service life prediction model such as Life-365 and DuraCrete, the model predicts the initiation period assuming diffusion to be the dominant mechanism [7, 8]. There are many papers describing this approach [9-12]. Thus, D_c is a useful tool to evaluate the service life of concrete structures.

The current work focuses on estimating the D_c in fly ash concrete through the electrical resistivity of concrete. Fly ash has been widely used as supplementary cementitious material (SCM) in concrete to improve the durability of concrete. Moreover, the incorporation of fly ash in concrete can significantly reduce the D_c of chloride into cement paste, mortar, or concrete [13-15]. The chloride penetration has also been evaluated by accounting for the chloride binding for the cement paste using fly ash [16-18]. Specifically, Thomas et al. [16] have studied one Class C and one Class F fly ash with a 25% replacement rate of cement paste. In addition, Qiao et al. [17] investigate the chloride biding of the cement paste for 20%, 40% and 60% replacement rates of a Class C fly ash while Ishida et al. [18] uses a Class F fly ash at 20% and 40% replacement rates to examine the chloride binding. All of these publications found that while fly ash does affect the chloride binding capacity of the cement paste, the results in those studies show that the binding of the chlorides is insignificant when the chloride concentration is around 1.0 mol/L regardless of

the fly ash source and replacement rate [16-18]. Because of this, the salt concentrations in this study are limited to 0.6 mol/L.

Recent studies employ electrical resistivity techniques to improve the estimation of the D_c of concrete [4, 19-23]. These efforts have used the Nernst-Einstein equation to investigate the interrelationship between the electrical resistivity [1, 5, 24, 25]. The Nernst-Einstein equation has been reported as a helpful approach to predict D_c since this equation applies to electrolytes, for ion travel can be likened to that of electrical charges [21, 26]. However, those studies mainly focus on studying concrete with fly ash of limited chemistry. Because of this, a study is needed about investigating the correlation between D_c and electrical resistivity in cement paste, as it is a simpler system, with a large number of fly ashes by applying the Nernst-Einstein equation.

In this study, an approach using the transmission X-ray microscopy (TXM) is applied to examine the D_c for a cement paste containing fly ash. This technique is useful as it is non-destructive and rapid to investigate the apparent D_c and surface concentration (C_s). This approach has been presented in previous studies to image the movement of the ions in concrete materials using the potassium iodide (KI) solution as a tracer or contrast agent [27, 28]. The current work examines the cement paste to investigate the apparent iodide diffusion coefficient (D_{ic}) as the pore structure of the cement paste matrix is related to the ion diffusion in concrete [29]. Moreover, using cement paste is helpful to minimize intervention from aggregates [28]. The surface electrical resistivity (ρ_{sr}) is also investigated in the current study for fly ash concrete using the four-point Wenner probe measurements as per AASHTO T 358 [30]. In all of this work, the term D_{ic} and ρ_{sr} will refer to the apparent iodide diffusion coefficient of the paste and the surface electrical resistivity of the concrete, respectively.

This study aims to evaluate the possibility of determining D_{ic} using ρ_{sr} in concrete materials including fly ash and provides insights into the relationship between D_{ic} and ρ_{sr} for 20% fly ash

replacement at 45, 90, and 135 days of hydration by using the Nernst-Einstein equation. This provides important insights into the relationship between the electrical resistivity and D_c in concrete structures.

5.2 Raw materials and experimental methods

5.2.1 Raw materials

ASTM C150 Type I ordinary portland cement (OPC) [31] was used as a cement, and the properties of OPC are described in Table 5.1. Limestone and natural sand from Oklahoma were prepared as coarse and fine aggregate, respectively. The specific gravities of coarse and fine aggregate were the same as 2.60, and the absorption for each aggregate was shown as 0.64% and 0.55%, respectively. No chemical admixtures were used in any mixtures to minimize the variables.

Nineteen different fly ash sources were investigated in this study. The fly ashes were produced from various coal sources, boiler designs, and collection conditions in the United States. The fly ashes were classified into twelve Class C and seven Class F fly ashes according to ASTM C618 [32]. The properties of fly ash, bulk oxides, and particle information were investigated with the automated scanning electron microscopy (ASEM) method. Details about the ASEM method was presented in previous chapters and publications [33-36].

Table 5.1 Chemical and phase properties of Type I ordinary portland cement.

Chemical composition (%)								**Phase Composition (%)**			
SiO_2	**Al_2O_3**	**Fe_2O_3**	**CaO**	**MgO**	**SO_3**	**Na_2O**	**K_2O**	**C_3S**	**C_2S**	**C_3A**	**C_4AF**
20.8	4.6	2.6	62.7	2.4	3.2	0.2	0.3	52.1	20.2	7.7	8.0

5.2.2 Diffusion test for developing apparent diffusion coefficient (D_{ic})

5.2.2.1 Sample preparation

Paste samples were prepared for the ion penetration test, and the mixture design of the paste samples is shown in Table 5.2. A total of twenty mixtures was prepared including one mixture with 100% OPC and nineteen mixtures with 20% fly ash replacement by mass. A 0.45 water-to-cement ratio was used at the 20% fly ash replacement rate by mass of cement for all the mixtures. Any chemical admixtures were not incorporated into the mixtures to minimize the potential variables. All the mixtures were prepared as per ASTM C305 [37]. Vials with a 9.5 mm diameter and 46.0 mm height were used for the paste samples, and then these samples were sealed and cured in the curing room (100% relative humidity at 23°C) until either 45, 90, or 135 days. Three samples were prepared for each hydration date for each mixture.

Table 5.2 Mixture design for the paste specimen.

Mixture	**Water (g)**	**Cement (g)**	**Fly ash (g)**	**W/C**
OPC	400	888.9	-	0.45
20% Fly ash	400	711.1	177.8	0.45

5.2.2.2 TXM ion penetration test and data analysis

The 0.6 mol/L of KI solution was used as a tracer of the moisture penetration to investigated the D_{ic} of fly ash paste. The concentration of the KI solution was determined because the preliminary experiments in the previous study showed this was the optimum concentration to attain suitable contrast between the paste and solution [28]. As presented in the introduction, other publications have shown that the chloride binding capacity with the 0.6 mol/L solution was not affected by different fly ash sources [16-18]. Furthermore, previous studies found that the diffusion profiles

for iodide and chloride in paste were quite comparable, and the difference in the calculated diffusion coefficient at 28 days of ponding for each solution was about 10% [27, 28].

After curing, all the samples were ponded with the KI solution for 28 days. Then the radiographs of the ponded samples were taken with a Skyscan 1172 mCT scanner. The KI solution was replaced with a new solution every seven days to keep a constant KI concentration. While ponding, the sealed vials were stored in a container at 23°C.

The D_{ic} was calculated by approximating Fick's second law with an error function as shown in Eq.(5.1) [38, 39]. All the data analysis was conducted with the MATLAB programming environment. More details for the experimental settings and theoretical background for the data analysis were reported in previous publications [27, 28] and can be found in Appendix J. The equation used is:

$$C_{(x,t)} = C_{is}(1 - \text{erf}(\frac{x}{2\sqrt{D_{ic}t}})) \qquad \text{Eq.(5.1)}$$

where, x is the distance from the sample surface, t is the denotes time, erf is the error function, D_{ic} is the apparent iodide diffusion coefficient, C_{is} is the iodide surface concentration, and $C_{(x,t)}$ is the total iodide concentration at the depth of x from the surface after t.

5.2.3 Concrete sample preparation

The concrete mixtures used 20% of the binder as fly ash by mass except for one mixture with 100% portland cement. Table 5.3 shows the mixture proportions for the mixtures. A 0.45 water-to-cementitious material ratio (w/cm) was used for all the mixtures. No chemical admixtures were used in any mixtures to minimize the variables. Details for the concrete mixing procedure can be found in Appendix M.

After mixing, concrete samples were formed in 100 mm by 200 mm cylindrical containers according to ASTM C31 [40]; they were being cured at 23°C and 100% RH for 24 h in the curing room after sealing the container. The samples were then demolded and placed into the curing room until the samples were ready for the surface electrical resistivity test.

Table 5.3 Concrete mixture proportions of specimens for ρ_{sr} test.

Mixture design	**W/C**	**Cement (kg/m^3)**	**Fly ash (kg/m^3)**	**Water (kg/m^3)**	**Coarse aggregate (kg/m^3)**	**Fine aggregate (kg/m^3)**
OPC	0.45	283	0	127	863	564
20% Fly ash	0.45	227	57	127	862	562

5.2.4 Surface electrical resistivity (ρ_{sr}) with the Wenner probe

A non-destructive electrical resistivity test, the four-point Wenner probe, was performed to measure the ρ_{sr} of the concrete according to AASHTO T358 [30] at 3, 7, 14, 28, 56, 90, and 180 days of hydration. Four lines were marked on the circular face of each concrete cylinder at 0, 90, 180, and 270 degrees before the measurement. The ρ_{sr} was measured at each angle. This means that 12 measurements were collected at each time period. The average value of twelve measurements was used as the representative ρ_{sr} for each fly ash at specific curing time. All specimens were in the saturated surface dry (SSD) status while the resistivity test was conducted.

The ρ_{sr} values for 45 and 135 days of hydration were linearly interpolated from the measured data. This helped to eliminate the time variable in the comparison of ρ_{sr} and D_{ic}. The values of ρ_{sr} for 45 days of hydration were interpolated by using the measured values of 28 and 56 days of hydration, while the values of ρ_{sr} for 135 days of hydration were interpolated by using the measured values of 90 and 180 days of hydration for each fly ash.

5.2.5 Investigation of the correlation between ρ_{sr} and D_{ic}

The Nernst-Einstein equation in Eq.(5.2) was used to investigate the correlation between ρ_{sr} and D_{ic}. This approach has been widely used because the test method for the electrical resistivity is quick, easy and non-destructive to measure, and it helps to avoid the time-consuming grinding of the samples [4, 22, 23, 41]. This means that theoretically the service life of the concrete structure can be simply estimated from the resistivity of the concrete.

The constant value K was calculated by using all the dataset, only Class C fly ash dataset and only Class F fly ash dataset. Then it was used to interpret the relationship between two performances under different use of datasets. Furthermore, the R-squared value for each derived equation was investigated to discuss the correlation between the two properties. The Nernst-Einstein equation is:

$$D_{ic} = K/\rho_{sr} \qquad \text{Eq.(2)}$$

where, D_{ic} is the apparent iodide diffusion coefficient [$x10^{-11}$, m^2/s]; ρ_{sr} is the surface electrical resistivity of the concrete sample [$k\Omega \cdot cm$]; K is a factor that shows the correlation between D_{ic} and ρ_{sr}.

5.3 Result and discussion

5.3.1 Bulk chemical composition

Table 5.4 shows the bulk chemical composition result from the ASEM method for nineteen fly ash sources used in the mixtures. The fly ashes with "C#" and "IC#" represent Class C fly ash while the fly ashes with "F#" and "IF#" represent Class F fly ash. All the fly ashes are classified as either Class C or F fly ash according to ASTM C618 which means Class C fly ash has > 18% of CaO while Class F fly ash has < 18% of CaO [32].

Table 5.4 Bulk chemical composition from the ASEM.

Source	SiO_2	Al_2O_3	Fe_2O_3	CaO	MgO	SO_3	Na_2O	K_2O	TiO_2	P_2O_5	SrO
C1	36.20	21.72	5.35	23.15	5.38	0.67	3.58	1.01	0.80	1.90	0.23
C2	35.82	19.18	5.60	26.88	5.49	0.98	3.00	0.88	0.73	1.25	0.18
C3	25.32	19.26	5.22	32.50	7.76	2.60	3.42	0.63	1.08	1.89	0.32
C4	36.70	22.82	4.53	22.45	4.33	1.19	3.44	0.95	1.28	1.09	1.22
C5	31.25	22.46	5.38	26.06	5.95	0.56	4.30	0.84	0.84	2.11	0.23
C6	27.66	22.88	4.23	21.54	4.52	2.55	12.61	0.76	1.27	0.67	1.32
C7	35.28	20.61	4.74	24.72	4.93	0.74	4.26	1.23	1.64	0.82	1.00
C11	30.96	20.77	6.38	27.15	7.14	1.59	3.45	0.73	0.78	0.83	0.23
IC1	31.82	22.87	5.68	28.24	5.52	1.08	2.28	1.02	0.78	0.46	0.25
IC2	25.15	21.20	6.22	30.47	7.78	1.04	4.02	0.56	1.22	2.18	0.15
IC3	29.66	21.03	5.92	30.29	5.35	1.87	2.22	0.55	1.04	1.61	0.46
IC4	29.85	17.66	4.73	31.75	9.32	1.19	2.57	0.76	0.83	1.08	0.24
F1	48.76	23.79	7.39	12.53	2.97	0.48	0.86	2.05	0.78	0.09	0.29
F2	50.40	20.91	3.89	17.09	3.69	0.54	1.04	1.37	0.70	0.05	0.32
F3	48.81	26.62	6.65	9.30	1.95	0.28	1.75	1.93	1.46	0.14	1.10
F4	45.34	27.39	4.00	14.61	3.59	0.70	1.48	0.65	1.09	0.37	0.76
F5	53.18	25.36	11.21	2.06	0.19	0.89	0.97	4.43	0.71	0.03	0.96
F6	51.87	25.71	12.32	2.50	0.32	0.67	1.61	4.13	0.66	0.05	0.16
IF1	58.33	21.87	6.87	3.67	1.42	0.59	2.17	4.25	0.22	0.36	0.24

5.3.2 Correlation between ρ_{sr} and D_{ic}

The value of K in Eq.(5.2) can be varied depending on the test method for determining the D_{ic}, the pore solution composition, the use of SCM in concrete materials, etc [4]. Since diffusivity is higher and electrical resistivity is lower in the more porous materials, the value of K tends to increase with concrete porosity [21].

5.3.2.1 Correlations between ρ_{sr} and D_{ic} with and without fly ash

To describe the effect of fly ash on the relationship between the ρ_{sr} and D_{ic}, Fig. 5.1 presents the comparison results between the ρ_{sr} and D_{ic} for all the measurements of samples with fly ash and without fly ash. A total of 57 comparisons are made for the samples with fly ash and three mixtures with only OPC. The mixtures with OPC do not show changes in D_{ic} or ρ_{sr} between 45 d and 135 d. However, the samples with fly ash showed that 19 out of 57 or 33% of the D_{ic} are higher than the D_{ic} of OPC. This is surprising as every ρ_{sr} value is higher for fly ash than OPC. However, once the $\rho_{sr} > 25$ kΩ·cm, the D_{ic} values are $< 0.5 \times 10^{-11}$ m^2/s of the value for OPC. This is true for 22 out of 26 or 85% of the samples. This indicates two important things; (1) when the ρ_{sr} is > 25 kΩ·cm there is a high possibility to improve the D_{ic}, and (2) when the $\rho_{sr} < 25$ kΩ·cm then the performance is quite variable.

Since OPC samples show quite consistent value on both the ρ_{sr} and D_{ic} for all the measurements, the K value is not examined for OPC. On the contrary, the K value is calculated as 13.16 by employing all the measurements for the samples with fly ash, and the black curve is shown in Fig. 5.1 with a K value of 13.16; however, a poor correlation is found with 0.67 R-squared value.

The variability of the apparent diffusion coefficient has been reported in several studies by using the coefficient of variation (CV). Tang [42] has evaluated the precision of diffusion coefficient through various test methods such as immersion test (Nordtest method NT build 492), rapid migration test (Nordtest method NT build 443), and measurement of chloride ion ingress test (EN 13396). This work showed that the CV of these tests is 24%, 28%, and 36%, respectively. Moreover, ASTM C1556 (bulk chloride diffusion test) provides 39.8% as the limit of CV to evaluate the precision (single laboratory) of determining the apparent diffusion coefficient of cementitious mixtures [43]. Based on the test results of those studies, this work uses +/- 30% value to determine the variability of predicting D_{ic}.

A value of +/- 30% has been added in Fig. 5.1 as the dashed pink line as an estimate for the variability of the D_{ic} measurement. The result shows that only 31 out of 57 or 54% of the comparisons are within +/- 30%. In other words, just about a half of the D_{ic} of 20% fly concrete can be estimated by using ρ_{sr} if a single K value is used. Thus, more investigation may be needed to improve for determining D_{ic} by using ρ_{sr} with K.

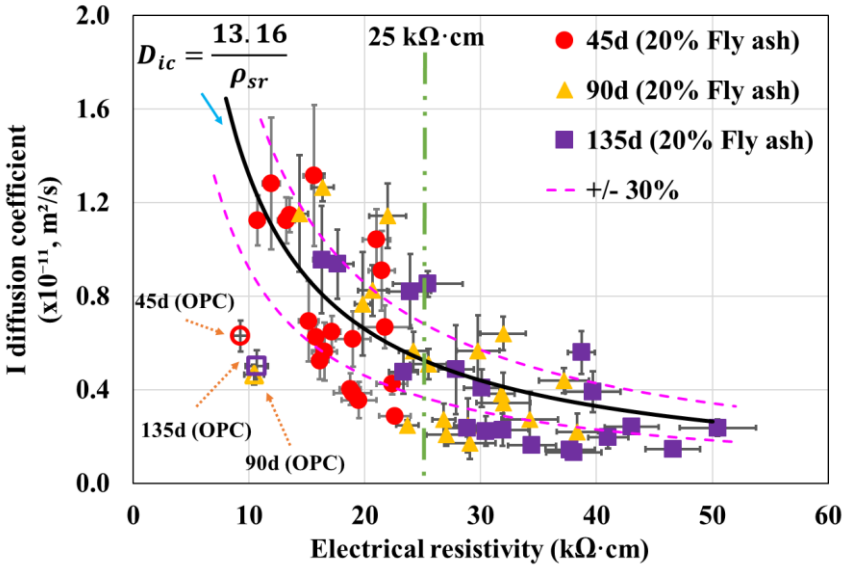

Fig. 5.1 Comprehensive correlation between the ρ_{sr} and D_{ic} for samples with fly ash and OPC.

Table 5.5 shows the calculated values of K and the percentages of comparison that are within +/- 30% for different days of hydration. All the K values are quite similar to each other and the derived K value by using all the measurements is 13.16 as shown in Fig. 5.1. Furthermore, all the R-squared values and the percentages of comparison that are within +/- 30% are quite low. This indicates that there are no impacts by the days of hydration on the relationship between the ρ_{sr} and D_{ic}. Thus, further investigation regarding the days of hydration is not conducted in this study.

Table 5.5 K and R-squared values for samples with fly ash for each hydration date.

Days of hydration (days)	K (95% confidence intervals)	R-squared	Percentage within +/- 30%
45	12.56 (10.48, 14.58)	0.41	63%
90	14.41 (11.63, 17.19)	0.53	58%
135	13.26 (10.74, 15.78)	0.61	42%

5.3.2.2 Impact of the type of fly ash on the relationships between the ρ_{sr} and D_{ic}

The relationships between the ρ_{sr} and D_{ic} with considering the type of fly ash are investigated further. Fig. 5.2 shows the comparison between the ρ_{sr} and D_{ic} of Class C fly ashes while Fig. 5.3 shows the comparison for Class F fly ashes. Overall, the Class F fly ashes exhibit a higher ρ_{sr} and lower D_{ic} than that of Class C fly ashes. The values of K and R-squared values of each comparison, as well as the number of points within +/-30%, are summarized in Table 5.6. Poor correlations have been found in each comparison between the ρ_{sr} and D_{ic} with the R-squared value of 0.53 for Class C and 0.60 for Class F. The value of K is calculated as 14.42 and 9.22 for the comparison of Class C fly ash and Class F fly ash, respectively. A value of +/- 30% to the regression line of Class C and Class F fly ash has been added respectively in Fig. 5.2 and Fig. 5.3 as the dashed pink line as a conservative estimate for the variability of the results. For Class C fly ash, 18 out of 36 or 50% comparisons are within +/- 30%, while 16 out of 21 or 76% comparisons are within +/- 30% for Class F fly ash. The results indicate that the K value is affected by the type of fly ash so that different K values might be used for different types of fly ash. Further, the results provide some insights that even though the D_{ic} could not be accurately predicted to use a single regression through the ρ_{sr} for Class C fly ash, an accurate prediction of the D_{ic} using ρ_{sr} for class F fly ash is reasonable.

While the Class F fly ash shows a lower variability than Class C fly ash, the D_{ic} values have a low variability after 25 kΩ·cm of ρ_{sr}. For the data points with ρ_{sr} > 25 kΩ·cm, the D_{ic} is between 0.13 x 10^{-11} m^2/s and 0.44 x 10^{-11} m^2/s, which is quite narrow. On the other hand, the ρ_{sr} shows a significant change from 26.82 kΩ·cm to 50.46 kΩ·cm in the same comparisons. In other words, D_{ic} for Class F fly ash is almost not changed after about 25 kΩ·cm, and so practically it is not necessary to use ρ_{sr} to estimate the D_{ic}.

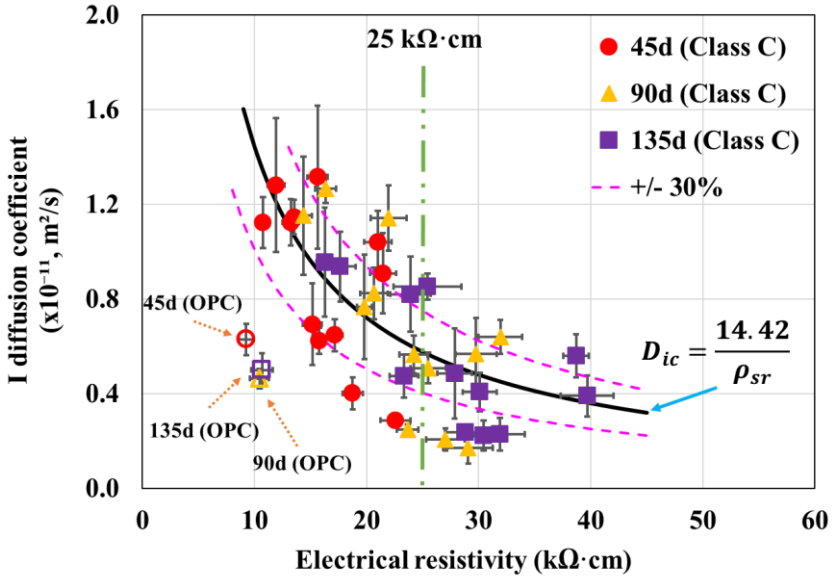

Fig. 5.2 Correlation between the ρ_{sr} and D_{ic} for Class C fly ashes.

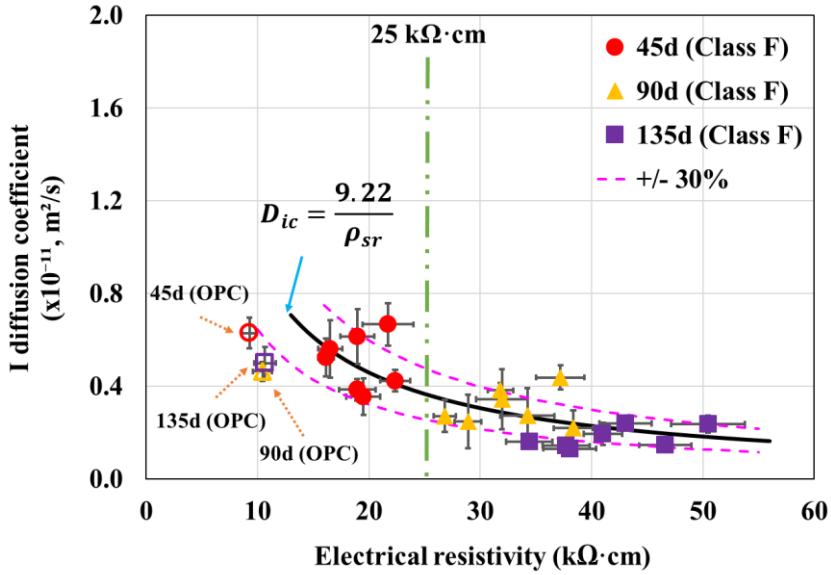

Fig. 5.3 Correlation between the ρ_{sr} and D_{ic} for Class F fly ashes.

Table 5.6 K and R-squared values for different types of fly ash.

Class of fly ash	K (95% confidence intervals)	R-squared	Percentage within +/- 30%
Class C	14.42 (12.84, 16.00)	0.53	50%
Class F	9.22 (8.02, 10.42)	0.60	76%

5.3.3 Calculate D_{ic} cement paste with fly ash through the ρ_{sr}

The current study focuses on examining the possibility of determining the D_{ic} through the ρ_{sr} by applying the Nernst-Einstein equation, and investigating the empirical relationship between D_{ic} of the fly ash-cement paste and ρ_{sr} from fly ash concrete. It has been published that the pore solution composition can affect the electrical resistivity, and therefore, these factors should be considered to accurately predict D_c [44, 45]. This has been done by controlling the pore solution chemistry of the concrete through a chosen soak solution or from measuring the pore solution chemistry and calculating a term called the formation factor [17, 46, 47]. The formation factor may improve the

ability to predict the D_c; however, the results in this study show that ρ_{sr} seems to be accurate for Class F fly ash.

5.3.4 Practical implication

In this study, the possibility of applying the Nernst-Einstein equation to estimate D_{ic} of 20% fly ash replacement of cement paste by using the ρ_{sr} at 45, 90 and 135 days of hydration. The results show that it is not recommended to use a single K value to interpret the empirical relationship between D_{ic} and ρ_{sr} of fly ash concrete. Although the correlations between two performances are quite poor, both Class C and Class F, employing the Nernst-Einstein equation on different types of fly ash provide insights that the variability of the comparison D_{ic} and ρ_{sr} could be affected by the type of fly ash used. However, the work shows that a single K value for class F fly ash is more reliable. Further, the work shows that the D_{ic} improved to be better than OPC when the ρ_{sr} is > 25 kΩ·cm. However, this occurred with all of the Class F fly ash after 90 d of hydration.

5.4 Conclusion

The present work employs the Nernst-Einstein equation to investigate the empirical relationship between the surface electrical resistivity and apparent diffusion coefficient for 20% fly ash replacement concrete materials between 45 and 135 days of hydration. This study shows that it is not accurate to use single regression analysis to relate the apparent iodide diffusion coefficient and the surface electrical resistivity. However, an accurate prediction of the apparent iodide diffusion coefficient for class F fly ash is reasonable.

The following conclusions can be made:

1. A poor correlation (0.67 R-squared value) and only 54% of the data is within +/- 30% of the predicted values when all fly ash is investigated with one equation for predicting the apparent iodide diffusion coefficient by using the surface electrical resistivity. This did

not improve when investigating different days of hydration.

2. A poor correlation (0.53 R-squared value) and only half (50%) of the data is within +/- 30% of the predicted values when Class C fly ash is investigated with one equation for predicting the apparent iodide diffusion coefficient by using the surface electrical resistivity.
3. While a poor correlation (0.60 R-squared value) is found when Class F fly ash is investigated with one predictive equation, 76% of the data is within +/- 30% of the predicted values one predictive equation which means that using a single predictive equation can be possible for Class F fly ash.
4. The apparent iodide diffusion coefficient becomes quite low and consistent for fly ash concrete for an electrical resistivity value > 25 kΩ·cm.

This work provides a practical application of the approach using the Nernst-Einstein equation to predict the diffusion coefficient. Future works studying the pore structure, ion types and concentration of pore solution in concrete for combining with the approach in this work should be done to better understand the relationship between the electrical resistivity and diffusion coefficient of fly ash concrete.

Acknowledgments

This work was sponsored by funding from the Illinois Department of Transportation [Project ICT R27-180], and the FHWA [EAR project # BAA No. 693JJ3-18-BAA-0001]. The authors would like to thank Dr. Daniel Cook for the assistance and discussion of this work.

Reference

[1] R. Van Noort, M. Hunger, P. Spiesz, Long-term chloride migration coefficient in slag cement-based concrete and resistivity as an alternative test method, Constr Build Mater 115 (2016) 746-759.

[2] R. He, H. Ye, H. Ma, C. Fu, X. Jin, Z. Li, Correlating the Chloride Diffusion Coefficient and Pore Structure of Cement-Based Materials Using Modified Noncontact Electrical Resistivity Measurement, J Mater Civil Eng 31(3) (2019) 04019006.

[3] L. Basheer, J. Kropp, D.J. Cleland, Assessment of the durability of concrete from its permeation properties: a review, Constr Build Mater 15(2-3) (2001) 93-103.

[4] Y. Liu, F.J. Presuel-Moreno, M.A. Paredes, Determination of Chloride Diffusion Coefficients in Concrete by Electrical Resistivity Method, ACI Materials Journal 112(5) (2015).

[5] X. Lu, Application of the Nernst-Einstein equation to concrete, Cement Concrete Res 27(2) (1997) 293-302.

[6] A.A. Torres-Acosta, F. Presuel-Moreno, C. Andrade, Electrical Resistivity as Durability Index for Concrete Structures, ACI Materials Journal 116(6) (2019) 245-253.

[7] B. Violetta, Life-365 service life prediction model, Concrete international 24(12) (2002) 53-57.

[8] A. Siemes, C. Edvardsen, Duracrete: service life design for concrete structures, Ottawa: NRC Research Press1999.

[9] E.P. Nielsen, M.R. Geiker, Chloride diffusion in partially saturated cementitious material, Cement Concrete Res 33(1) (2003) 133-138.

[10] A. Ababneh, F. Benboudjema, Y. Xi, Chloride penetration in nonsaturated concrete, J Mater Civil Eng 15(2) (2003) 183-191.

[11] A.V. Saetta, R.V. Scotta, R.V. Vitaliani, Analysis of chloride diffusion into partially saturated concrete, Materials Journal 90(5) (1993) 441-451.

[12] M. Masi, D. Colella, G. Radaelli, L. Bertolini, Simulation of chloride penetration in cement-based materials, Cement Concrete Res 27(10) (1997) 1591-1601.

[13] M. Thomas, Marine performance of PFA concrete, Magazine of Concrete Research 43(156) (1991) 171-185.

[14] O. Al-Amoudi, M. Maslehuddin, I.M. Asi, Performance and correlation of the properties of fly ash cement concrete, Cement, Concrete and Aggregates 18(2) (1996) 71-77.

[15] R.K. Dhir, E.A. Byars, PFA concrete: chloride diffusion rates, Magazine of Concrete Research 45(162) (1993) 1-9.

[16] M. Thomas, R. Hooton, A. Scott, H. Zibara, The effect of supplementary cementitious materials on chloride binding in hardened cement paste, Cement Concrete Res 42(1) (2012) 1-7.

[17] C. Qiao, P. Suraneni, T.N.W. Ying, A. Choudhary, J. Weiss, Chloride binding of cement pastes with fly ash exposed to CaCl2 solutions at 5 and 23° C, Cement and Concrete Composites 97 (2019) 43-53.

[18] T. Ishida, S. Miyahara, T. Maruya, Chloride binding capacity of mortars made with various Portland cements and mineral admixtures, Journal of Advanced Concrete Technology 6(2) (2008) 287-301.

[19] W.J. McCarter, G. Starrs, T.M. Chrisp, Electrical conductivity, diffusion, and permeability of Portland cement-based mortars, Cement Concrete Res 30(9) (2000) 1395-1400.

[20] R.J. Kessler, R.G. Powers, E. Vivas, M.A. Paredes, Y.P. Virmani, Surface resistivity as an indicator of concrete chloride penetration resistance, 2008 Concrete Bridge ConferenceFederal Highway AdministrationNational Concrete Bridge CouncilMissouri Department of TransportationAmerican Concrete Institute (ACI), 2008.

[21] P. Linares-Alemparte, C. Andrade, D. Baza, Porosity and electrical resistivity-based empirical calculation of the oxygen diffusion coefficient in concrete, Constr Build Mater 198 (2019) 710-717.

[22] C. Andrade, R. d'Andrea, N. Rebolledo, Chloride ion penetration in concrete: The reaction factor in the electrical resistivity model, Cement and Concrete Composites 47 (2014) 41-46.

[23] L. Xiao, Z. Ren, W. Shi, X. Wei, Experimental study on chloride permeability in concrete by non-contact electrical resistivity measurement and RCM, Constr Build Mater 123 (2016) 27-34.

[24] O. Sengul, O.E. Gjørv, Electrical resistivity measurements for quality control during concrete construction, ACI Materials Journal 105(6) (2008) 541.

[25] C. Andrade, Calculation of chloride diffusion coefficients in concrete from ionic migration measurements, Cement Concrete Res 23(3) (1993) 724-742.

[26] E.J. Garboczi, Permeability, diffusivity, and microstructural parameters: a critical review, Cement Concrete Res 20(4) (1990) 591-601.

[27] M. Khanzadeh Moradllo, M.T. Ley, Comparing ion diffusion in alternative cementitious materials in real time by using non-destructive X-ray imaging, Cement and Concrete Composites 82 (2017) 67-79.

[28] M.K. Moradllo, Q. Hu, M.T. Ley, Using X-ray imaging to investigate in-situ ion diffusion in cementitious materials, Constr Build Mater 136 (2017) 88-98.

[29] K. Stanish, R.D. Hooton, M.D. Thomas, Testing the Chloride Penetration Resistance of Concrete: A Literature Review, United States. Federal Highway Administration, 2001.

[30] AASHTO T 358:2015Method Of Test For Surface Resistivity Indication Of Concrete'S Ability To Resist Chloride Ion Penetration, 2015.

[31] ASTM C150, Standard Specification for Portland Cement, American Society for Testing and Materials, West Conshohocken, PA, 2019.

[32] ASTM C618, Standard Specification for Coal Fly Ash and Raw or Calcined Natural Pozzolan for Use in Concrete, American Society for Testing and Materials, West Conshohocken, PA, 2019.

[33] Q. Hu, M. Aboustait, M.T. Ley, J.C. Hanan, V. Rose, R. Winarski, Combined three-dimensional structure and chemistry imaging with nanoscale resolution, Acta Mater 77 (2014) 173-182.

[34] Q. Hu, M.T. Ley, J. Davis, J.C. Hanan, R. Frazier, Y. Zhang, 3D chemical segmentation of fly ash particles with X-ray computed tomography and electron probe microanalysis, Fuel 116 (2014) 229-236.

[35] T. Kim, Q. Hu, M.T. Ley, M. Aboustait, J.W. Bullard, Using Particle Characterization to Study Fly Ash Dissolution and Leaching in Water and KOH Solution, ACI Materials Journal 116(4) (2019).

[36] T. Kim, M. Moradian, M.T. Ley, Dissolution and leaching of fly ash in nitric acid using automated scanning electron microscopy, Advances in Civil Engineering Materials 7(1) (2018) 291-307.

[37] ASTM C305, Standard Practice for Mechanical Mixing of Hydraulic Cement Pastes and Mortars of Plastic Consistency, American Society for Testing and Materials, West Conshohocken, PA, 2014.

[38] J. Crank, The mathematics of diffusion, Oxford university press1979.

[39] S. Sadati, M.K. Moradllo, M. Shekarchi, Long-term durability of onshore coated concrete — chloride ion and carbonation effects, Frontiers of Structural and Civil Engineering 10(2) (2016) 150-161.

[40] ASTM C31, Standard Practice for Making and Curing Concrete Test Specimens in the Field, American Society for Testing and Materials, West Conshohocken, PA, 2019.

[41] E. Ryan, E. Burdette, R. Ankabrandt, R. Nidiffer, B. Buchanan, Comparison of two methods to assess the resistance of concrete to chloride ion penetration, J Mater Civil Eng 26(4) (2014) 698-704.

[42] L. Tang, Guideline for practical use of methods for testing the resistance of concrete to chloride ingress, CHLORTEST-EU funded Research Project'Resistance of concrete to chloride ingress-from laboratory tests to in-field performance'G6RD-CT-2002-00855, Deliverable D23 (2008).

[43] ASTM C1556, Standard Test Method for Determining the Apparent Chloride Diffusion Coefficient of Cementitious Mixtures by Bulk Diffusion, American Society for Testing and Materials, West Conshohocken, PA, 2016.

[44] P. Gao, J. Wei, T. Zhang, J. Hu, Q. Yu, Modification of chloride diffusion coefficient of concrete based on the electrical conductivity of pore solution, Constr Build Mater 145 (2017) 361-366.

[45] C. Shi, Effect of mixing proportions of concrete on its electrical conductivity and the rapid chloride permeability test (ASTM C1202 or ASSHTO T277) results, Cement Concrete Res 34(3) (2004) 537-545.

[46] W.J. Weiss, T.J. Barrett, C. Qiao, H. Todak, Toward a specification for transport properties of concrete based on the formation factor of a sealed specimen, Advances in Civil Engineering Materials 5(1) (2016) 179-194.

[47] W.J. Weiss, R.P. Spragg, O.B. Isgor, M.T. Ley, T. Van Dam, Toward performance specifications for concrete: linking resistivity, RCPT and diffusion predictions using the formation factor for use in specifications, High tech concrete: Where technology and engineering meet, Springer2018, pp. 2057-2065.

CHAPTER VI

CONCLUSION

The research presented in this dissertation provides an advanced approach of the Particle Model that predicts the performances of the fly ash in concrete by using the individual fly ash particle characteristics. The 52,000 particles from 26 fly ash sources are investigated using the automated scanning electron microscope. Nine distinct groups of fly ash particles are provided through machine learning that is used for deriving predictive models. The fitting coefficients in the derived predictive models give important insights into the varying effects of different fly ash particles over time. Furthermore, the empirical correlation between the electrical resistivity and the diffusion coefficient is provided for the materials with partially replaced fly ash to cement. These are an important step to build accurate predictive models for fly ash performance in concrete.

The main conclusions of this dissertation are:

6.1 Predicting the Compressive Strength of Fly Ash Concrete with the Particle Model

- Overall, over 91% of the fly ash particles investigated are classified into nine groups based on the chemical composition of each particle.
- About 95% of all measurements at 20% fly ash replacement and 81% of all

- measurements at 40% replacement of the compressive strength are predicted within +/- 10% through the predictive models through the Particle Model method.
- The R-squared value for the compressive strength prediction of the Particle Model is ≈ 0.99, while the Class C and F classification model is < 0.50 for 20% and 40% fly ash replacement between 3 to 180 days of hydration.
- Group 2, 3, 5, 7, and 9 are correlated with strength gain for both 20% and 40% fly ash replacement and show similar trends at both replacement levels.
- Group 4, 6, and 8 have a poor contribution or a reduction to the compressive strength for 20% and 40% replacement.
- Group 1 showed the largest coefficient over the first 56 days for 20% replacement while there is no impact for the compressive strength for 40% replacement.

6.2 Using the Particle Model to Predict Electrical Resistivity Performance of Fly Ash in Concrete

- The Class C and F classification method does not work well to predict electrical resistivity of fly ash concrete.
- There are no correlations found between the electrical resistivity and the median particle size as all R-squared values of the investigated trend lines are < 0.5 and < 0.3 at 20% and 40% fly ash replacement level, respectively.
- The Particle Model can predict the electrical resistivity within +/- 10% for 80% of all measurements at 20% replacement and 75% of all measurements at 40% replacement.
- The R-squared value for the electrical resistivity prediction of the Particle Model is > 0.98 for both 20% and 40% fly ash replacement between 3 to 180 days of hydration.
- Group 4, 5, 7, and 8 increased the resistivity between 3 and 180 days of hydration at both 20% and 40% replacement.

- Group 1 has the largest coefficient at the later ages for both 20% and 40% replacement while there was no impact at an early age. The impact of Group 9 is ≈ 0 until 90 days of hydration while it has a big impact at 180 days of hydration for both 20% and 40% replacement.
- Group 2 decreases the resistivity at 20% replacement and increases the resistivity at 40% replacement between 3 and 180 days of hydration. Although the actual value of coefficients for Group 3 is quite small for all the measured hydration times for 20% and 40% fly ash replacement levels, it showed a similar trend of coefficient change to Group 2. On the other hand, Group 6 increases the resistivity at 20% replacement while it decreases the resistivity at the 40% replacement.

6.3 Predicting Ion Diffusion in Fly Ash Cement Paste through Particle Analysis

- Between 45 and 135 days of hydration, the apparent iodide diffusion coefficient is decreased over time for all the fly ash sources except for C6. Furthermore, iodide surface concentration shows similar values to the OPC for all the investigated fly ash sources.
- At 45 and 90 days of hydration, 8 of the 12 Class C fly ashes show a greater iodide diffusion coefficient than OPC, and at the 135 days of hydration, the number of Class C fly ashes decreases to 6.
- The R-squared values of the relationship between the measured values and mean particle size of nineteen fly ashes are less than 0.3 which means the mean particle size showed poor correlation over the apparent iodide diffusion coefficient.
- For the apparent iodide diffusion coefficient, all the R-squared values of predictive models are > 0.95.
- The predicted and measured apparent iodide diffusion coefficient in paste shows that 81% of all measurements can be predicted within the variation of the test method (+/-

30%) between 45 to 135 days of hydration at 20% fly ash replacement.

- Groups 2 and 5 decrease the apparent iodide diffusion coefficient which means these groups help to improve the mass transport of the sample. Group 5 is the only particle group that showed improvement at all periods while Group 2 showed improvement at 90d.
- Group 1, 3, and 6 increase the apparent iodide diffusion coefficient between 45 and 135 days of hydration. Group 8 increases the apparent iodide diffusion coefficient at 90d and 135d while Group 9 increases the apparent iodide diffusion coefficient at only 45d. Group 4 and 7 have no impacts on the apparent iodide diffusion coefficient between 45d and 135d hydration.

6.4 The Relationship between the Apparent Diffusion Coefficient and Electrical Resistivity of Fly Ash Concrete

- A poor correlation (0.67 R-squared value) and only 54% of the data is within +/- 30% of the predicted values when all fly ash is investigated with one equation for predicting the apparent iodide diffusion coefficient by using the surface electrical resistivity. This did not improve when investigating different days of hydration.
- A poor correlation (0.53 R-squared value) and only half (50%) of the data is within +/- 30% of the predicted values when Class C fly ash is investigated with one equation for predicting the apparent iodide diffusion coefficient by using the surface electrical resistivity.
- While a poor correlation (0.60 R-squared value) is found when Class F fly ash is investigated with one predictive equation, 76% of the data is within +/- 30% of the predicted values one predictive equation which means that an accurate prediction of the apparent iodide diffusion coefficient for class F fly ash is reasonable.

- The apparent iodide diffusion coefficient becomes quite low and consistent for fly ash concrete for an electrical resistivity value > 25 kΩ·cm.

6.5 Future Work

Even though this research focuses on the fly ash performance on compressive strength, surface electrical resistivity, and diffusion, the application of the Particle Model can be extended to predict the fly ash performance in different concrete performances and longer hydration times. The following is a list of proposed future work:

- The Particle Model method can be used to predict the different durability mechanisms such as the alkali-silica reaction of fly ash concrete over time. Furthermore, the developed methods can be applied to investigate the impact of fly ash in fresh concrete properties such as slump and air contents.
- The suggested nine fly ash particle groups can be used to predict the longer period (after 180 days) of fly ash concrete performance.
- The suggested nine groups of fly ash and the Particle Model method can be used to more accurately predict the performance of blended fly ash in concrete.
- The reactivity and the phase composition of each group should be studied for more understanding of the nine groups of fly ash particles. This can help to improve the reliability and accuracy or the Particle Model.
- Studying the pore structure, ion types and concentration of pore solution in concrete for combining with the approach using the Nernst-Einstein equation should be done to better understand the relationship between the electrical resistivity and diffusion coefficient of fly ash concrete.

APPENDICES

Appendix A. Consistency of the ASEM method

Table A.1 shows the results of the average SD for three times the ASEM investigation of 50 fly ash particles on the same sample [1]. The SD of three times investigation was relatively small which means that the results from the ASEM method were quite consistent.

Table A.1 The average standard deviation for three times the ASEM investigation of 50 fly ash particles on the same sample.

Element	**SD (%)**
Silicon, Si	0.3
Aluminum, Al	0.4
Iron, Fe	0.7
Calcium, Ca	0.8
Magnesium, Mg	0.3
Potassium, K	0.6
Sodium, Na	0.6
Sulfur, S	0.2
Phosphorus, P	1.6
Morphology	**SD**
Average diameter (μm)	0.1
Perimeter (μm2)	0.4

Appendix B. Bulk chemical composition comparison between the results of XRF and ASEM

Table B.1 shows the comparison results of the eleven oxides between the result obtained with the ASEM method and the XRF method for twenty fly ashes. It showed that 96% of the comparisons were shown less than a 5% absolute difference between them. This suggests that the two methods agree well with each other.

Table B.1 Chemical composition of fly ashes by XRF and ASEM (C: Class C fly ash and F: Class F fly ash).

Fly ash		Chemical composition (% by mass)										
		SiO_2	Al_2O_3	Fe_2O_3	CaO	MgO	SO_3	Na_2O	K_2O	TiO_2	P_2O_5	SrO
C1	XRF	38.4	19.8	6.2	21.9	5.3	1.4	1.8	0.6	1.4	1.7	0.4
	ASEM	36.2	21.7	5.3	23.2	5.4	0.7	3.6	1.0	0.8	1.9	0.2
C2	XRF	36.2	19.9	6.7	24.0	5.2	1.4	1.7	0.5	1.4	1.4	0.4
	ASEM	35.8	19.2	5.6	26.9	5.5	1.0	3.0	0.9	0.7	1.2	0.2
C3	XRF	33.2	17.0	5.8	28.1	7.0	1.9	1.9	0.4	1.4	1.4	0.4
	ASEM	25.3	19.3	5.2	32.5	7.8	2.6	3.4	0.6	1.1	1.9	0.3
C4	XRF	37.6	23.2	5.5	21.8	4.2	1.0	1.7	0.6	1.6	1.6	0.4
	ASEM	36.7	22.8	4.5	22.4	4.3	1.2	3.4	1.0	1.3	1.1	1.2
C5	XRF	37.9	19.5	5.7	22.9	5.6	0.9	2.0	0.5	1.4	1.5	0.4
	ASEM	31.3	22.5	5.4	26.1	6.0	0.6	4.3	0.8	0.8	2.1	0.2
C6	XRF	37.0	20.6	5.3	15.6	3.6	2.9	9.2	0.7	1.3	0.7	0.7
	ASEM	27.7	22.9	4.2	21.5	4.5	2.5	12.6	0.8	1.3	0.7	1.3
C7	XRF	39.1	20.0	6.2	22.3	4.9	1.0	1.8	0.7	1.4	1.1	0.4
	ASEM	35.3	20.6	4.7	24.7	4.9	0.7	4.3	1.2	1.6	0.8	1.0
C8	XRF	40.0	20.9	5.9	21.5	5.0	0.8	1.6	0.7	-	-	-
	ASEM	40.1	22.6	4.5	19.4	5.7	0.8	3.7	0.9	0.6	1.4	0.1
C9	XRF	36.0	22.4	5.5	24.0	4.8	1.2	1.7	0.5	-	-	-
	ASEM	31.5	24.0	6.0	25.7	5.3	1.0	3.7	0.6	0.9	1.1	0.1
C10	XRF	35.9	18.0	6.7	25.8	6.1	1.8	1.8	0.4	1.2	0.8	0.5
	ASEM	36.0	19.3	5.1	22.7	7.8	2.0	4.8	0.6	1.0	0.3	0.5
F1	XRF	56.3	20.1	5.7	10.3	3.0	0.5	0.6	1.4	1.2	0.1	0.3
	ASEM	48.8	23.8	7.4	12.5	3.0	0.5	0.9	2.1	0.8	0.1	0.3
F2	XRF	52.0	16.4	4.4	18.7	2.9	0.9	0.8	0.9	1.0	0.3	0.2
	ASEM	50.4	20.9	3.9	17.1	3.7	0.5	1.0	1.4	0.7	0.1	0.3
F3	XRF	59.2	24.4	6.2	4.0	1.2	0.4	1.4	1.1	1.1	0.1	0.1
	ASEM	48.8	26.6	6.6	9.3	2.0	0.3	1.7	1.9	1.5	0.1	1.1
F4	XRF	49.7	24.2	4.7	12.9	3.3	0.7	1.0	0.6	1.7	0.5	0.3
	ASEM	45.3	27.4	4.0	14.6	3.6	0.7	1.5	0.6	1.1	0.4	0.8

F5	XRF	51.5	23.2	11.9	3.9	1.1	0.9	0.9	2.4	1.3	0.2	0.1
	ASEM	53.2	25.4	11.2	2.1	0.2	0.9	1.0	4.4	0.7	0.0	1.0
F6	XRF	49.0	20.9	16.1	4.9	0.9	1.6	1.1	2.5	1.1	0.1	0.0
	ASEM	51.9	25.7	12.3	2.5	0.3	0.7	1.6	4.1	0.7	0.1	0.2
F7	XRF	47.7	24.9	14.7	3.7	0.9	0.7	0.7	1.7	1.3	0.3	0.1
	ASEM	51.9	26.3	8.0	3.3	0.5	1.7	4.0	2.5	0.9	0.6	0.1
F8	XRF	56.9	22.6	4.6	7.3	2.3	0.3	1.7	1.2	-	-	-
	ASEM	56.9	23.9	3.4	6.2	2.1	0.1	4.1	1.7	0.3	1.2	0.1
F9	XRF	53.5	19.2	6.3	13.2	3.1	0.6	0.6	1.1	-	-	-
	ASEM	48.3	25.0	5.9	12.6	3.3	0.5	1.3	1.8	1.1	0.2	0.1
F10	XRF	57.7	24.5	4.1	8.1	2.0	0.3	0.2	0.9	-	-	-
	ASEM	53.6	27.8	2.8	10.5	2.5	0.5	0.3	1.3	0.4	0.3	0.0

Appendix C. The comprehensive procedure of ASEM method

ASEM method has been introduced and published [2] and was processed with three steps as shown below in Fig. C.1.

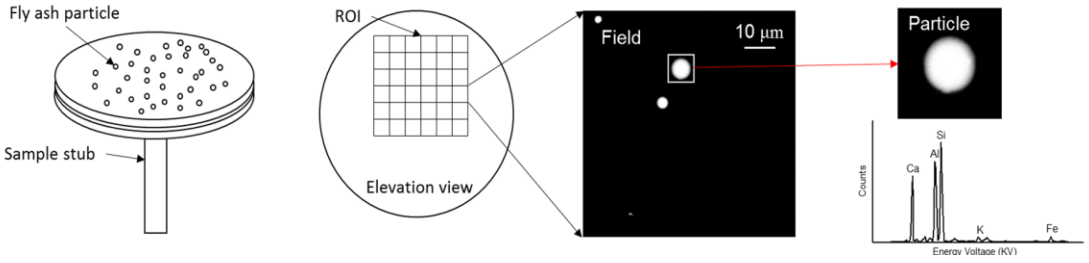

a) Sample preparation b) ASEM analysis c) Data Collection

Fig. C.1 The schematic of the ASEM procedure.

The first step was the sample preparation. A fly ash sample of 16.5mg (±1.5mg) was taken and placed in a plastic vial with 50 ml of alcohol solution. Since fly ash is a reactive material with water, it is important using a non-reactive solution for dispersion of fly ash particles without any reactions. The vial was capped, sealed, and sonicated for 30 min to disperse the fly ash particles and keep them in the suspension. Then, three to four droplets of the suspension with dispersed fly

ash particles were placed using a pipette on the sample holder with double-sided adhesive carbon tape.

Then the ASEM analysis was conducted. The prepared sample was then placed in the ASEM vacuum chamber and started the analysis using the settings in Table C.1. The probe current was kept constant using a Faraday Cup and Pico-ammeter to maintain the consistency of beam energies. The ASEM automatically detects and analyzes the size, shape, and chemistry for 500 individual particles per hour.

Table C.1 Summary of instrument settings, scanning settings, and EDS settings used for ASEM.

Instrument Setting	**Value**
Accelerating Voltage	20 keV
Probe Current	1.20 nA
Magnification	2500x
Working Distance	17-18 mm
Aspect Ratio	1.3
Search dwell time	16 μs
Measure dwell time	32 μs
Minimum Count Rate	3500 counts/s
Acquisition time	5s

Data conversion was the last step. Since fly ash particles are not flat like the 2D images from ASEM analysis, this violates one of the fundamental assumptions of classical quantitative EDS analysis. As discussed, the correction models have been developed by Armstrong and Love-Scott [3, 4] and Armstrong – Buseck [5, 6] to take into account the shape of the particle and make corrections to the collected k-ratios of 11 elements (Si, Al, Fe, Ca, Mg, S, Na, K, Ti, P, and Sr). The elemental composition of each particle was then corrected by the atomic number dependent

scattering, adsorption, and fluorescence effects (ZAF correction). The corrections were performed by using the software package called CalcZAF [7, 8].

Appendix D. Determination of the maximum spectral angle

The value of the spectral angle helps to measure which group is the closest one from an individual particle. Each particle had nine spectral angle values, and this can be calculated by Eq. (D.1).

$$\theta = \arccos\frac{\vec{a}\cdot\vec{b}}{|\vec{a}||\vec{b}|} \qquad \text{Eq. (D.1)}$$

where the $\vec{a}$ indicates a compositional vector of each group, and the $\vec{b}$ indicates the compositional vector of individual fly ash particles.

To determine either each fly ash particle can be classified as one of nine groups or not, a certain limit of spectral angle also known as the max spectral angle was needed. Since all particles will not fit each group, the max spectral angle helps to decide which they are the best fit. This means that group composition for each fly ash is highly contingent on what max spectral angle is used because more particles can be classified into the nine groups by using a larger max spectral angle. Therefore, it was decided to use one spectral angle to a value that either improves or at least maintains the performance of the SOM analysis. Furthermore, this is helpful to keep the useful particles in the nine groups as well as improve the modeling analysis results by excluding particles that may not be helpful in further model analyses.

Each particle has nine spectral angle values that indicate the distance from the particle to each of the nine groups. The smallest spectral value was used to decide to which group each particle belongs. If the smallest spectral angle showed under the max spectral angle, the particle was classified into the group that showed the smallest spectral angle. This process helps to classify

fly ash particles into one of the nine groups if they are in a reasonable range of the chemistry reported in Table 2.4. The ones that do not fit any of the nine groups were recorded as unclassified fly ash particles. Therefore, the percentage of classified particles for each fly ash also could be changed by using different maximum spectral angles.

The following process was conducted to determine the optimum maximum spectral angle. 52,000 particles, were classified by using different thresholds. The threshold was changed from 0.10 rad then increased incrementally by 0.10 rad interval to 0.60 rad so that six thresholds were investigated as a potential maximum spectral angle (0.10, 0.20, 0.30, 0.40, 0.50, and 0.60 rad). Since twenty-six fly ashes were investigated in this study, twenty-six percentage values were calculated based on the number of classified particles for each fly ash (2,000 is 100% for each fly ash). Then the comprehensive percentage of classified particles and SD of twenty-six fly ash percentage values were calculated for each investigated potential maximum spectral angle.

Table D.1 shows the changes for the comprehensive percentage of classified particles and STDEV of twenty-six fly ash percentage values on each different max spectral angle. The results of the STDEV from 0.1 rad to 0.3 rad showed significant changes with changing the max spectral angle but it turned to a highly consistent level after the point of 0.3 rad. The lower STDEV by using over 0.4 rad implied that the data might have higher stability in expecting the modeling analysis. Furthermore, the difference of the comprehensive percentage of classified particles between 0.3 rad and 0.4 rad was about 6% which means more particles can be included in nine groups if 0.4 rad is used as a max spectral angle rather than 0.3 rad.

Table D.1 Statistical analysis results with different max spectral angles.

Spectral Angle (θ, rad)	**0.10**	**0.20**	**0.30**	**0.40**	**0.50**	**0.60**
The percentage of classified particles (%)	14.17	65.38	88.99	95.36	97.91	98.80
SD (%)	6.10	14.38	5.31	1.93	1.33	1.02

To determine which value performs the best for predicting the compressive strength, the linear regression analysis was conducted with 0.3, 0.4 and 0.5 rad as the max spectral angle. Fig. D.1 shows the comprehensive comparison results of the significance of the probability of each nine groups for each model with different maximum spectral angles on different performance data. It shows how each group is significant in its model. 3d, 28d, and 180d of 20% fly ash concrete performance data were investigated for the linear regression analysis using nine groups on compressive strength (Fig. D.1(a)). 28d and 180d at 20% fly ash concrete data were investigated for the linear regression analysis using nine groups on the electrical resistivity (Fig. D.1(b)). The linear regression analysis using nine groups at 45d of D_{iC} and C_{iS} was investigated (Fig. D.1(c)). Each model was derived using all nine groups with the significance of variables from the MLR analysis and compared. The R-squared value of each model also compared and the results are shown in Table D.2. All the R-squared values showed over 0.99 which is quite high for all the analyses. This means that all of these potential maximum spectral angles did a good job on the modeling. The results with 0.3 rad max spectral angle showed some differences to modeling results with 0.4 rad and 0.5 rad max spectral angle. On the other hand, the significance of each group between 0.4 rad and 0.5 rad was almost the same as each other. The results indicate that about 6% of particles between 0.3 rad and 0.4 rad spectral angle affect the result of the modeling analysis. In other words, these particles cannot be excluded for further modeling analysis because of the reliability. Furthermore, the particles that showed over a 0.4 rad spectral angle may not affect the model analysis results so that these particles can be considered as outliers and excluded from nine groups. Thus, 0.4 rad was used as the max spectral angle in this study.

Table D.2 R-squared value of each linear regression model on different hydration time data with different max spectral angle used.

Max spectral angle	3d	28d	180d
0.3 rad	0.995	0.995	0.995
0.4 rad	0.997	0.996	0.996
0.5 rad	0.997	0.997	0.996

3d of 20% fly ash concrete			
Angle	Significance of variables		
	0.3	0.4	0.5
Group 1		*	*
Group 2	***	***	**
Group 3	***	***	***
Group 4	***	***	***
Group 5	**	***	***
Group 6		.	.
Group 7	***	***	***
Group 8	*	*	*
Group 9		*	**

28d of 20% fly ash concrete			
Angle	Significance of variables		
	0.3	0.4	0.5
Group 1	*	***	***
Group 2	***	***	***
Group 3	***	***	***
Group 4	***	***	***
Group 5	***	***	***
Group 6			
Group 7	***	***	***
Group 8			
Group 9	.	***	***

180d of 20% fly ash concrete			
Angle	Significance of variables		
	0.3	0.4	0.5
Group 1		*	*
Group 2	***	***	***
Group 3	***	***	***
Group 4	***	***	***
Group 5	***	***	***
Group 6	*	*	*
Group 7	***	***	***
Group 8			
Group 9	.	**	**

'***' : Pr(>|t|) ≤ 0.001, '**' : 0.001 < Pr(>|t|) ≤ 0.01, '*' : 0.01 < Pr(>|t|) ≤ 0.05, '.' : 0.05 < Pr(>|t|) ≤ 0.1

(a) Compressive strength

28d of 20% fly ash concrete			
Angle	Significance of variables		
	0.3	0.4	0.5
Group 1	***		
Group 2		**	***
Group 3	**	*	.
Group 4	***	***	***
Group 5	.	***	***
Group 6	***	***	***
Group 7	***	***	***
Group 8	***	***	***
Group 9	***	***	**

180d of 20% fly ash concrete			
Angle	Significance of variables		
	0.3	0.4	0.5
Group 1		*	**
Group 2	*	*	.
Group 3			
Group 4	***	***	***
Group 5	***	***	***
Group 6	**		
Group 7	***	***	***
Group 8	***	***	***
Group 9	.	*	***

'***' : Pr(>|t|) ≤ 0.001, '**' : 0.001 < Pr(>|t|) ≤ 0.01, '*' : 0.01 < Pr(>|t|) ≤ 0.05, '.' : 0.05 < Pr(>|t|) ≤ 0.1

(b) Electrical resistivity

D_C for 45d of 20% fly ash paste			
Angle	Significance of variables		
	0.3	0.4	0.5
Group 1			
Group 2	***	***	***
Group 3	***	***	***
Group 4	***	***	***
Group 5			
Group 6			
Group 7		.	*
Group 8	.	***	***
Group 9	*	***	***

C_S for 45d of 20% fly ash paste			
Angle	Significance of variables		
	0.3	0.4	0.5
Group 1			
Group 2	*		
Group 3	**	***	***
Group 4	***	***	***
Group 5	***	***	***
Group 6			
Group 7	***	***	***
Group 8			
Group 9		.	*

'*' : Pr(>|t|) ≤ 0.001, '**' : 0.001 < Pr(>|t|) ≤ 0.01, '*' : 0.01 < Pr(>|t|) ≤ 0.05, '.' : 0.05 < Pr(>|t|) ≤ 0.1**

(c) Diffusion

Fig. D.1 Comprehensive results of the linear regression model analysis with different max spectral angles on different hydration time data.

Appendix E. The procedure for the MLR analysis for the compressive strength

While the model could be returned that uses all nine groups, it was possible that some of the identified groups do not have any influence on concrete performance. The significance of the variables was investigated from the MLR analysis to determine which, if any, of the groups are significant to the analysis. The variable which showed over 0.10 was not considered as a significant value from the result. The significance of value was tested by determining the t-value of the coefficient. The t-value can be simply calculated by dividing the coefficient by the standard error which is shown in the 2nd (Coefficient) and 3rd (Std. Error) column in Table E.1. As an example, Table E.1 showed the initial model performance with all nine groups for 20% fly ash concrete at 28d curing with the result of the MLR.

Table E.1 The initial model results of MLR for predicting the compressive strength of 20% fly ash concrete at 28d curing.

Group	Coefficient	Std. Error	t value	Pr(>|t|)
Group 1	265.02	75.39	3.515	0.001
Group 2	223.97	37.21	6.019	0.000
Group 3	91.43	12.27	7.452	0.000
Group 4	44.40	10.59	4.193	0.000
Group 5	90.53	11.49	7.879	0.000
Group 6	**-17.25**	**22.58**	**-0.764**	**0.449**
Group 7	51.22	5.13	9.984	0.000
Group 8	**10.35**	**23.03**	**0.449**	**0.655**
Group 9	156.84	39.92	3.929	0.000

*Bold with underlined groups: Groups showed non-significant (over 0.1) of Pr(>|t|)

Non-significant variables can be removed, and then the model was simplified. According to the result of example analysis in Table E.1, Group 6 and Group 8 showed the non-significant value of Pr(>|t|) as 0.449 and 0.655, respectively. To improve the reliability of the modeling process, the model analysis was re-conducted after removing only Group 8 which shows the highest non-significant Pr(>|t|) value. Pr(>|t|) value of Group 6 on the re-conducted model was changed from 0.449 to 0.505. Since Pr(>|t|) of Group 6 was still high and non-significant, the model analysis should be conducted again without Group 6. This process needs to be conducted until Pr(>|t|) values of remaining groups show significant, at least marginally significant (between 0.05 to 0.10).

Table E.2 shows the model analysis result after two groups removed, and all the Pr(>|t|) values of remaining groups showed as significant. Therefore, the final model for compressive strength of 20% fly ash concrete at 28d curing can be simplified with the remaining groups, and the final equation was determined as Eq. (E.1). Since only 28d curing time compressive strength data was

used in the analysis, the model does not require a time element. The R-squared value of the final model showed as 0.997 (R-squared value of the initial model was 0.996) after the equation was simplified.

Table E.2 Particle Model result for predicting the compressive strength of 20% fly ash concrete at 28d curing time using seven significant groups.

Group	Coefficient	Std. Error	t value	Pr(>|t|)
Group 1	295.66	55.86	5.293	0.000
Group 2	204.69	27.66	7.400	0.000
Group 3	83.82	7.57	11.073	0.000
Group 4	48.29	9.13	5.289	0.000
Group 5	84.72	7.02	12.068	0.000
Group 7	50.46	4.81	10.491	0.000
Group 9	170.09	25.82	6.588	0.000

Compressive Strength of 20% fly ash concrete at 28d (psi)

$$= 295.66(\%Group1) + 204.69(\%Group2) + 83.82(\%Group3) + 48.29(\%Group4) + 84.72(\%Group5) + 50.46(\%Group7) + 170.09(\%Group9) \quad \text{Eq. (E.1)}$$

Appendix F. Determine the nine distinct groups from SOM analysis

As discussed, 52,000 fly ash particles data from twenty-six fly ashes were collected by using ASEM, and each particle has eleven pieces of chemical composition data (Na_2O, MgO, Al_2O_3, SiO_2, P_2O_5, SO_3, K_2O, CaO, TiO_2, Fe_2O_3, and SrO_2). The SOM was used to determine distinct groups [9]. To conduct the SOM analysis, a certain model geometry should be selected to determine the number of datum points to classify the fly ash particles, and nine geometry was used in this study based on the result of previous publication [1].

The main purpose of using SOM was not just grouping fly ash particles into nine groups, but to find a representative set of nine groups to classify the fly ash particles and apply these nine groups to model analysis. The representative nine groups were determined through the following three steps: 1) Running SOM 200 times with the 52,000 particle database so that 200 possible sets of nine groups were derived. 2) Pick one set and compare all nine groups with nine groups from all the other 199 sets. Each group can be identified with the composition of eleven chemistry provided from ASEM analysis. 3) Collect all the groups that showed similar chemical composition from 200 sets as one. The average and standard error for each chemical composition were calculated for each group.

Table F.1 (same as Table 2.4) showed the chemical composition of each group, and each group showed a unique composition of eleven chemicals. The standard error was investigated for the 200 comparisons on each chemical for each group, and the result is shown in Table F.2. The result showed that just one result was 0.10, and all the other values were under 0.06. These values were quite low, and this means that nine groups derived by using the SOM method were quite repeatable and consistent. Therefore, nine groups in Table F.1 were determined as the representative nine groups.

Table F.1 Chemical composition of determined nine distinct groups with SOM analysis.

Group	SiO_2	Al_2O_3	Fe_2O_3	CaO	MgO	SO_3	Na_2O	K_2O	TiO_2	P_2O_5	SrO
Group1	10.56	5.42	77.81	2.80	0.72	0.98	0.91	0.18	0.28	0.20	0.10
Group2	8.35	33.41	6.35	33.71	6.62	2.06	0.47	0.01	0.81	6.96	1.14
Group3	8.67	15.83	8.17	42.63	9.34	6.21	0.23	0.03	2.00	6.49	0.28
Group4	38.35	31.09	4.48	6.65	2.89	1.29	12.13	1.95	0.56	0.20	0.37
Group5	36.16	26.69	4.64	20.99	6.55	0.43	2.35	0.13	1.29	0.30	0.43
Group6	23.86	21.54	4.80	34.81	7.90	1.54	0.45	0.01	1.70	2.90	0.43
Group7	48.75	32.36	6.39	3.82	1.65	0.42	2.97	2.85	0.43	0.02	0.32
Group8	60.58	14.82	4.75	7.11	2.75	0.33	5.90	2.83	0.46	0.04	0.39
Group9	84.46	5.43	2.03	2.19	0.51	0.20	2.62	2.06	0.10	0.00	0.38

Table F.2 The standard error for each chemical for nine groups.

Group	SiO_2	Al_2O_3	Fe_2O_3	CaO	MgO	SO_3	Na_2O	K_2O	TiO_2	P_2O_5	SrO
Group 1	0.01	0.01	0.03	0.06	0.01	0.02	0.00	0.03	0.02	0.10	0.00
Group 2	0.01	0.02	0.10	0.04	0.04	0.02	0.00	0.05	0.01	0.02	0.01
Group 3	0.01	0.03	0.05	0.04	0.04	0.04	0.00	0.06	0.03	0.02	0.00
Group 4	0.04	0.01	0.03	0.03	0.01	0.02	0.01	0.03	0.02	0.02	0.01
Group 5	0.02	0.02	0.04	0.04	0.01	0.01	0.00	0.05	0.03	0.01	0.01
Group 6	0.01	0.01	0.04	0.06	0.03	0.02	0.00	0.05	0.04	0.01	0.00
Group 7	0.02	0.01	0.03	0.03	0.00	0.01	0.01	0.02	0.01	0.02	0.00
Group 8	0.03	0.02	0.06	0.05	0.00	0.01	0.01	0.04	0.01	0.01	0.00
Group 9	0.02	0.01	0.02	0.05	0.00	0.00	0.01	0.01	0.00	0.01	0.00

Appendix G. The comprehensive results of the coefficient values for the predictive models of the compressive strength

The coefficients of each group for the model used for predicting the compressive strength are shown in Table G.1. The predictive models were constructed by applying the coefficient values to the Eq. (2) for both 20% and 40% fly ash replacements at seven specific times.

Table G.1 Coefficients for each group at different curing times.

Mixture	Curing	Group 1	Group 2	Group 3	Group 4	Group 5	Group 6	Group 7	Group 8	Group 9
20% Fly ash	3 days	96.50	79.40	56.94	42.92	29.85	25.06	35.35	32.19	49.30
	7 days	222.86	144.55	71.05	45.91	54.44	-	39.54	-	125.45
	14 days	226.16	167.32	80.02	49.40	75.67	-	46.17	-	128.52
	28 days	295.66	204.69	83.81	48.29	84.72	-	50.46	-	170.09
	56 days	364.94	193.79	94.85	56.72	103.25	-	60.91	-	204.87
	90 days	262.89	245.19	136.83	50.55	150.02	-74.03	73.67	-	186.76
	180 days	239.32	272.40	142.75	60.05	159.46	-77.40	83.75	-	186.45
40% Fly ash	3 days	-	83.52	17.62	-	43.87	49.25	24.06	-	45.82
	7 days	-	119.63	48.95	-	55.15	44.48	28.65	-	77.55
	14 days	-	178.06	82.00	-	95.84	-	32.88	-	91.57
	28 days	-	212.96	102.60	-	110.01	-	51.25	-	69.28
	56 days	-	254.92	99.78	-	125.77	-	56.89	-	114.86
	90 days	-	246.19	116.46	-	135.93	-	71.30	-	107.35
	180 days	-	280.54	126.19	-	134.31	-	72.56	-	125.26

Appendix H. The procedure for simplifying the prediction model for the surface electrical resistivity

While the model could be returned that uses all nine groups, it was possible that some of the identified groups do not have any influence on the resistivity. The significance of the variables was investigated using an MLR analysis to determine which, if any, of the groups are significant to the analysis. The variable which showed over 0.10 was not considered as a significant value from the result. The significance of value was tested by determining the t-value of the coefficient. The t-value can be simply calculated by dividing the coefficient by the standard error which is shown in the 2nd (Coefficient) and 3rd (Std. Error) column in Table H.1. As an example, Table H.1 showed the initial model performance with all nine groups for 40 % fly ash concrete at 28d curing with the result of the MLR analysis.

Table H.1 The initial model result from MLRfor predicting the resistivity of 40% fly ash concrete at 28d curing.

Group	Coefficient	Std. Error	t value	Pr(>|t|)
Group 1	1.23	0.25	4.92	0.00
Group 2	0.85	0.13	6.54	0.00
Group 3	0.19	0.04	4.75	0.00
Group 4	**-0.01**	**0.04**	**-0.25**	**0.85**
Group 5	0.52	0.04	13.00	0.00
Group 6	-0.19	0.08	-2.38	0.02
Group 7	0.11	0.02	5.50	0.00
Group 8	0.40	0.07	5.71	0.00
Group 9	**0.10**	**0.13**	**0.77**	**0.45**

*Bold with underlined groups: Groups showed non-significant (over 0.1) of Pr(>|t|)

Non-significant variables can be removed, and then the model was simplified. According to the result of example analysis in Table H.1, Group 4 and Group 9 showed the non-significant value

of Pr(>|t|) as 0.85 and 0.45, respectively. To improve the reliability of the modeling process, the model analysis was re-conducted after removing only Group 4 which shows the highest non-significant Pr(>|t|) value. Pr(>|t|) value of Group 9 on the re-conducted model was changed from 0.45 to 0.44. Since Pr(>|t|) of Group 9 was still high and non-significant, the model analysis should be conducted again without Group 9. This process needs to be conducted until Pr(>|t|) values of remaining groups show significant, at least marginally significant (between 0.05 to 0.10).

Table H.2 shows the model analysis result after two groups removed, and all the Pr(>|t|) values of remaining groups showed as significant. Therefore, the final model for resistivity of 40% fly ash concrete at 28d curing can be simplified with the remaining groups, and the final equation was determined as Eq. (H.1). Since only 28d curing time resistivity data was used in the analysis, the model does not require a time element. The R-squared value of the final model showed as 0.984 (R-squared value of the initial model was 0.985) after the equation was simplified (Particle Model).

Table H.2 Particle Model result for predicting the resistivity of 40% fly ash concrete at 28d curing time using seven significant groups.

Group	**Coefficient**	**Std. Error**	**t value**	**Pr(>|t|)**
Group 1	1.10	0.18	6.11	0.00
Group 2	0.85	0.07	12.14	0.00
Group 3	0.20	0.04	5.00	0.00
Group 5	0.51	0.04	12.75	0.00
Group 6	-0.19	0.07	-2.71	0.01
Group 7	0.12	0.01	12.00	0.00
Group 8	0.44	0.05	8.80	0.00

The resistivity of 40% fly ash concrete at 28d (kΩ·cm)

= 1.10(%Group1) + 0.85(%Group2) + 0.20(%Group3) + 0.51(%Group5) - 0.19(%Group6) +

0.12(%Group7) + 0.44(%Group8) Eq. (H.1)

Appendix I. The comprehensive results of the coefficient values for the predictive models of surface electrical resistivity

The coefficients of each group for the model used for predicting the electrical resistivity are shown in Table I.1. The predictive models were constructed with applying the coefficient values to the Eq.(3.2) for both 20% and 40% fly ash replacements at seven specific times.

Table I.1 Coefficient values for each of the nine groups at different curing times for 20% and 40% fly ash replacement rates.

Mixture	Curing	Group 1	Group 2	Group 3	Group 4	Group 5	Group 6	Group 7	Group 8	Group 9
20% Fly ash	3 days	-	-0.07	0.02	0.09	-0.02	0.18	0.06	0.16	-0.06
	7 days	-	-0.06	0.01	0.13	-0.02	0.22	0.08	0.18	-0.09
	14 days	-	-0.18	-0.05	0.26	0.02	0.32	0.10	0.20	-0.14
	28 days	-	-0.18	-0.04	0.37	0.10	0.33	0.14	0.42	-0.37
	56 days	0.99	-0.67	-0.07	0.59	0.28	0.43	0.22	0.45	-
	90 days	1.09	-0.60	-	0.61	0.45	0.36	0.30	0.73	-
	180 days	1.47	-0.58	-	0.61	0.63	0.31	0.44	1.04	0.79
40% Fly ash	3 days	-	-	0.02	0.04	0.07	0.07	0.04	0.06	0.08
	7 days	-	0.23	0.04	-	0.10	0.06	0.06	0.06	0.11
	14 days	0.92	0.33	0.05	-	0.24	0.06	0.02	-0.09	0.58
	28 days	1.10	0.85	0.20	-	0.51	-0.19	0.12	0.44	-
	56 days	2.34	1.23	0.17	0.28	0.99	-0.40	0.28	0.81	-
	90 days	3.75	2.24	0.36	0.31	1.65	-1.14	0.47	1.34	-
	180 days	3.64	1.20	-	1.09	2.13	-0.46	0.90	-	4.09

Appendix J. Experimental settings for the KI diffusion test

Fig. J.1 shows the schematic diagram of the experimental setup for the sample vial [10]. 0.6 mm thickness of aluminum wire was set on the side of the sample vial. The wire helps align the images and also acts as a standard material between scans [10]. The TXM settings are shown in Table J.1.

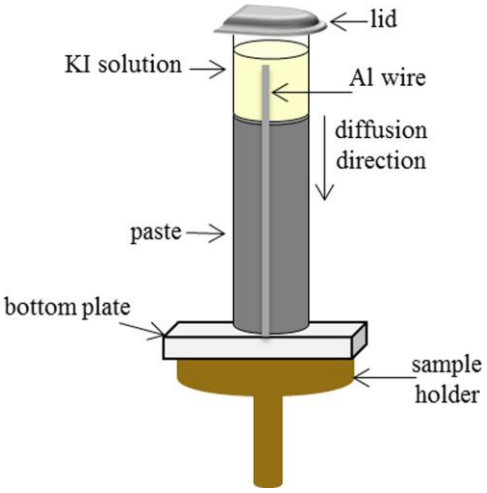

Fig. J.1 Schematic diagram of the diffusion test setup [10].

Table J.1 Summary of TXM instrument setting [10].

Parameter	Setting
Voltage (keV)	100
Current (μA)	100
Chamber condition	Air
Filter	0.5mm Al + 0.5mm Cu
Pixel size (μm)	8.8

The D_{ic} and C_{is} of the sample for each radiograph were calculated with the following steps. First, take the sample area from the radiograph by removing all other parts to avoid any background

attenuation effect. Next, match the height of the surface between the reference paragraph and the 28d ponding time radiograph to measure the gray value from the same area. Then, measure the hundreds of lines of the specified area in several seconds, and calculate the D_{ic} and C_{is}. Beer-Lambert Law (Eq.(J.1)) [11, 12] was applied to calculate a change in attenuation due to I ($\Delta\mu$) at different depths of the sample.

$$(\Delta\mu)_x = \ln\left(I_{ref}\right)_x - \ln(I_t)_x \qquad \text{Eq.(J.1)}$$

where, $(I_{ref})_x$ is the gray value at depth x on the reference profile, and $(I_t)_x$ is the gray value at the same location at a future time.

Then the D_{ic} and C_{is} were calculated with the help of Fick's second law (Eq.(4.1)) [13, 14]. All the data analysis was conducted with the MATLAB programming environment.

Appendix K. The procedure for the MLR analysis for apparent iodide diffusion coefficient

Even though the model could be returned that uses all nine groups, some of the groups cannot have any influence on the diffusion coefficient or surface concentration. The significance of the variables was used to determine the groups which are significant to the model. The variable which showed the probability (Pr(>|t|)) over 0.10 was not considered as a significant value from the result. The significance of value was tested by determining the t-value of the coefficient. Table K.1 provides MLR analysis results for the initial model performance with all nine groups of the diffusion coefficient at 90 days of hydration.

Table K.1 The initial model result of MLR for predicting the diffusion coefficient at 90 days of hydration.

Group	Coefficient	Std. Error	t value	Pr(>|t|)
Group 1	**0.049**	**0.039**	**1.256**	**0.216**
Group 2	- 0.038	0.018	- 2.111	0.041
Group 3	**0.010**	**0.006**	**1.667**	**0.128**
Group 4	**0.001**	**0.005**	**0.200**	**0.792**
Group 5	- 0.030	0.006	- 5.000	0.000
Group 6	0.053	0.011	4.818	0.000
Group 7	**0.001**	**0.003**	**0.333**	**0.869**
Group 8	**0.014**	**0.011**	**1.273**	**0.215**
Group 9	**0.008**	**0.020**	**0.400**	**0.693**

*Bold with underlined groups: Groups showed non-significant (over 0.1) of Pr(>|t|)

The model was simplified by removing the non-significant variables. According to the result of example analysis in Table K.1, Group 1, 3, 4, 7, 8, and 9 showed the non-significant Pr(>|t|) value. To improve the reliability of the model process, the model analysis was re-conducted after removing a group that showed the highest non-significant Pr(>|t|) value which is Group 7 in Table K.1. Group 4 showed the highest Pr(>|t|) value among the remaining eight groups as 0.808 which is non-significant. The model analysis was conducted after removing the Group 4, and Group 9 showed the highest Pr(>|t|) among the remaining seven groups as 0.429 which is non-significant. The model analysis was conducted again after removing the Group 9, and then all the Pr(>|t|) value of the remaining six groups were < 0.1. The process was conducted until Pr(>|t|) values of remaining groups show significant, at least marginally significant (between 0.05 to 0.10).

Table K.2 shows the final model analysis result after three groups removed. Thus, the predictive model for the diffusion coefficient at 90 days of hydration can be derived using the result, and the

final predictive model equation was determined as Eq.(K.1). The R-squared value of the final model showed as 0.923 (0.919 for the initial model) after the equation was simplified.

Table K.2 Particle Model result for predicting the diffusion coefficient at 90 days of hydration using six significant groups.

Group	**Coefficient**	**Std. Error**	**t value**	**Pr(>|t|)**
Group 1	0.048	0.026	1.846	0.071
Group 2	- 0.033	0.010	- 3.300	0.002
Group 3	0.011	0.005	2.200	0.046
Group 5	- 0.029	0.005	- 5.800	0.000
Group 6	0.051	0.009	5.667	0.000
Group 8	0.021	0.006	3.500	0.001

D_{ic} at 90 days of hydration ($x10^{-11}$, m^2/sec)

= 0.048(%Group1) - 0.033(%Group2) + 0.011(%Group3) - 0.029(%Group5) + 0.051(%Group6) + 0.021(%Group8) Eq.(K.1)

Appendix L. Comprehensive results of the coefficient values for the predictive models of apparent iodide diffusion coefficient

Table L.1 shows the coefficients of each group to predict the D_{ic} at 45, 90, and 135 days of hydration. The numerical value for each group shows how significant it is at each time. Positive or negative values are shown to increase or decrease the D_{ic} while the ages without a coefficient mean that those groups did not influence the D_{ic} at that time period.

Table L.1 Coefficients of each group on the predictive models for D_{ic}.

Group	D_{ic}		
	45d	**90d**	**135d**
Group 1	0.084	0.048	0.038
Group 2	-	-0.033	-
Group 3	0.010	0.011	0.012
Group 4	-	-	-
Group 5	-0.024	-0.029	-0.020
Group 6	0.039	0.051	0.027
Group 7	-	-	-
Group 8	-	0.021	0.011
Group 9	0.049	-	-

Appendix M. Concrete mixing procedure

The moisture content for both coarse and fine aggregates was determined before the mixing process and the batch proportions for the aggregates and water were adjusted. Both aggregates were brought into the temperature-controlled mixing facility at least a day before conducting the moisture correction, and their batch weights were corrected for the moisture content. After adjusting the mixture proportion, all the mixtures were mixed according to the following steps. All aggregates were collected from the outside storage piles, and they were stored in a temperature-controlled room (23°C) for at least 24 hours. The aggregates were then placed in the mixer and spun; after that, a representative sample was taken for moisture correction. It should be noted here that aggregates have to be properly sealed to prevent water loss before the mixing. At the time of mixing, all aggregates and approximately one half of the mixing water were loaded into the mixer; they were being mixed for three minutes. This allowed the aggregates to approach the saturated surface dry (SSD) condition and to ensure that the aggregates were evenly

distributed. All the materials (the cement, fly ash, and the remaining water) were added into the mixer and were being mixed for three minutes. Then the mixture was rested for two minutes while the sides of the mixing drum were scraped. After that, the mixer was started to mix the concrete for three more minutes as well.

References for appendix

[1] T. Kim, J.M. Davis, M.T. Ley, S. Kang, P. Amrollahi, Fly ash particle characterization for predicting concrete compressive strength, Constr Build Mater 165 (2018) 560-571.

[2] M. Aboustait, T. Kim, M.T. Ley, J.M. Davis, Physical and chemical characteristics of fly ash using automated scanning electron microscopy, Constr Build Mater 106 (2016) 1-10.

[3] J.T. Armstrong, Quantitative Elemental Analysis of Individual Microparticles with Electron Beam Instruments, in: K.F.J. Heinrich, D.E. Newbury (Eds.), Electron Probe Quantitation, Springer US, Boston, MA, 1991, pp. 261-315.

[4] G. Love, V.D. Scott, Evaluation of a New Correction Procedure for Quantitative Electron-Probe Microanalysis, J Phys D Appl Phys 11(10) (1978) 1369-1376.

[5] J.T. Armstrong, P.R. Buseck, Quantitative Chemical-Analysis of Individual Microparticles Using Electron-Microprobe - Theoretical, Anal Chem 47(13) (1975) 2178-2192.

[6] J.T. Armstrong, P.R. Buseck, A General Characteristic Fluorescence Correction for the Quantitative Electron Microbeam Analysis of Thick Specimens, Thin-Films and Particles, X-Ray Spectrom 14(4) (1985) 172-182.

[7] M. Aboustait, Q. Hu, R. Frazier, Y. Zhang, B. Tabb, M. Ley, J. Hahan, Innovative prediction of fly ash performance in concrete, Oklahoma Transportation Center, Midwest City, OK, 2013.

[8] J.T. Armstrong, J. Donovan, P. Carpenter, CALCZAF, TRYZAF and CITZAF: The Use of Multi-Correction-Algorithm Programs for Estimating Uncertainties and Improving Quantitative X-ray Analysis of Difficult Specimens, Microscopy and Microanalysis 19(S2) (2013) 812-813.

[9] T. Kohonen, Self-Organizing Maps, Third ed., Springer, Berlin, Heidelberg1997.

[10] M. Khanzadeh Moradllo, M.T. Ley, Comparing ion diffusion in alternative cementitious materials in real time by using non-destructive X-ray imaging, Cement and Concrete Composites 82 (2017) 67-79.

[11] V.C. Tidwell, L.C. Meigs, T. Christian-Frear, C.M. Boney, Effects of spatially heterogeneous porosity on matrix diffusion as investigated by X-ray absorption imaging, Journal of Contaminant Hydrology 42(2) (2000) 285-302.

[12] L. Cavé, T. Al, Y. Xiang, P. Vilks, A technique for estimating one-dimensional diffusion coefficients in low-permeability sedimentary rock using X-ray radiography: Comparison with through-diffusion measurements, Journal of Contaminant Hydrology 103(1) (2009) 1-12.

[13] J. Crank, The mathematics of diffusion, Oxford university press1979.

[14] S. Sadati, M.K. Moradllo, M. Shekarchi, Long-term durability of onshore coated concrete — chloride ion and carbonation effects, Frontiers of Structural and Civil Engineering 10(2) (2016) 150-161.

VITA

Shinhyu Kang

Candidate for the Degree of

Doctor of Philosophy

Dissertation: PREDICTING FLY ASH PERFORMANCE IN CONCRETE FROM PARTICLE CHARACTERISTICS

Major Field: Civil Engineering

Biographical: Shinhyu Kang was born in Iksan, Jeollabuk-do, Republic of Korea on July 4th, 1983

Education:

Completed the requirements for the Doctor of Philosophy in Civil Engineering at Oklahoma State University, Stillwater, Oklahoma in May 2020.

Completed the requirements for the Master of Science in Materials Science and Engineering at Kyonggi University, Suwon, Gyeonggi-do, Republic of Korea in 2012.

Completed the requirements for the Bachelor of Science in Materials Science and Engineering at Kyonggi University, Suwon, Gyeonggi-do, Republic of Korea in 2010.

Experience:

Graduate Research Assistant, Oklahoma State University, Stillwater, OK, 2015-2020.
Development Engineer & Research Assistant, Iljin Diamond Co., Ltd., Eumseong, Republic of Korea 2011-2014
Graduate Research Assistant, Kyonggi University, Suwon, Gyeonggi-do, Republic of Korea, 2010-2011

Professional Memberships:

American Concrete Institute (ACI)
American Coal Ash Association (ACAA)
American Ceramic Society (ACerS)
American Society of Civil Engineers (ASCE)